

Measurements in bulk magnetic materials

Fausto Fiorillo

Istituto Nazionale di Ricerca Metrologica-INRIM, Torino, Italy

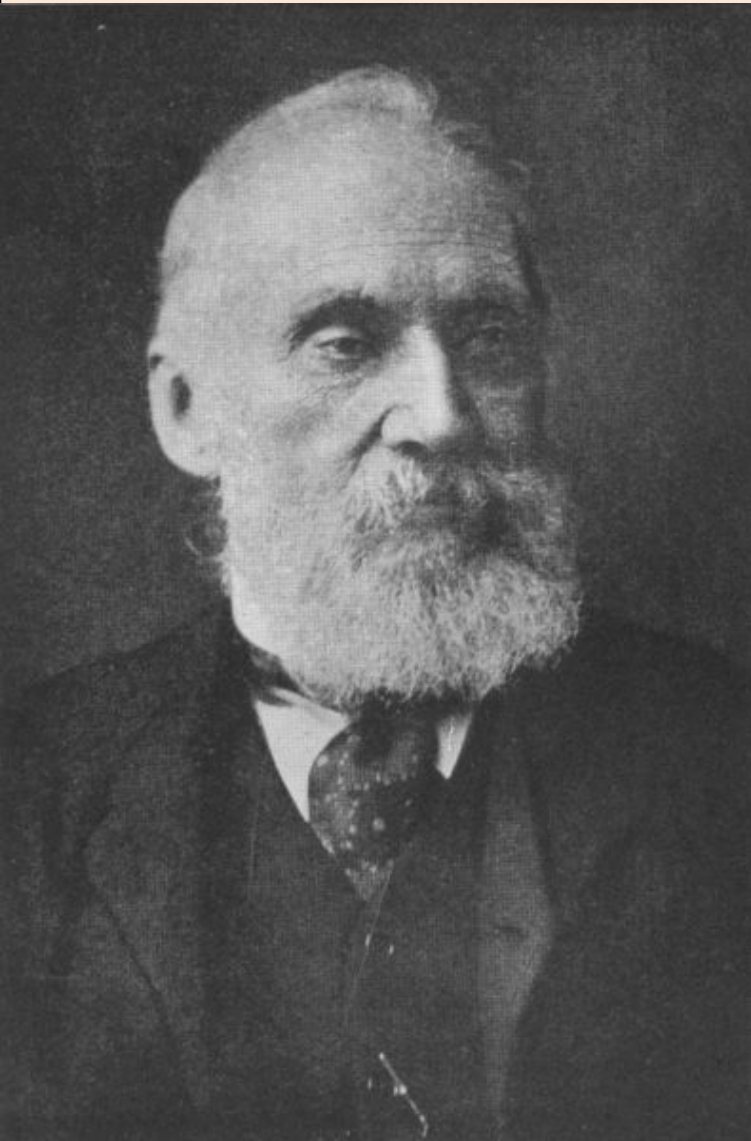
OUTLINE

- **Generation of high magnetic fields**
- **Neutron diffraction and the measurement of the intrinsic properties of magnetic materials.**
- **Measurements of magnetization curve, hysteresis, and the related parameters:**
 - a) **soft magnetic materials;** b) **permanent magnets.**

Magnets and measurements are everywhere

- ***Measurements mean knowledge. They are indispensable to science, industry, and commerce.***
- ***Measurements are the prerequisite for any conceivable development in the production and trading of goods.***
- ***Global market of magnetic materials: EUR € 35 10⁹***
- ***Magnetic materials satisfy basic demands of our society***
- ***Measurements are expensive: they cost about 5% of GNP in industrial countries***

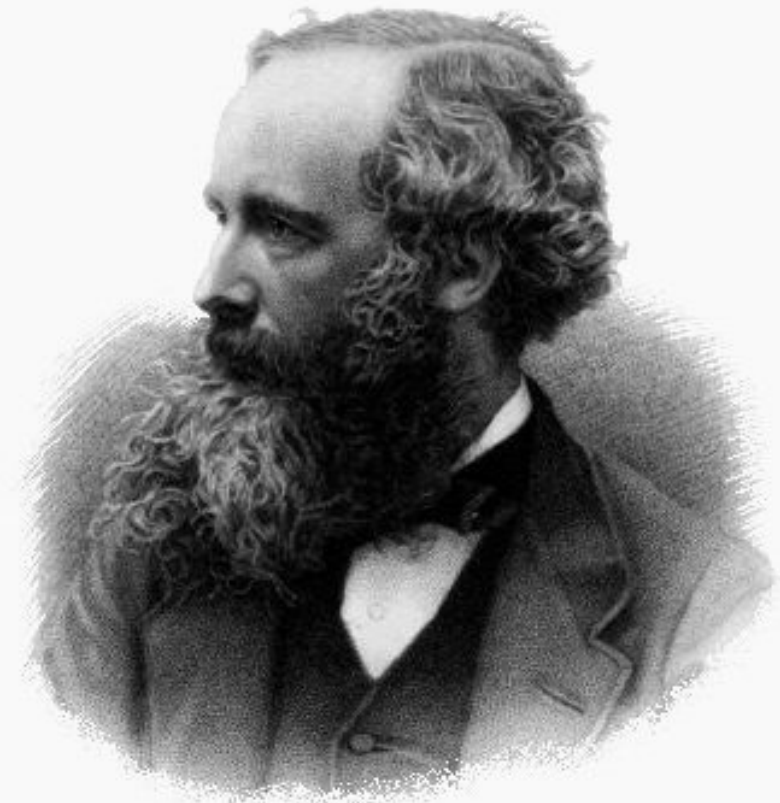
- **Whatever the specific aim of measurements, there is no shortcut to rigorous and physically grounded experimental methods.**
- **Measurements require good judgment and this is only possible if the underlying scientific issues are understood.**
- **Measurements are useful when there is consensus and standards are fixed.**
- **National Metrological Institutes (NMIs) and international metrological and standardization organizations play the key role in this respect. They provide traceability to the SI units.**
- **NMIs declare calibration and measurement capabilities. Intercomparisons are at the root of such declarations.**



Measurements are indispensable for achieving quantitative information on materials, favour their applications, and stimulate new physical theories.

“I often say that when you can measure what you are speaking about and express it in numbers you know something about it. But when you cannot measure it, when you cannot express it in numbers, your knowledge is of a meager and unsatisfactory kind.”

Lord Kelvin, 1883



“...we can scarcely avoid the conclusion that light consists in the transverse undulations of the same medium which is the cause of electric and magnetic phenomena”.

Lord Kelvin and Maxwell formulated the requirement for a **coherent system of units** with **base units** and **derived units**.

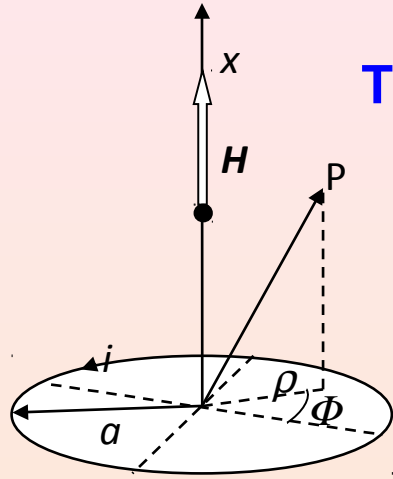
*A system of units is said to be **coherent** if all of its units are either base units, or are derived from the base units without using any numerical factors other than 1. The International System of Units (**SI**) is a coherent system.*

J.C. Maxwell 1831-1879

<i>Quantity</i>	<i>Symbol</i>	<i>SI units</i>	<i>Gaussian units</i>	<i>Conversion SI-Gaussian</i>
Magnetic moment	m	$\text{A}\cdot\text{m}^2, \text{J}\cdot\text{T}^{-1}$	$\text{erg}\cdot\text{G}^{-1}, \text{emu}$	$1 \text{ A}\cdot\text{m}^2 = 10^3 \text{ emu}$
Magnetic flux	Φ	$\text{Wb}, \text{V}\cdot\text{s}$	$\text{G}\cdot\text{cm}^2, \text{maxwell}$	$1 \text{ Wb} = 10^8 \text{ maxwell}$
Magnetic flux density	B	T	G	$1 \text{ T} = 10^4 \text{ G}$
Magnetic field	H	$\text{A}\cdot\text{m}^{-1}$	Oe	$1 \text{ A}\cdot\text{m}^{-1} = 1.2566 \cdot 10^{-2} \text{ Oe}$
Magnetization	M	$\text{A}\cdot\text{m}^{-1}$	$\text{erg}\cdot\text{G}^{-1}\cdot\text{cm}^{-3}, \text{emu}\cdot\text{cm}^{-3}$	$1 \text{ A}\cdot\text{m}^{-1} = 10^{-3} \text{ emu}\cdot\text{cm}^{-3}$
Magnetic polarisation	J	T	--	--
Magnetic susceptibility	χ	--	--	$\chi_{SI} = 4\pi\chi_G$

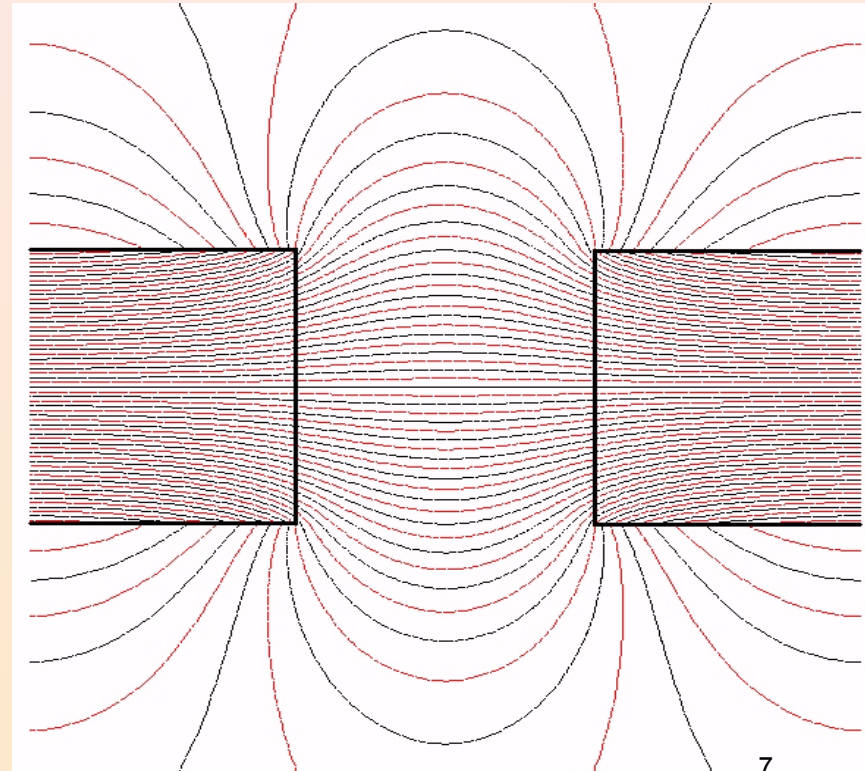
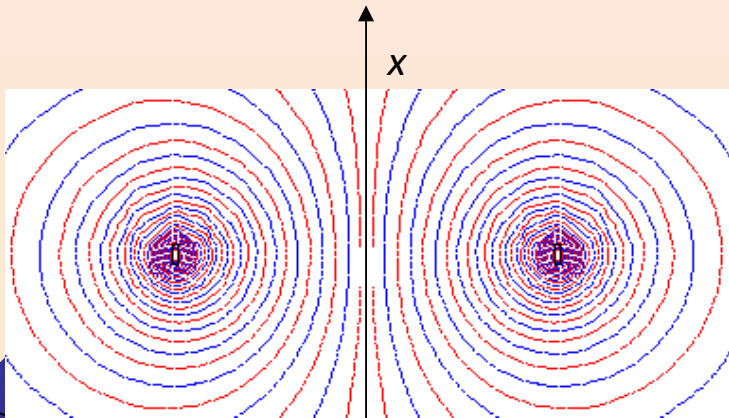
$$\mathbf{B} = \mu_0 \mathbf{H} + \mu_0 \mathbf{M} = \mu_0 \mathbf{H} + \mathbf{J}$$

The characterization of a magnetic material requires that an exciting field is generated. This can be done either by making electrical currents flowing in conductors or exploiting the ordered array of quantum-mechanical electronic currents circulating in a magnetic material.

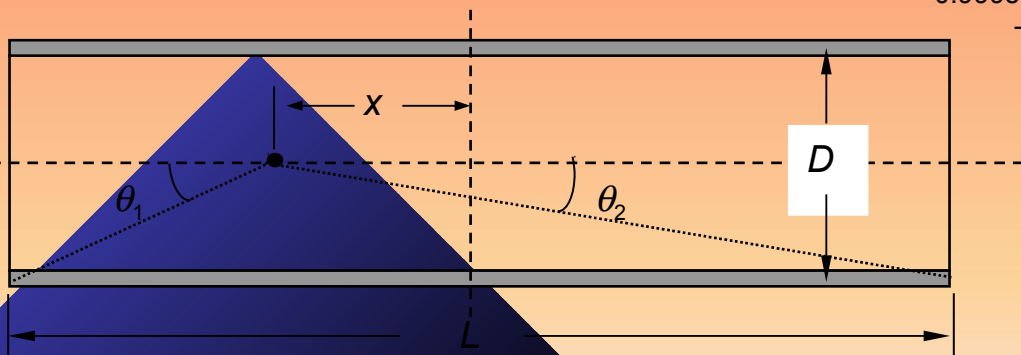
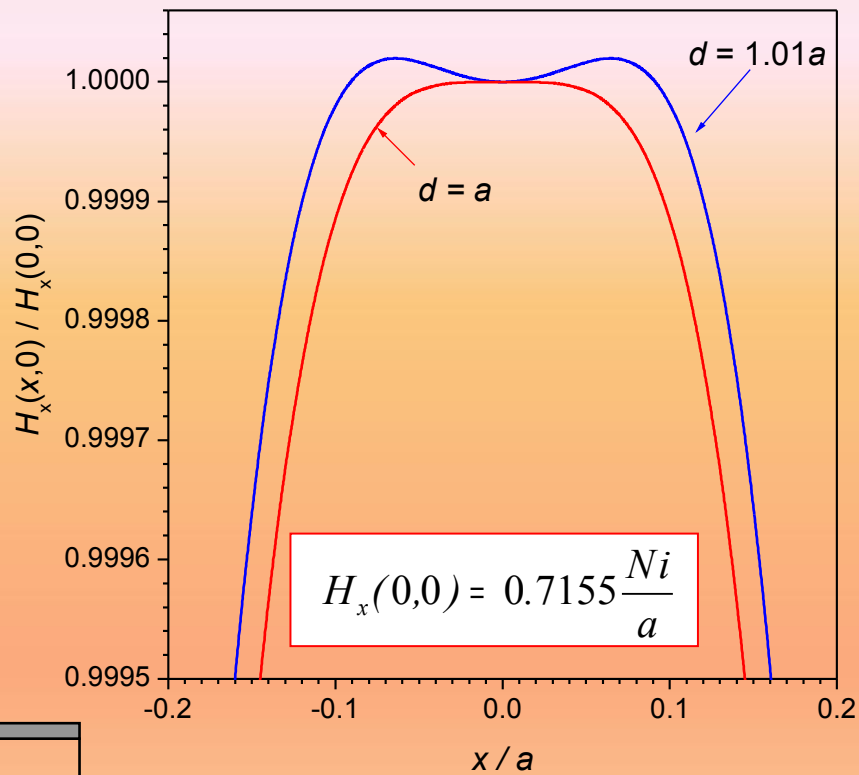
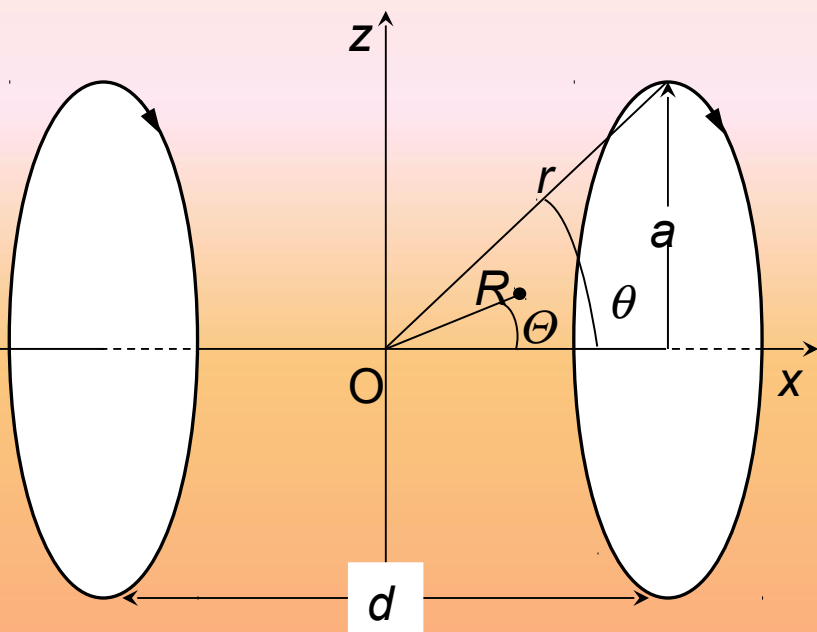


The Biot-Savart 's law

$$d\mathbf{H} = \frac{i d\mathbf{l} \times \mathbf{r}}{4\pi r^3}$$



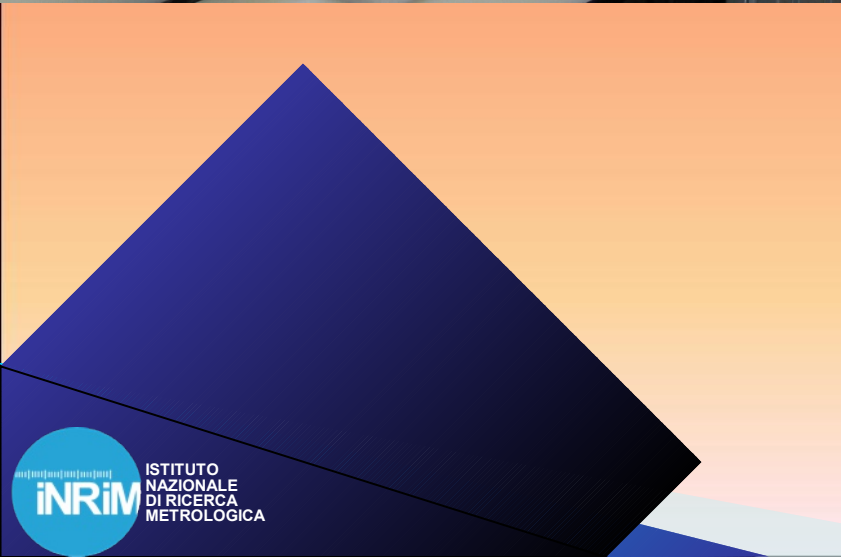
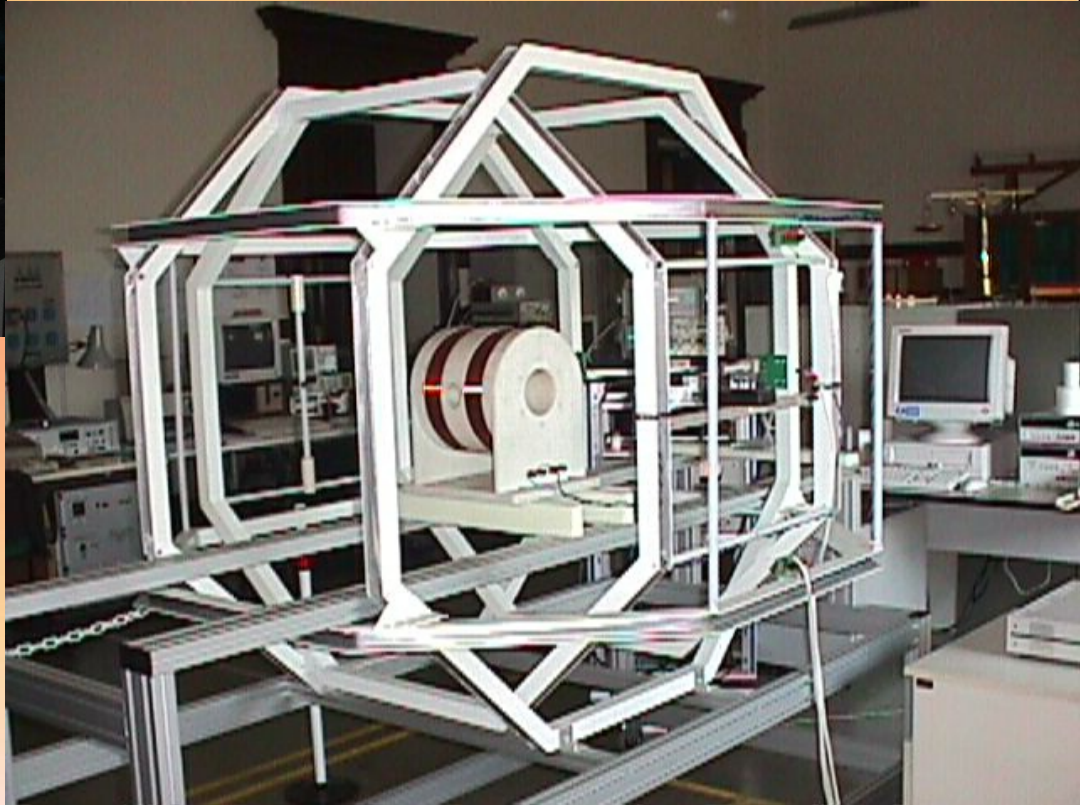
Two common wirewound field sources: the Helmholtz coil and the solenoid.



$$H_x(0) = \frac{Ni}{(D^2 + L^2)^{1/2}}$$



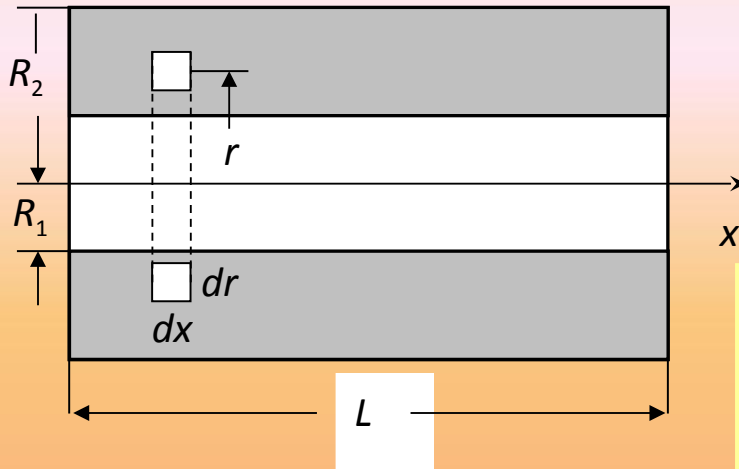
A reference magnetic field source



Due to obvious heating problems, the maximum available flux density in water-cooled windings is of the order of 0.1 T.

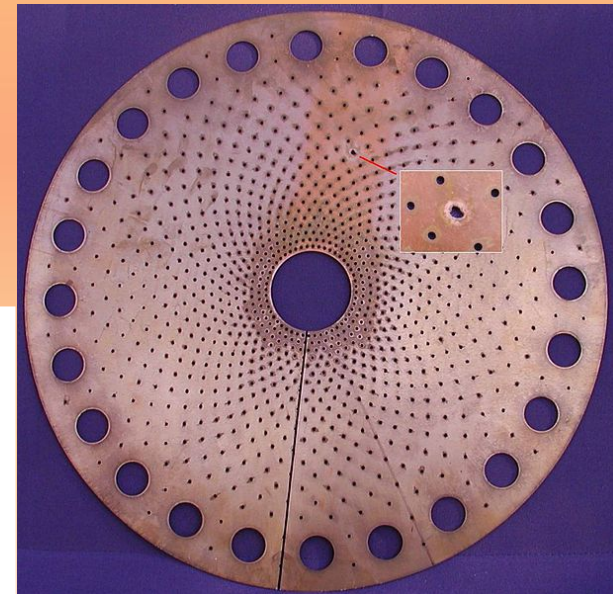
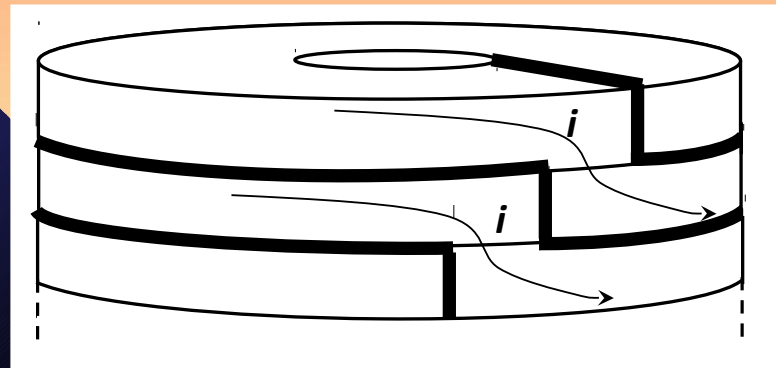
The power consumption

$$W = \frac{H^2}{G^2 \lambda} \rho R_1$$

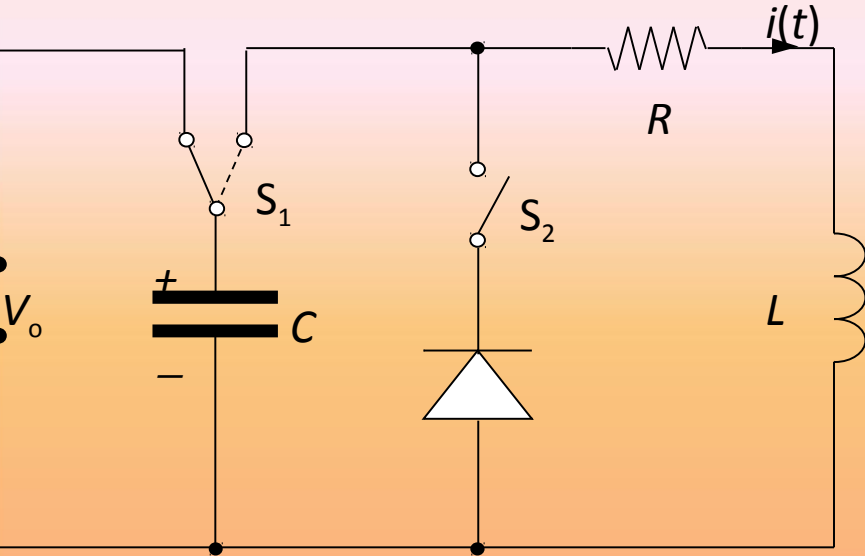


G is a function of R_2/R_1 ($G_{\max} = 0.17$), ρ is the resistivity, $\lambda < 1$ is the filling factor. With $\mu_0 H = 0.1$ T, $W = 1.5 - 3$ kW

Very high steady fields (up to about 40 T) are obtained with the Bitter coils. In order to dissipate the enormous amounts of generated heat (power loss of several MW) and withstand the large electrodynamic forces, the wire is substituted by a stack of tightly clamped copper disks.



Pulsed fields peaking up to about 10 T can be obtained by conventional solenoids, supplied by a discharging condenser bank.

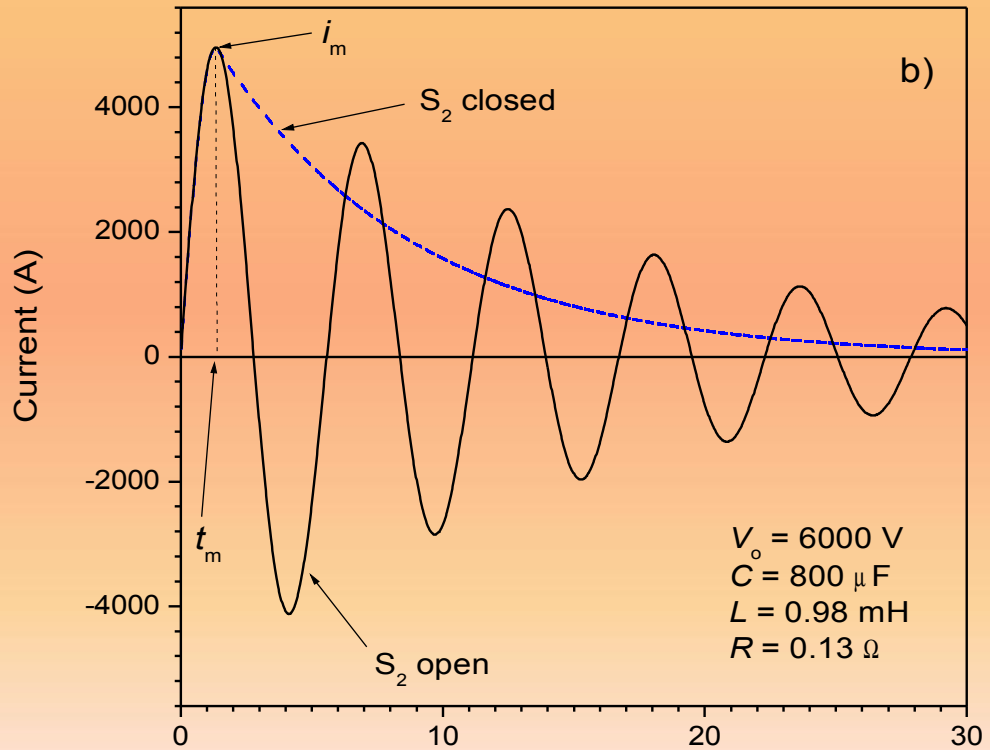


$$L \frac{\partial^2 i(t)}{\partial t^2} + R \frac{\partial i(t)}{\partial t} - \frac{1}{C} i(t) = 0$$

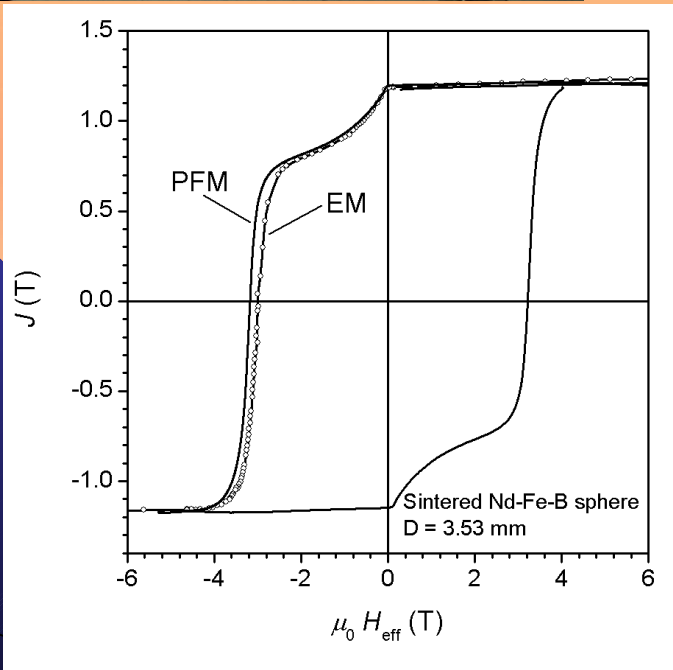
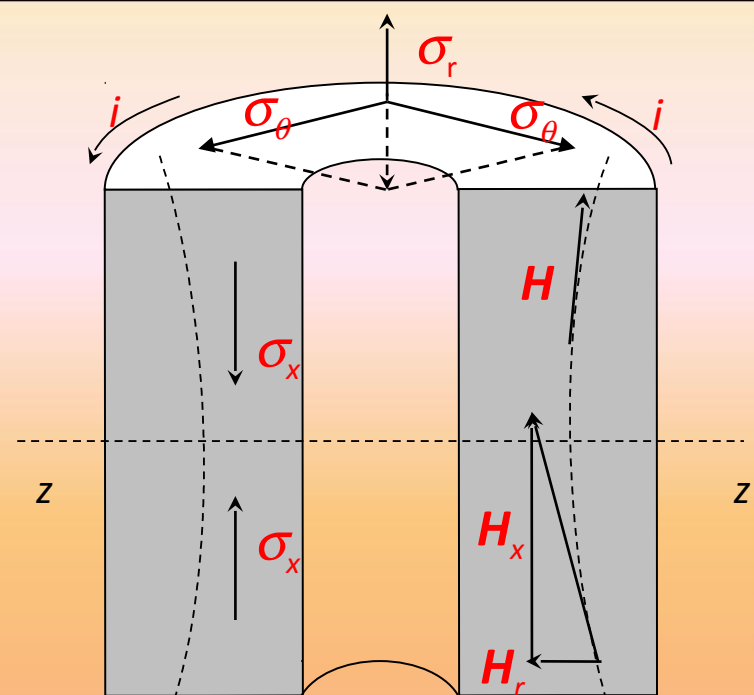
The oscillatory damped solution

$$i(t) = \frac{V_o}{L} \cdot \exp\left(-\frac{R}{2L} t\right) \cdot \frac{\sin \omega t}{\omega}$$

$$\tau = 2L / R$$



$V_o = 6000 \text{ V}$
 $C = 800 \mu\text{F}$
 $L = 0.98 \text{ mH}$
 $R = 0.13 \Omega$



E ~ 15 kW

L = 0.8 mH, C = 3.6 mF, V = 3 kV

High field strengths, up to about 2 T – 3 T, can be generated by means of magnetic cores.

We write for an ideal permanent magnet:

$$H_g l_g = - H_m l_m$$

$$B_m = B_g = \mu_0 H_g = \mu_0 H_m + J_m$$

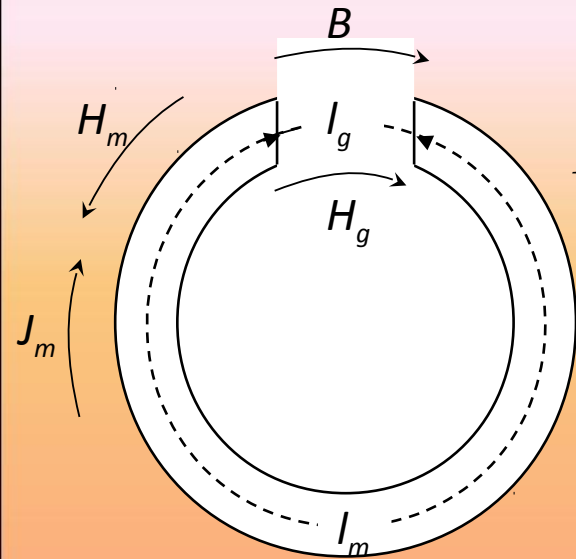
Combining these equations, we obtain the field in the gap

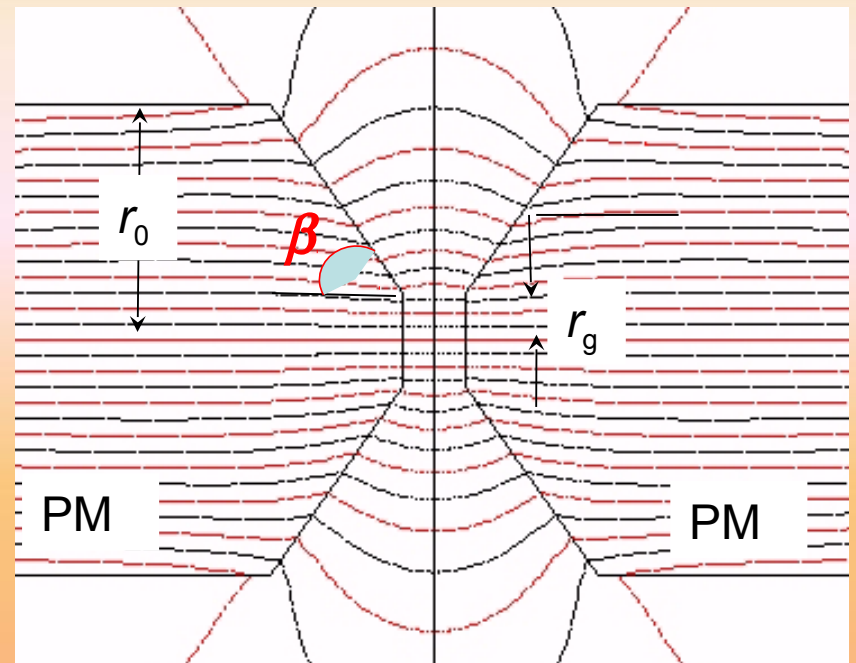
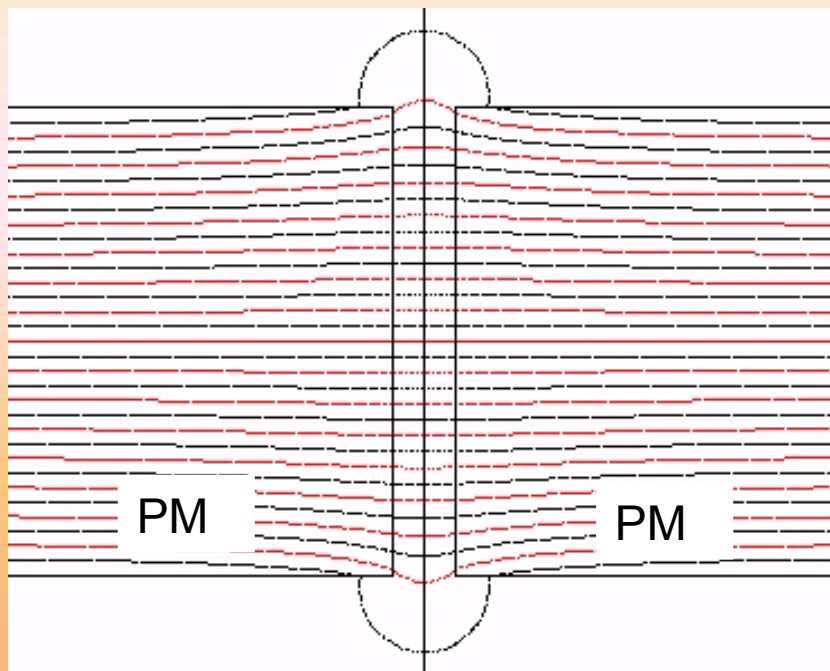
$$H_g = \frac{1}{\mu_0} \cdot \frac{l_m / l_g}{1 + l_m / l_g} J_m$$

The smaller the gap, the higher the field H_g . In the narrow slit limit ($l_g \ll l_m$) we get the upper limit for the available field strength

$$H_g \cong J_m / \mu_0 = M_m$$

For a Nd-Fe-B sintered magnet $\mu_0 H_{g,max} \sim J_s = 1.6 \text{ T}$





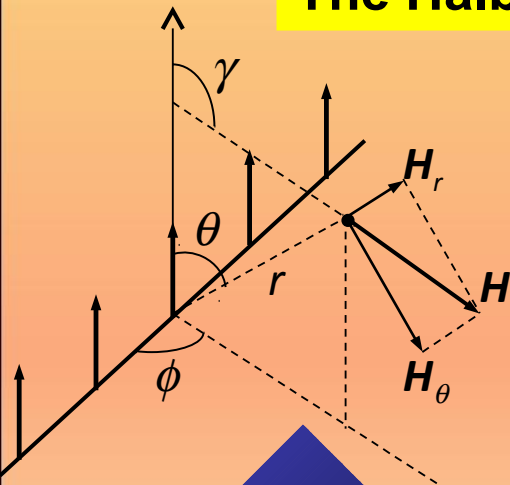
The fieldstrength in the gap can be increased by magnet tapering. For optimally skewed pole faces ($\beta = 54.74^\circ$) one gets

$$(H_g)_{\max} = \frac{2M}{3\sqrt{3}} \cdot \ln \frac{r_0}{r_g}$$

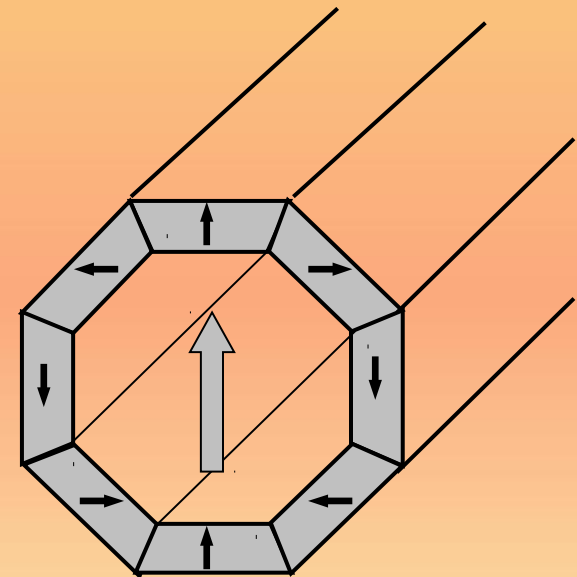
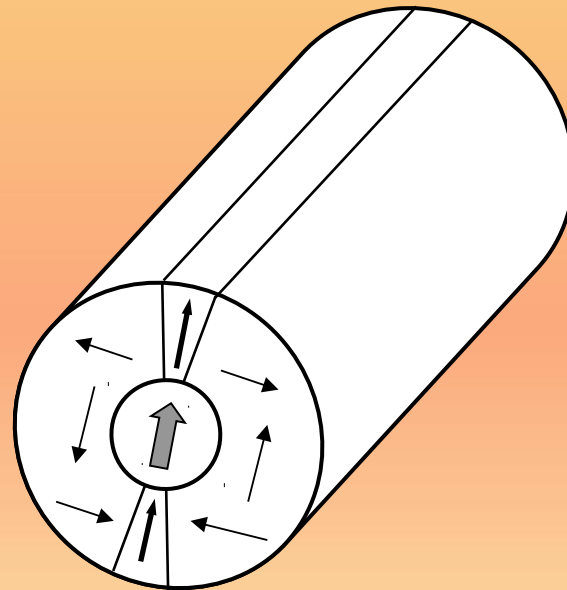
Requirement of reasonable gap volumes and field uniformity pose, however severe limits to the maximum attainable fieldstrength.

All-magnet field sources using rare-earth based building blocks can provide magnetic fields in excess of the material saturation M_s . The blocks act as permanent dipoles, which can be oriented to concurrently contribute to the field upon a suitable region. Rare-earth based magnets have so high coercivity that they are nearly transparent to the fields generated by themselves and other magnets.

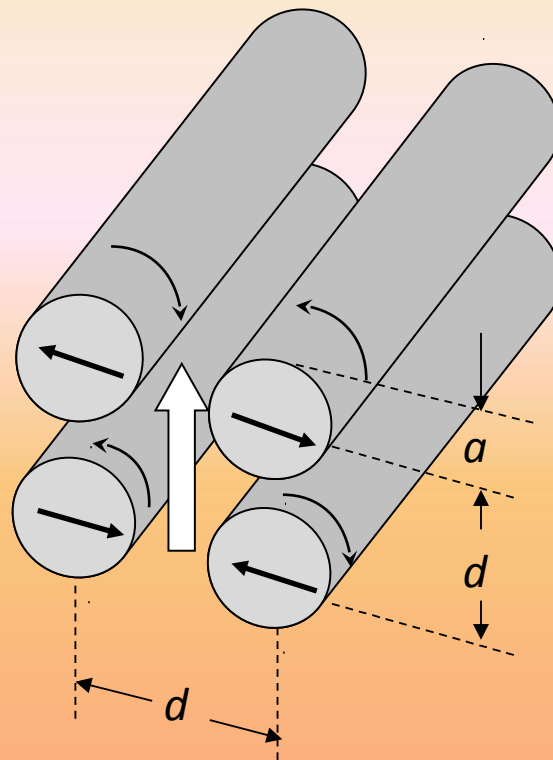
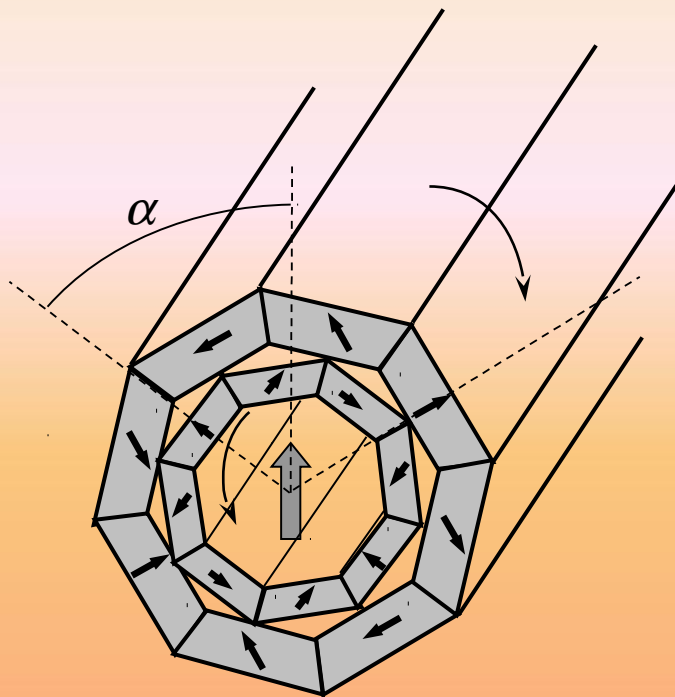
The Halbach cylinder



$$|H| = \frac{\lambda}{2\pi r^2}$$



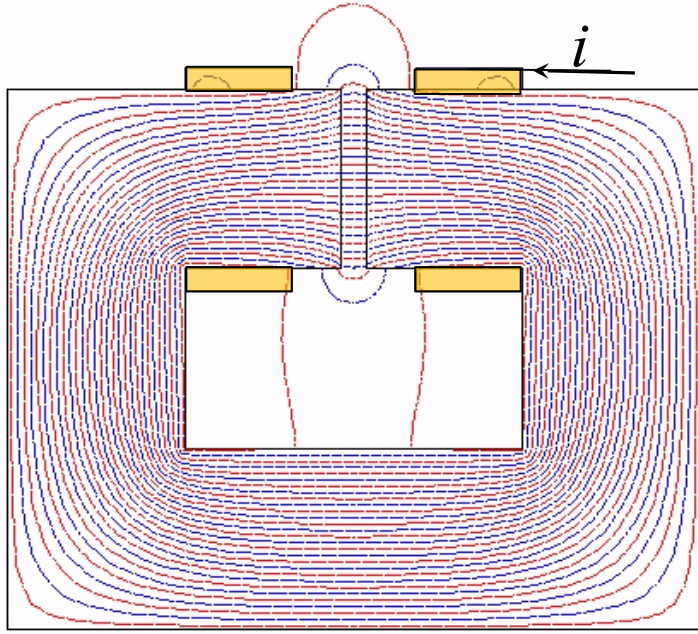
$$H = \frac{B_r}{\mu_o} \ln \frac{r_o}{r_g}$$



O. Cugat, P. Hansson, J.M.D. Coey, IEEE Trans. Magn. 30 (1994) 4602.

Two synchronously counter-rotating Halbach's cylinders having the same ratio between outside and inside diameters produce a field of amplitude continuously variable between $\pm 2H_0$ and fixed orientation. In a simplified realization of this device, four identical cylindrical rods, magnetized in the transverse direction, are made to counter-rotate.

A soft magnetic core, multiplying the flux supplied by the current flowing in the magnetizing winding, can be exploited for generating a field of variable amplitude. In such a case we have an electromagnet.



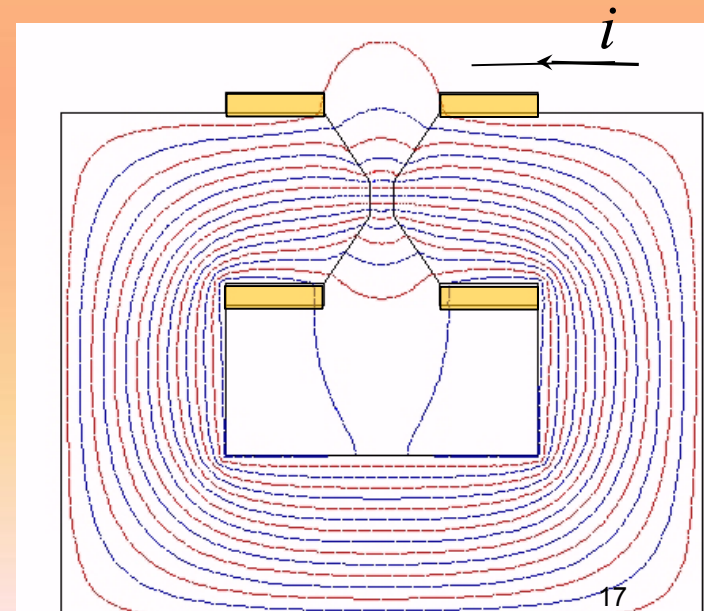
The previous equation for the field in the gap of the permanent magnet becomes

$$\mu_0 H_g = \frac{\mu_0 Ni / l_g + J_m \cdot l_m / l_g}{1 + l_m / l_g}$$

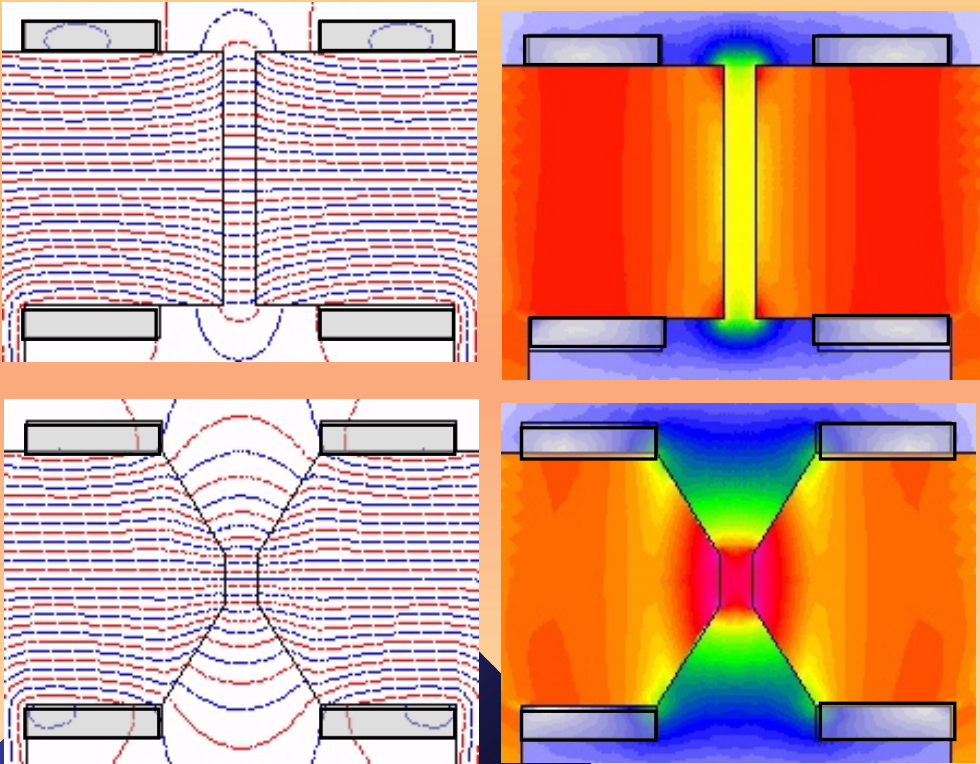
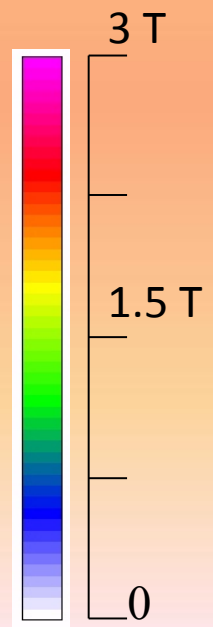
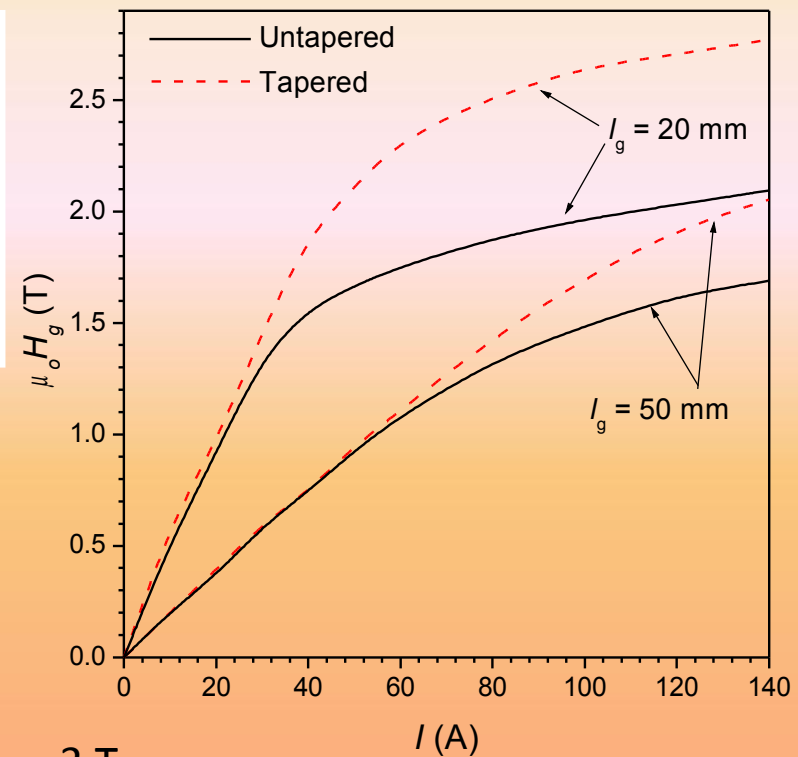
But now J_m is affected by the demagnetizing field at the gap and the magnetic core eventually saturates.

If the iron core is far from saturation and is endowed with high permeability (i.e. negligible reluctance, $\mu_r \gg l_m / l_g$), we obtain the maximum field in the gap

$$(\mu_0 H_g)_{\max} = \frac{\mu_0 Ni}{l_g}$$

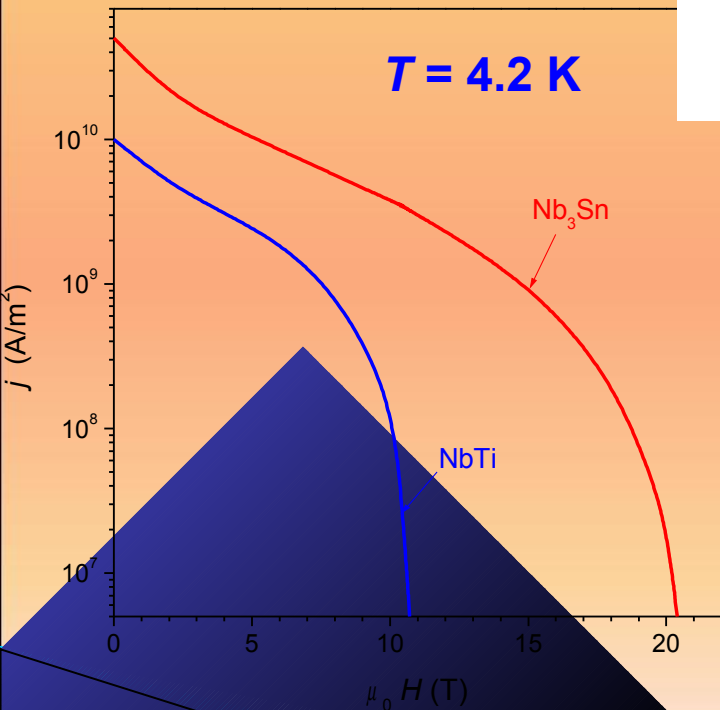
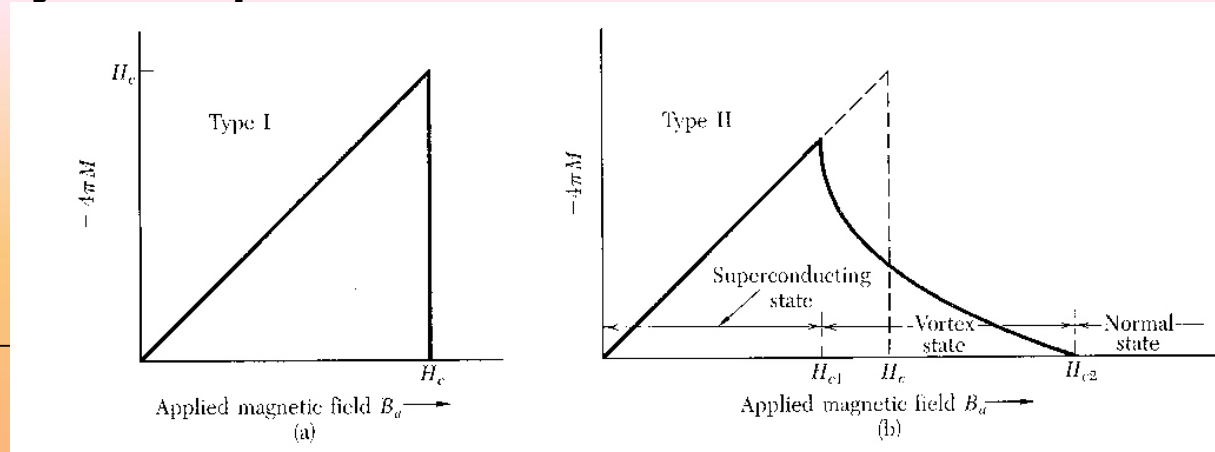


Core tapering provides practical advantage in electromagnets, especially if the pole faces are made of the high saturation polarization $\text{Fe}_{49}\text{Co}_{49}\text{V}_2$ alloy ($J_s = 2.35 \text{ T}$).



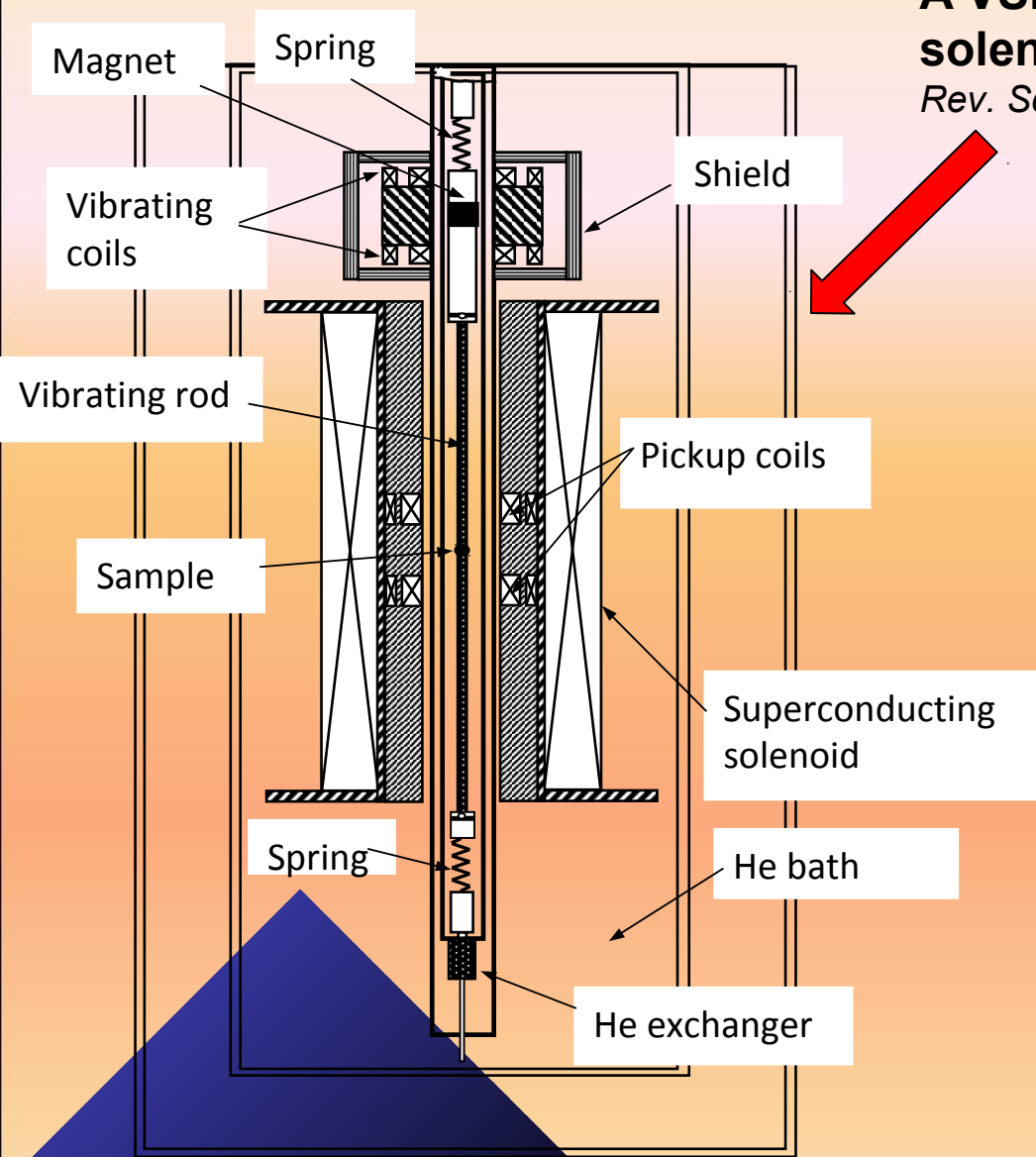
$N \cdot I = 125 \cdot 10^3 \text{ A}$

Superconducting solenoids are the standard solution for generation of steady magnetic fields above 2 T. It has become such after the discovery of a number of Type II superconducting alloys, egregiously withstanding the high fields generated by the supercurrents.

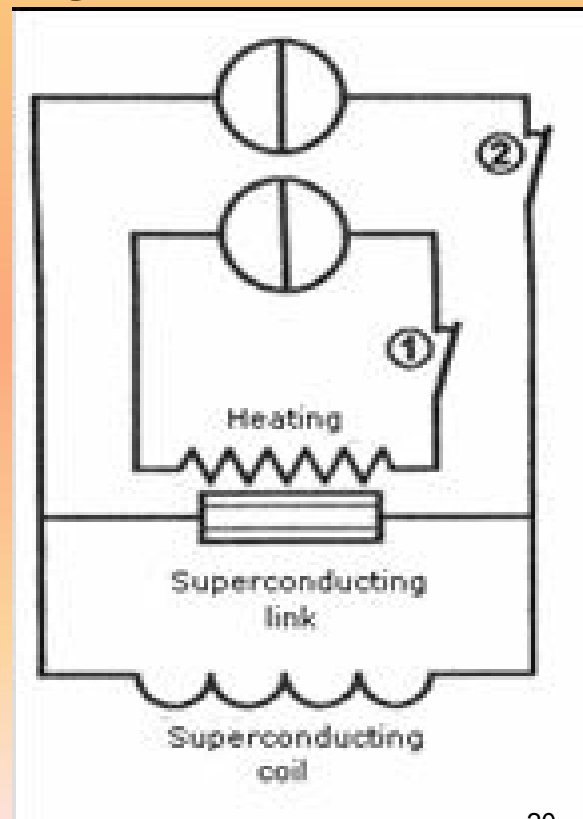


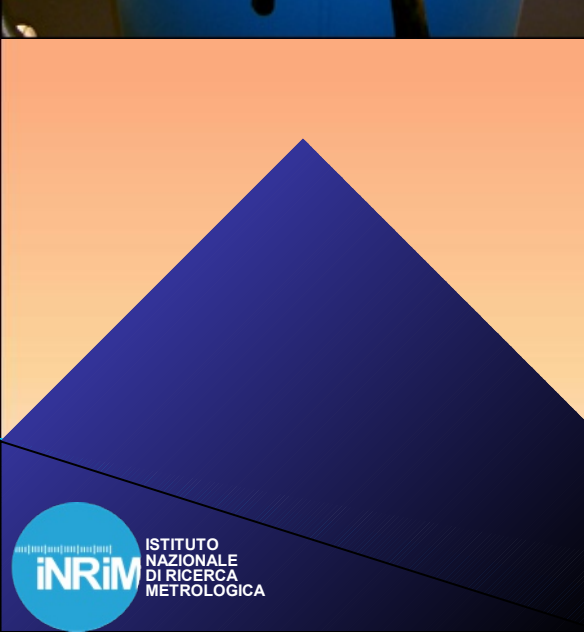
Critical curves for the two common technological Type II superconductors, NbTi and Nb_3Sn at $T = 4.2 \text{ K}$. Superconductivity prevails below the curves and normal resistivity above.

A VSM setup using a superconducting solenoid field source (D. Dufeu and P. Lethuillier, *Rev. Sci. Instr.* 70 (1999), 3035-3039).



A superconducting solenoid operating in a persistent mode



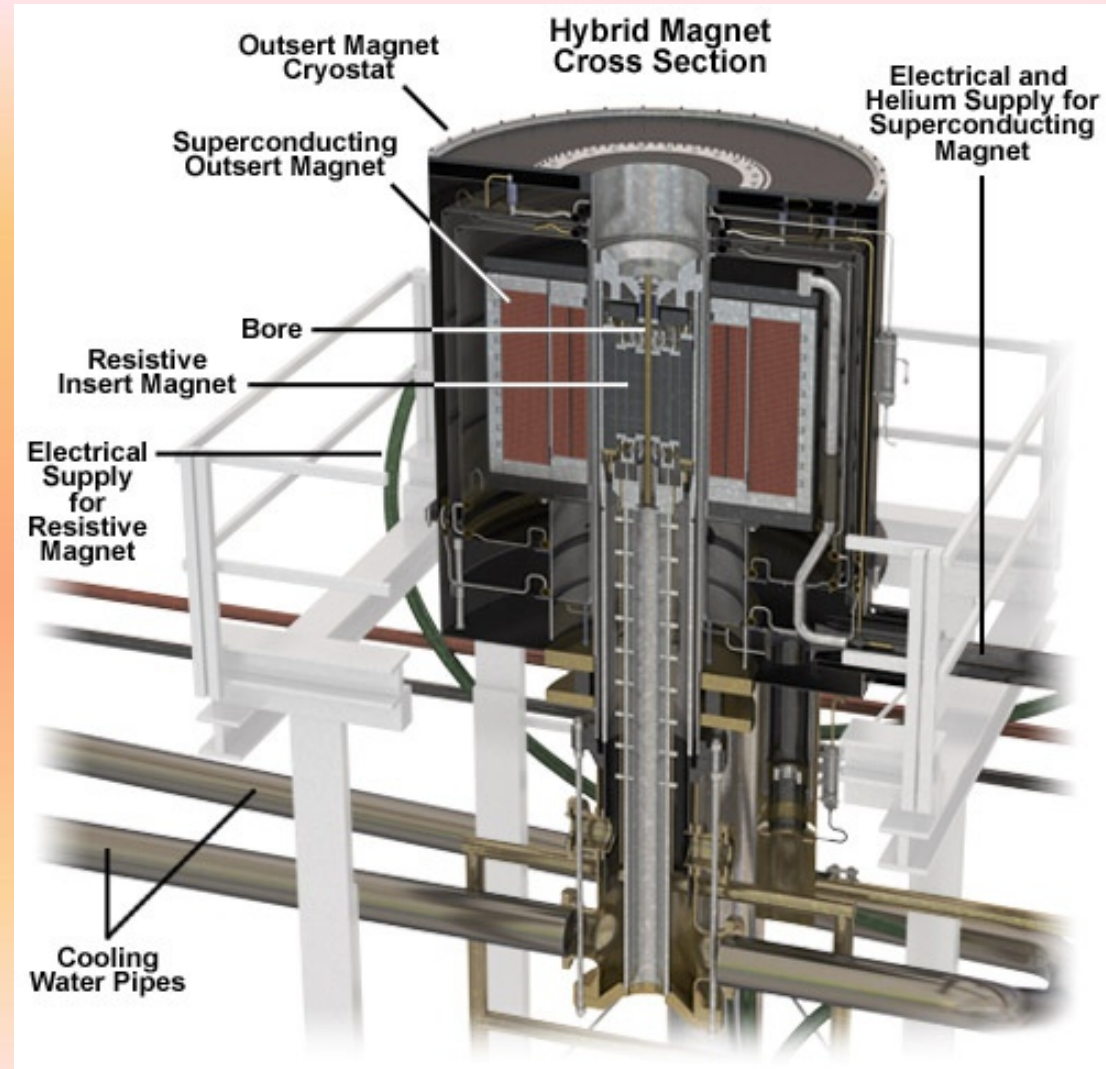


Destructive quenching of
a superconducting
solenoid

European School on
Magnetism ESM2013

The 45 T Hybrid Magnet in the NATIONAL HIGH MAGNETIC FIELD LABORATORY (USA)

This magnet combines a superconductive magnet of **11.5 T** with a Bitter magnet of **33.5 T**. It is connected to a closed system of pipes and machines that continually make and recycle 2 800 liters of liquid helium. About 250 liter/s cold water is needed to keep the resistive part from overheating, as it would otherwise do with the 33 MW of power it uses.



INVESTIGATING THE INTERNAL MAGNETIC STRUCTURE AND THE INTRINSIC PROPERTIES OF MAGNETIC MATERIALS

A stream of particles has wavelike attributes and can be used as a probe to investigate the material structure at the atomic level, if the wavelength compares to the interatomic distances.

The familiar X-Ray Diffraction technique is the standard tool for investigating the atomic arrangement in crystals, but it is ill suited for probing ordering of the magnetic moments. For the same reason, strong charge scattering, electron diffraction is impracticable for observing the arrangement of magnetic moments (although backscattered electrons in SEM microscopy can be exploited for magnetic domain observations).

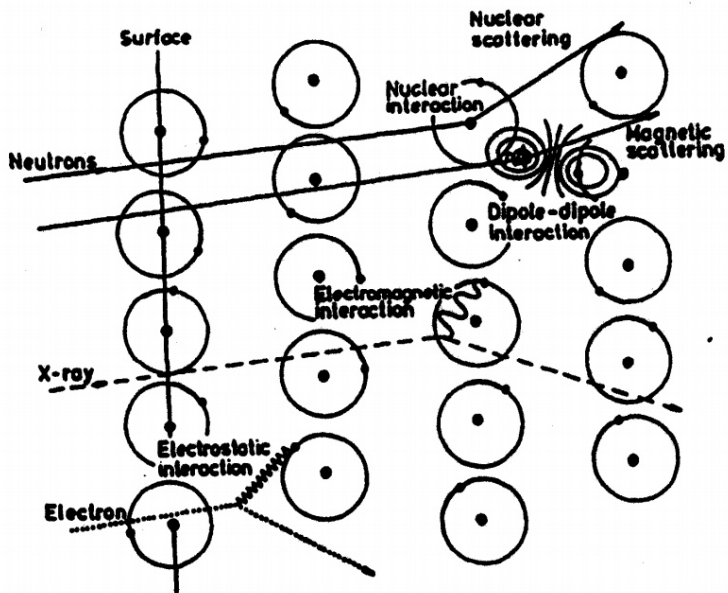
Neutrons, insensitive to the electrostatic interactions, are endowed with a magnetic moment, can penetrate even deeper than X-rays, and can be diffracted by atomic planes when their DeBroglie wavelengths are comparable to the interatomic distances

$s = 1/2$

n

$$\mu_n = -\gamma\mu_N = -1.913 \frac{e\hbar}{2m_p}$$

$$\mu_n / \mu_e \approx m_e / m_p = 1/2000$$

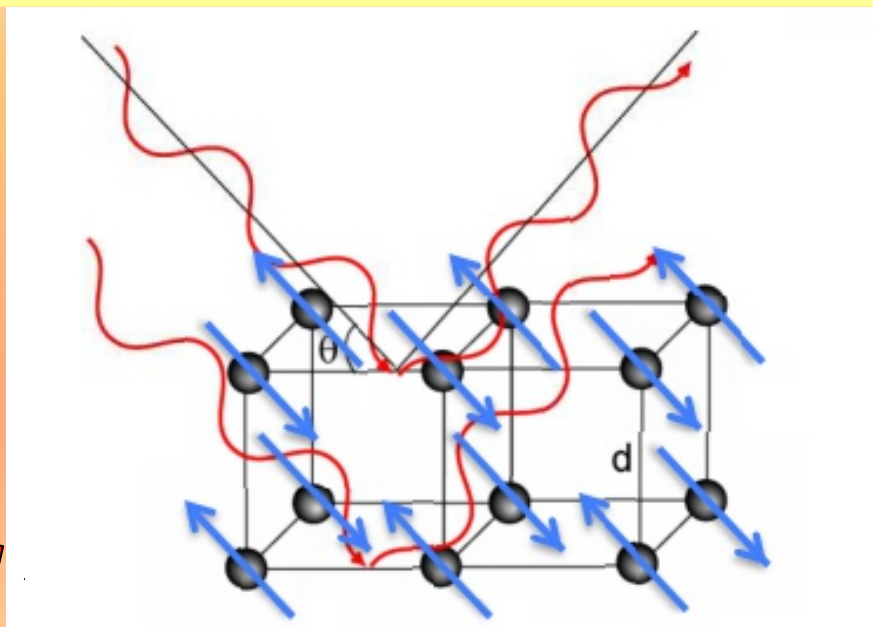


A thermal neutron

$$E = k_B T \sim 4 \cdot 10^{-21} \text{ J}$$

$$\text{Wavelength } \lambda = h/p = h/(2mE)^{1/2}$$

$$\lambda \sim 1.8 \cdot 10^{-10} \text{ m}$$

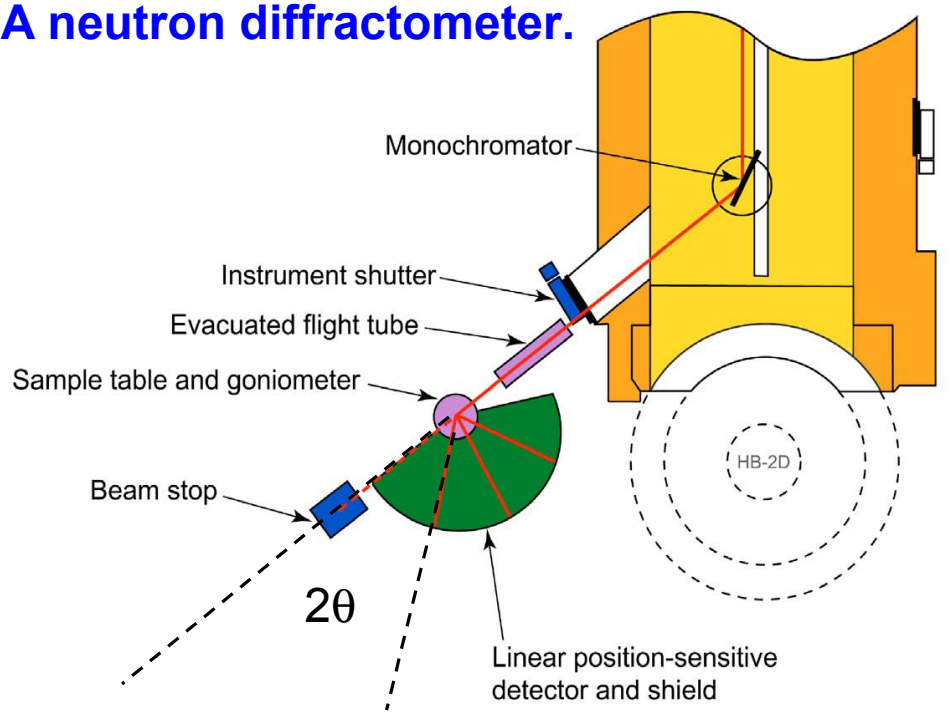


The neutron diffraction from crystals obeys the **Bragg's law** for constructive interference of the diffracted beams.

$$2d \sin \theta = n \lambda$$

C.G. Shull and J.S. Smart, Phys. Rev 110 (1949) 1256.

A neutron diffractometer.

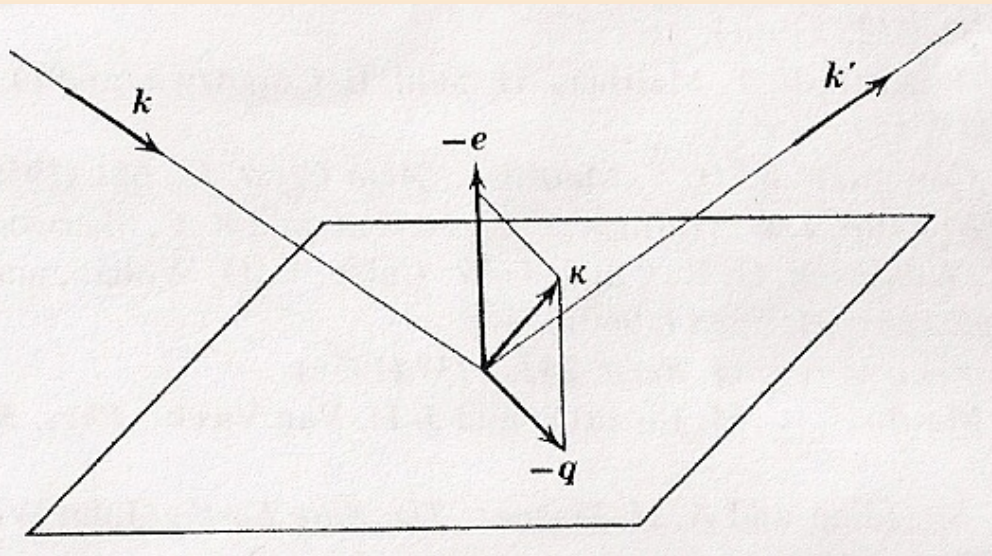


Neutrons are collimated and thermalized. A defined wavelength is selected by a single crystal monochromator. This can possibly be magnetized, so as to achieve a polarized neutron beam.

The test specimen can either be a single crystal or, more frequently, in powder form. The scattered neutron flux is around 10^8 neutrons /m²/s, much lower than the photon flux in XRD experiments.

Each diffraction line contains a nuclear isotropic part and a magnetic part, which depends on the orientation of the magnetic moments.

Combination of XRD and neutron diffraction experiments can provide complete information on atomic and magnetic moment arrangement.



The differential scattering cross-section for unpolarized neutrons is obtained as

$$\frac{\partial \sigma}{\partial \Omega} = C^2 + D^2 q^2$$

nuclear

magnetic

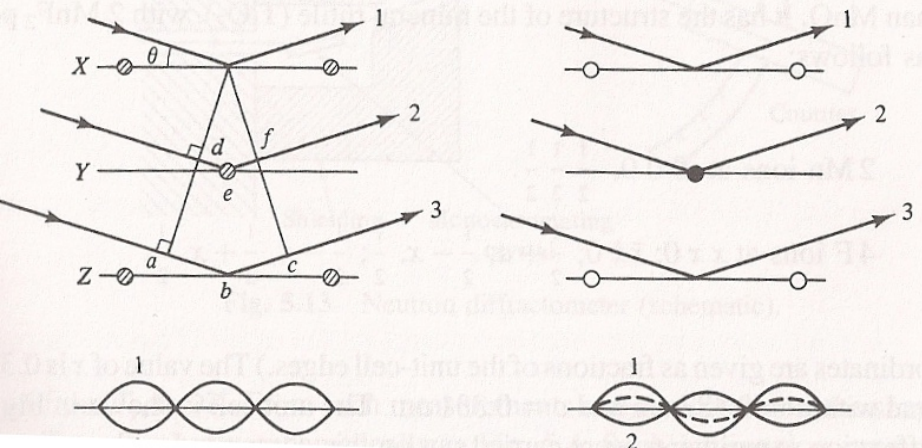
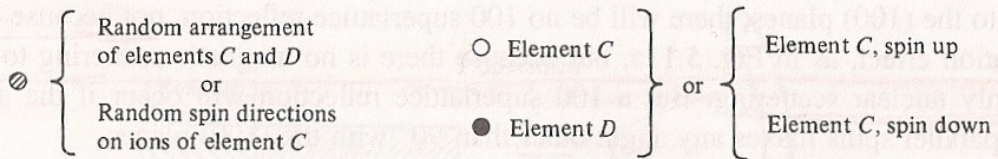
$\kappa \equiv$ unit vector directed with the magnetic moment

$e \equiv$ scattering vector, unit vector bisecting k and k'

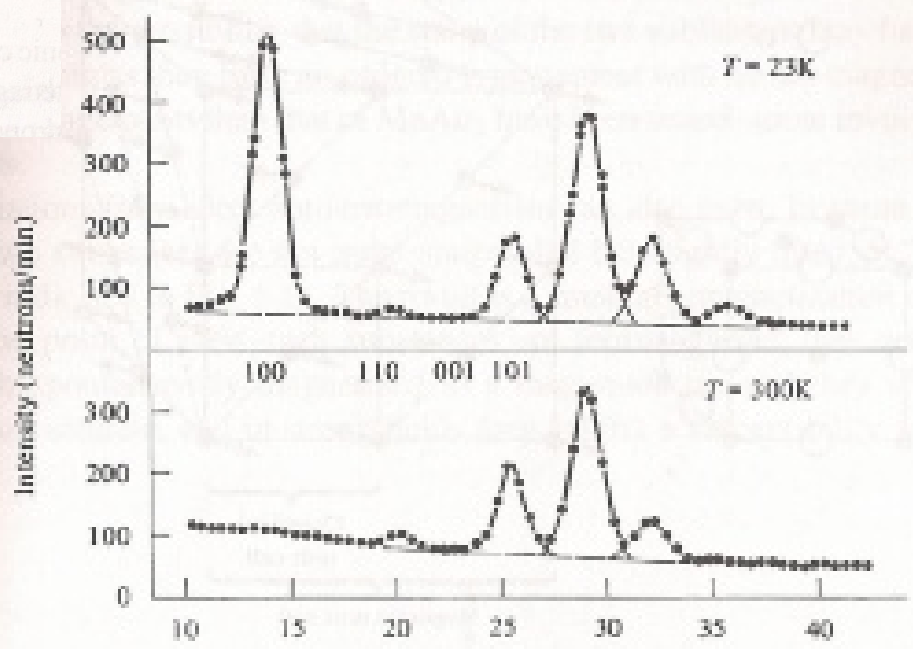
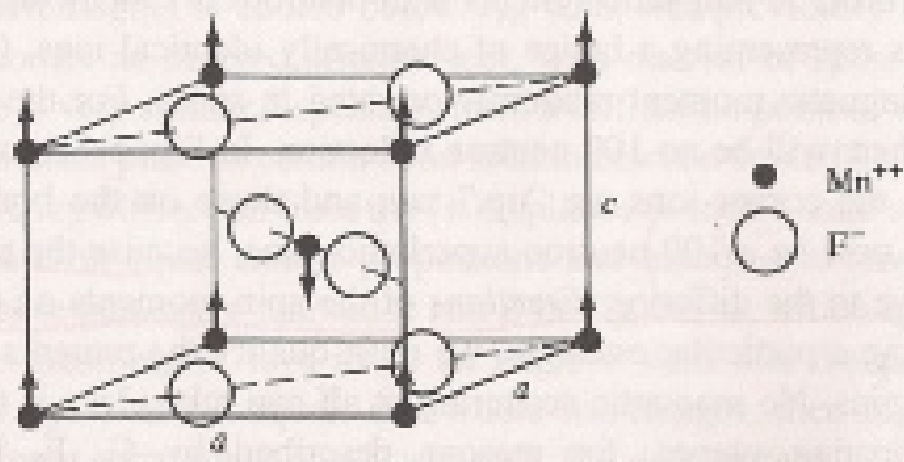
$$q = e(e \cdot \kappa) - \kappa$$

The magnetic part depends on the orientation of the magnetic moment. If $\kappa \equiv e$ the scattering cross-section is reduced to zero.

The magnetic scattering depends on applied field and temperature and can be separated from the nuclear scattering .

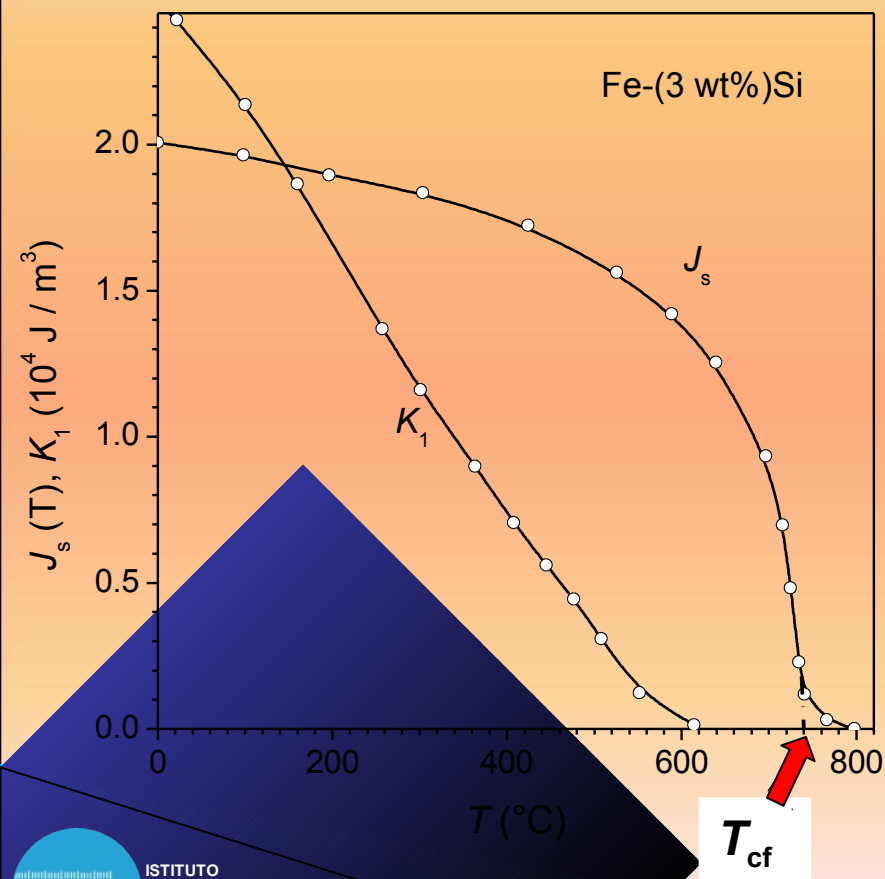


Antiferromagnetic ordering in MnF_2 is revealed by partially constructive interference of diffracted beams. The corresponding line in the powder diffraction pattern disappears above the Néel temperature T_N .

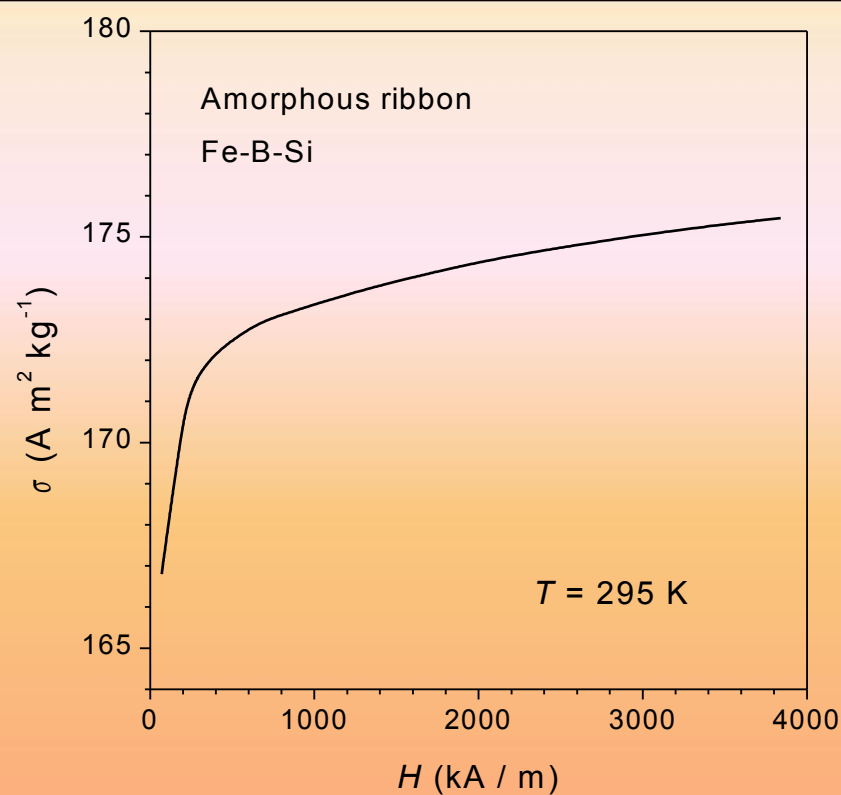
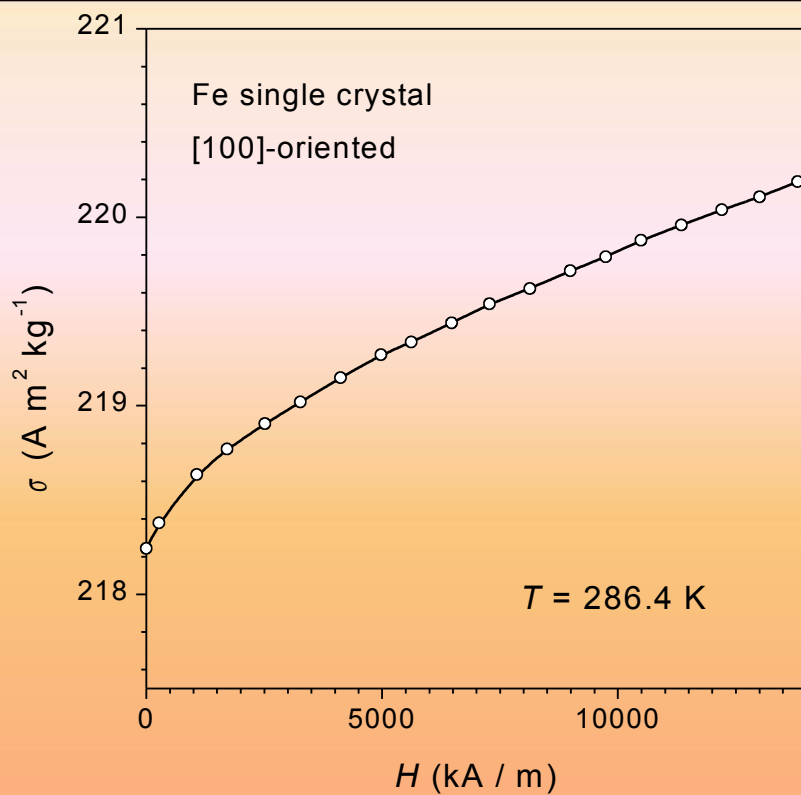


R.A. Erickson, Phys. Rev 90 (1953) 779.

The chemical composition and the crystallographic texture determine existence and arrangement of unpaired spins, whose outcome is measured in terms of intrinsic magnetic parameters. The fundamental intrinsic parameters of bulk magnets are the spontaneous magnetization M_s , the Curie (Néel) temperature T_c , and the magnetocrystalline anisotropy constants.



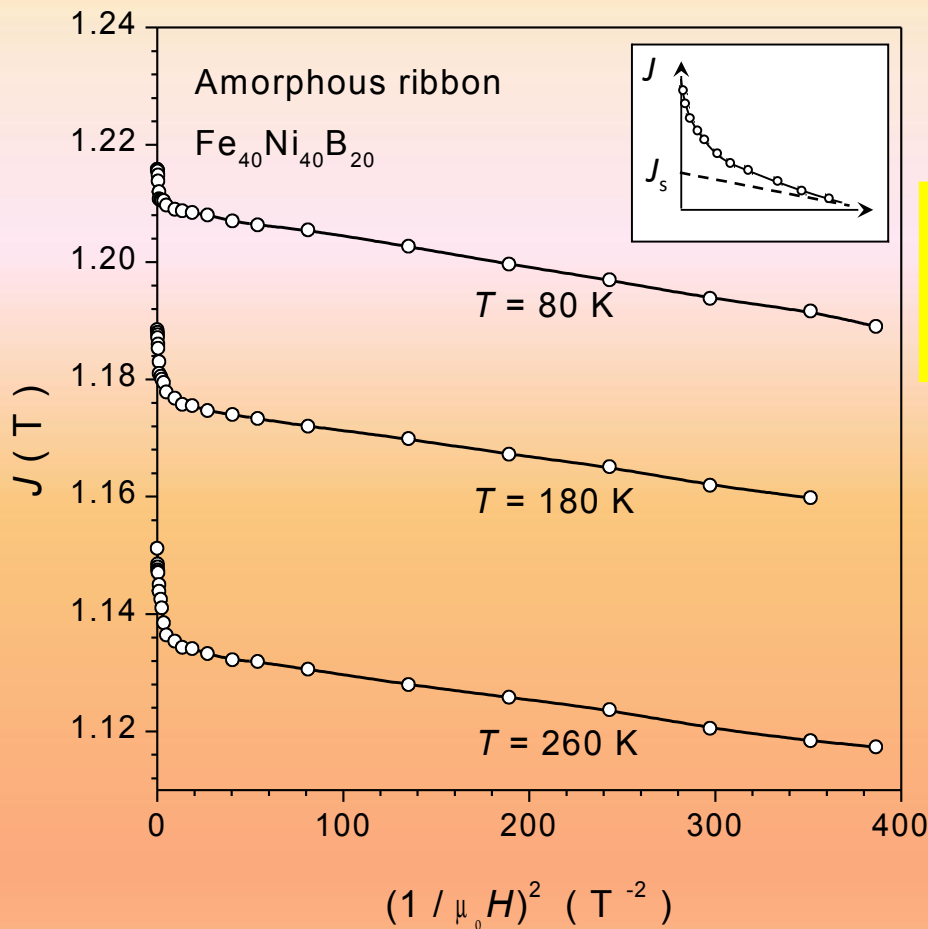
Saturation polarization J_s and anisotropy constant K_1 determined as a function of temperature in an Fe-(3 wt%)Si alloy.



The law of approach to saturation can be exploited in finding out the spontaneous magnetization at all temperatures

$$M(H) = M_s \left(1 - \frac{a}{H} - \frac{b}{H^2} \right) + k \cdot H$$

Forced magnetization term



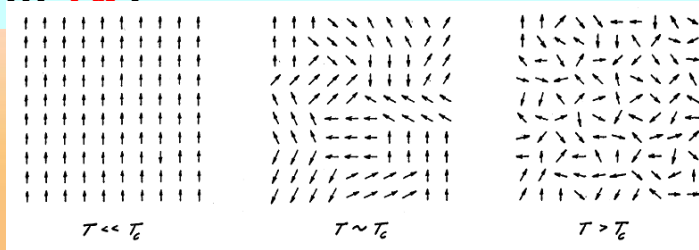
$1/H^2$ representation of magnetic polarization curves measured in an $\text{Fe}_{40}\text{Ni}_{40}\text{B}_{20}$ amorphous alloy.

H. Kronmüller, *IEEE Trans. Magn.* **15** (1979) 1218.

In the field interval $\sim 40 \text{ kA/m} \leq H \leq \sim 160 \text{ kA/m}$ the magnetization follows a $1/H^2$ law. The spontaneous magnetization is given by the intercept of the fitting straight lines with the ordinate axis. The steep increase of $J(H)$ towards $1/H^2 \rightarrow 0$ is associated with the forced paramagnetic effect.

The measurement of the spontaneous magnetization M_s becomes complicated on approaching the Curie temperature, because the forced magnetization can largely overcome M_s .

Neutron diffraction experiments suggest that long-range order gives way to short-range order at $T = T_{cf}$ and that the individual spins become independent of neighbors far from T_{cf} .



C. Shull, Phys. Rev. 103 (1956) 516.

The Weiss-Brillouin function for the spontaneous magnetization.

$$M_s = M_{so} \tanh\left(\frac{\mu_o m (H + \gamma M_s)}{kT}\right)$$

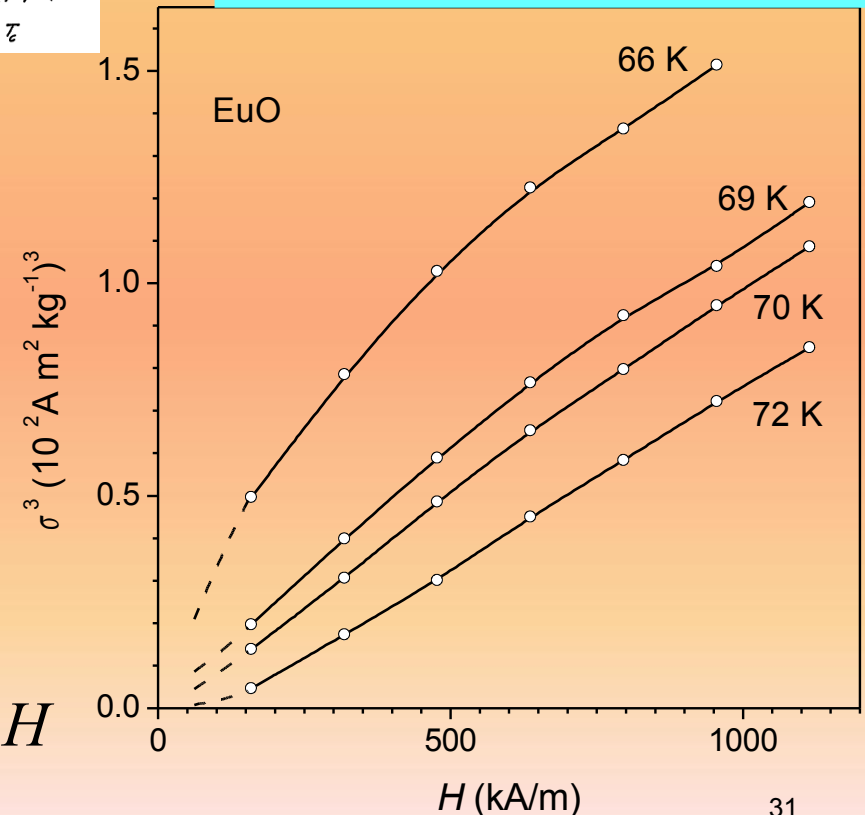
becomes for $M_s \ll M_{so}$ around T_{cf}

$$\frac{1}{3} \left(\frac{M_s}{M_{so}}\right)^3 + \left(\frac{T - T_{CF}}{T}\right) \cdot \frac{M_s}{M_{so}} = \frac{\mu_o m}{kT} H$$

and for $T = T_{cf}$

$$\frac{1}{3} \left(\frac{M_s}{M_{so}}\right)^3 = \frac{\mu_o m}{kT} H$$

Arrott's plots



The ferromagnetic phase transition is associated with a discontinuity of the physical quantities affected by magnetic order, like heat capacity, coefficient of thermal expansion, thermal coefficient of resistivity.

With zero applied field the magnetic contribution to the specific heat can be written

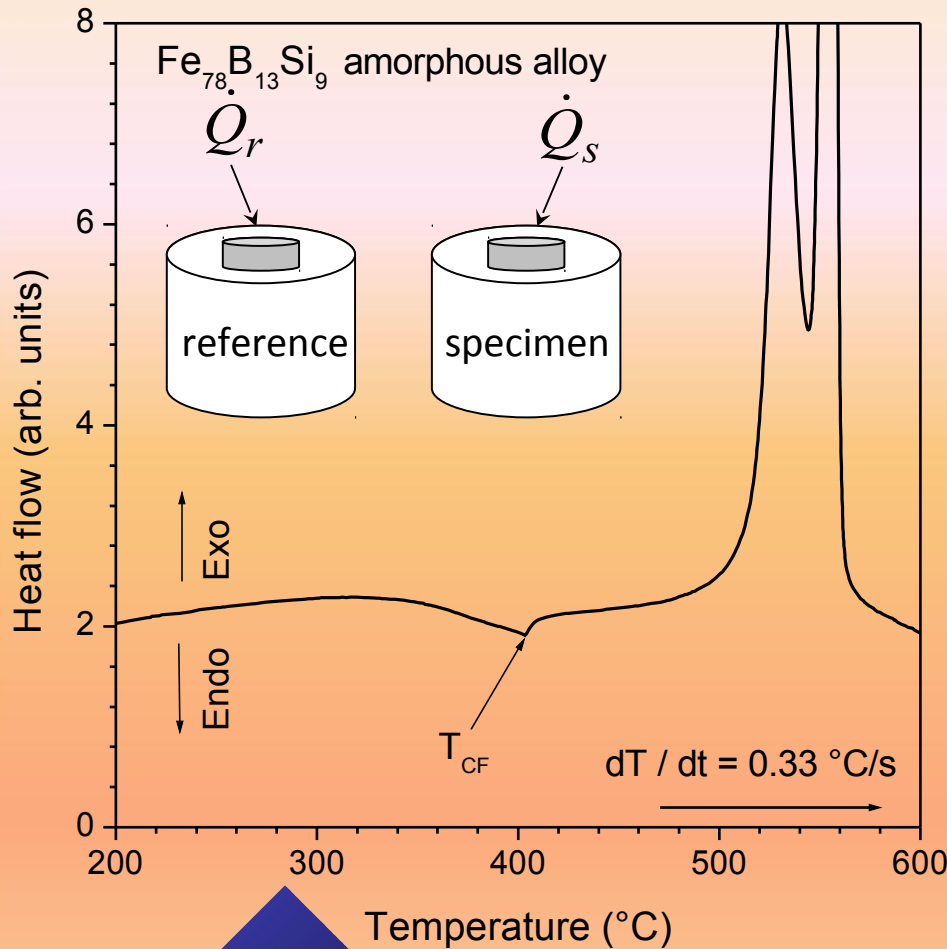
$$c_m = dU_m / dT \quad \text{where} \quad dU_m = -\mu_0 H_e dM_s$$

and $H_e = \gamma M_s$ is the Weiss mean field. c_m is thus expected to increase

with temperature as

$$c_m = -\frac{\mu_0 \gamma}{2} \cdot \frac{dM_s^2}{dT} \quad \text{and drop to zero at } T = T_{cf}.$$

Differential Thermal Analysis (**DTA**) and Differential Scanning Calorimetry (**DSC**) can be used to reveal the magnetic phase transition. They both analyze the response of the test sample to a defined heating schedule by comparison with a suitable reference sample, which has similar heat capacity and is immune from transformations in the temperature range of interest.



DSC trace obtained upon heating an amorphous alloy of composition **Fe₇₈B₁₃Si₉** at a constant rate of temperature change **$dT/dt = 0.33 \text{ } ^\circ\text{C/s}$** . It shows the increase of the heat capacity of the test sample and the drop occurring at the Curie temperature, together with the large exothermic peak associated with the crystallization process. **DSC** works on the principle of supplying the test sample and a reference sample with heat flows \dot{Q}_s and \dot{Q}_r in such a ratio that zero temperature difference is maintained between them.

MAGNETIC ANISOTROPY

Magnetic materials seldom behave isotropically. The classical Heisenberg exchange interaction $-J_{ij}\mathbf{S}_i \cdot \mathbf{S}_j$ is isotropic, but the spins individually interact with the crystalline field, which, being endowed with the symmetry properties of the host lattice, provides preferential orientations for the exchange-coupled spins.

The magnetocrystalline anisotropy energy

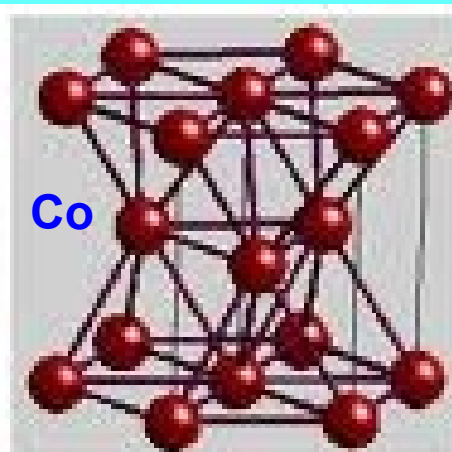
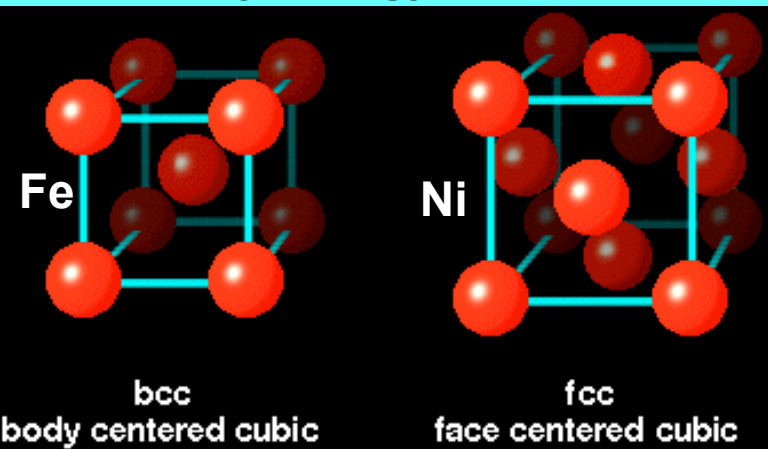
Cubic crystal (e.g. Fe, Ni) $E_a = K_1 \cdot (\alpha_1^2 \alpha_2^2 + \alpha_2^2 \alpha_3^2 + \alpha_3^2 \alpha_1^2) + K_2 \cdot \alpha_1^2 \alpha_2^2 \alpha_3^2$

Hexagonal crystal (e.g. Co) $E_a = K_1 \sin^2 \theta + K_2 \sin^4 \theta$

Soft crystalline magnets: cubic structure, low-to-medium anisotropy energy.

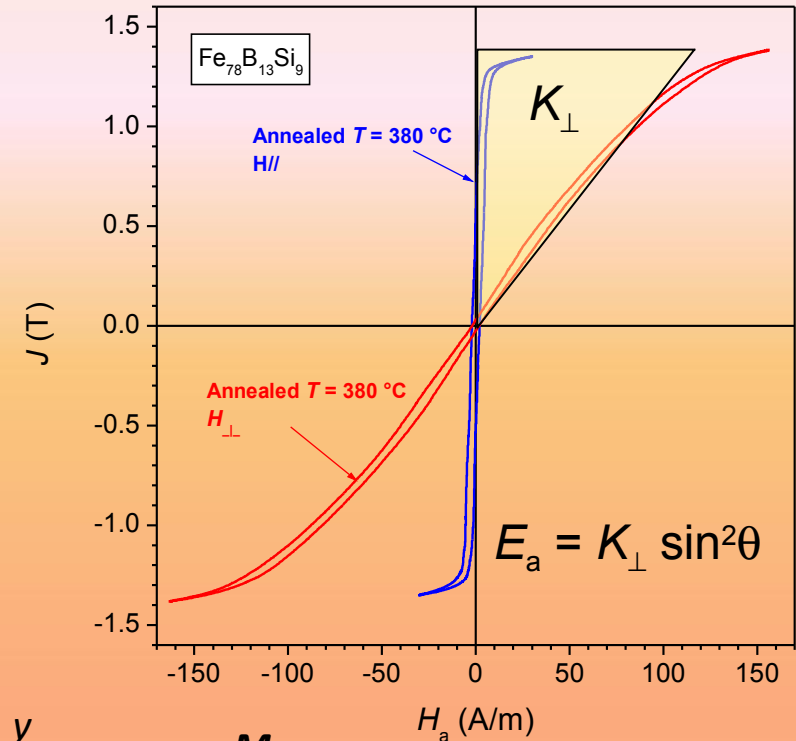
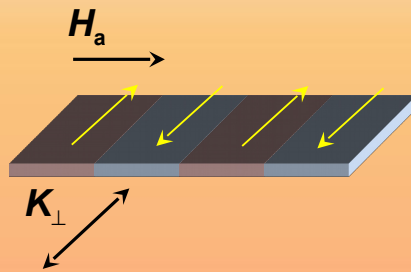
Permanent magnets: hexagonal structure, high anisotropy energy

Material	K_1 (J/m ³)
Fe <100> e.a.	$4.8 \cdot 10^4$
Ni <111> e.a.	$-0.57 \cdot 10^4$
Co [0001] e.a.	$50 \cdot 10^4$
BaFe ₁₂ O ₁₉	$25 \cdot 10^4$
Nd ₂ Fe ₁₄ B	$500 \cdot 10^4$
Sm ₂ Co ₁₇	$330 \cdot 10^4$
SmCo ₅	$1700 \cdot 10^4$



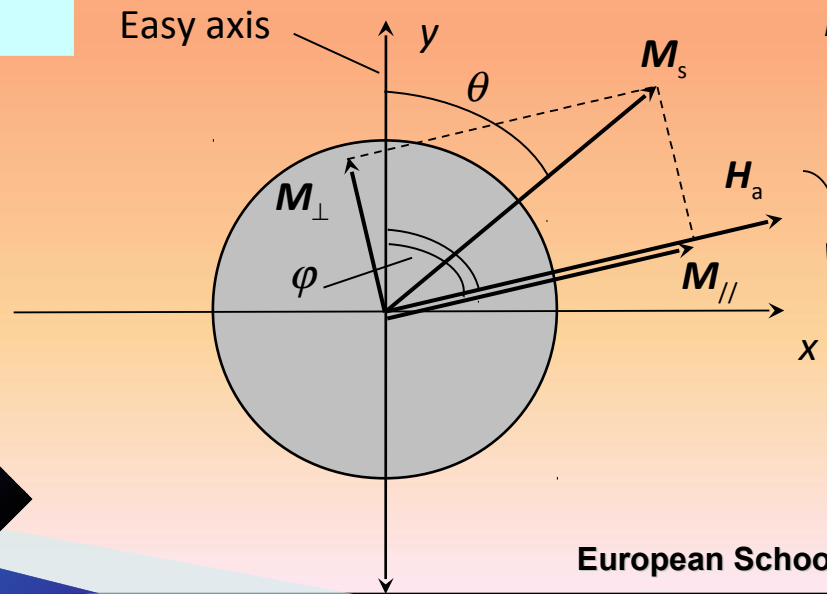
A number of methods can be applied to measure the anisotropy constants.

1) Measurement of the magnetization curve up to saturation in a single crystal along an easy axis and along different directions. The area between the curves is approximately equal to anisotropy energy.

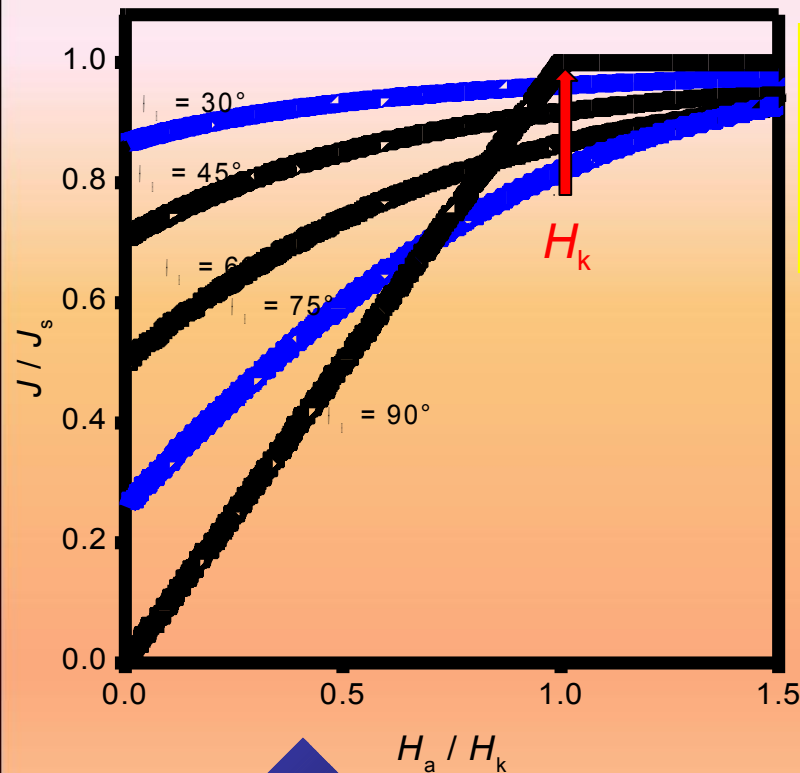


2) Measurement of the torque curves in single crystals.

$$\tau_K = K_u \sin 2\theta$$



3) Determination of the anisotropy field in hard magnets by the Singular Point Detection (SPD) technique.



A uniaxial particle magnetized transverse to the easy axis exhibits a linear magnetization curve, attaining the saturated state at a finite field value.

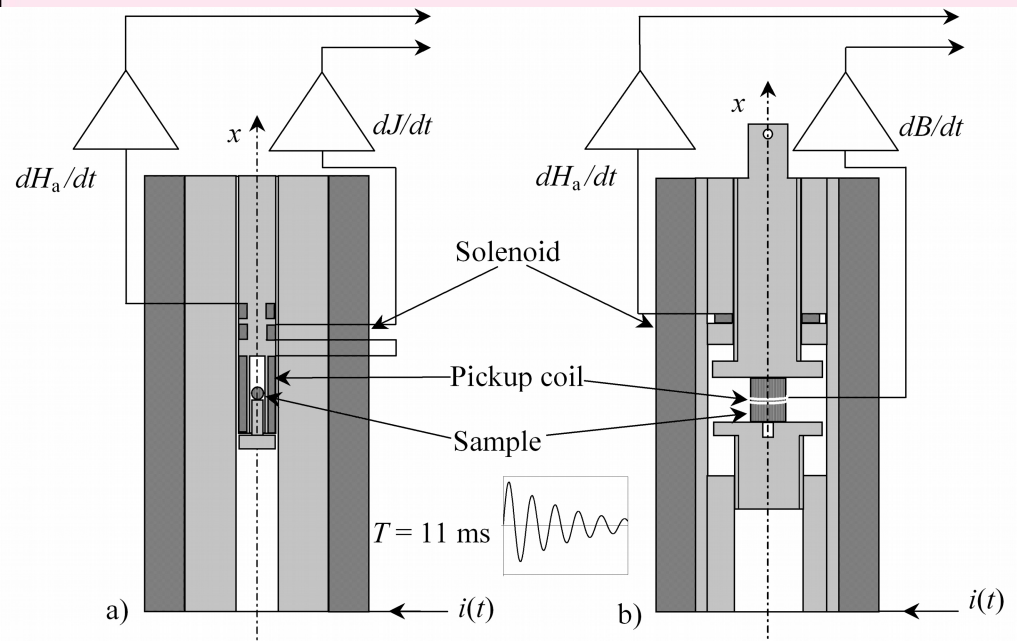
This is the anisotropy field H_k . The linear magnetization curve is obtained minimizing the sum of anisotropy and Zeeman energies

$$E = -\mu_0 \mathbf{M}_s \cdot \mathbf{H} + K_1 \sin^2 \theta + K_2 \sin^4 \theta$$

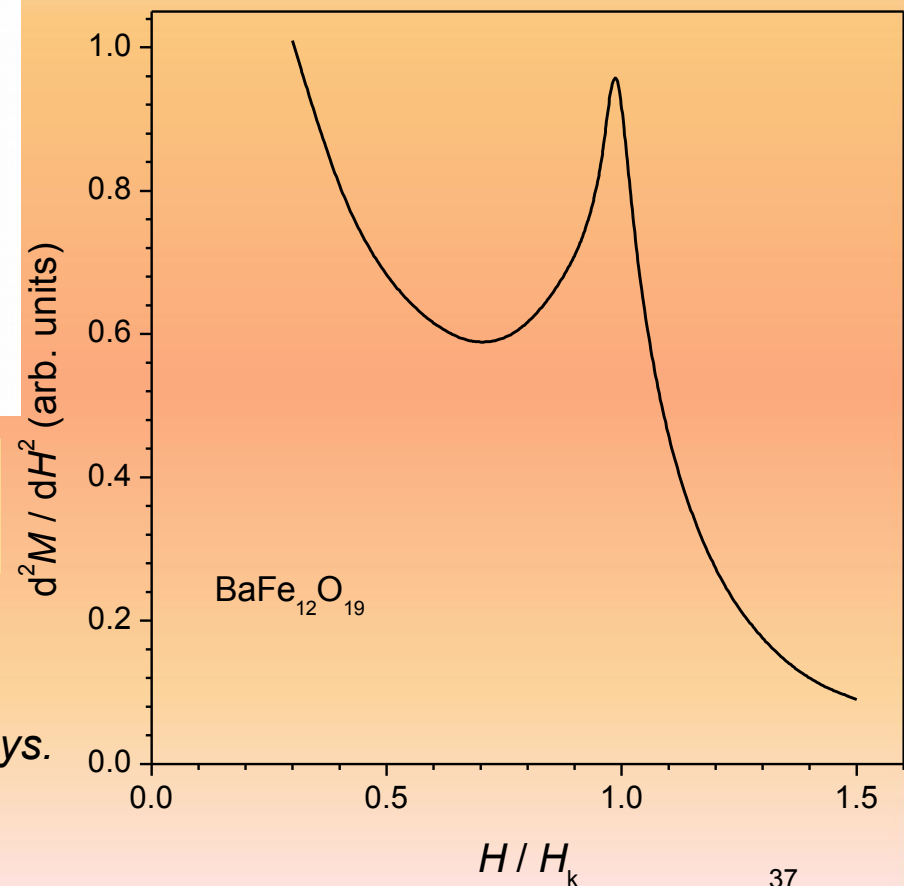
and we get
$$H_K = \frac{2(K_1 + 2K_2)}{\mu_0 M_s}$$

A permanent magnet is usually obtained as an assembly of uniaxial particles (either bonded or sintered). A certain proportion of these particles are expected to have easy axis along or close to a direction perpendicular to the applied field.

The derivative dM/dH of the magnetization curve of the transverse particles will show a discontinuity for $H = H_k$, which transforms into a cusp upon making the second derivative d^2M / dH^2 .



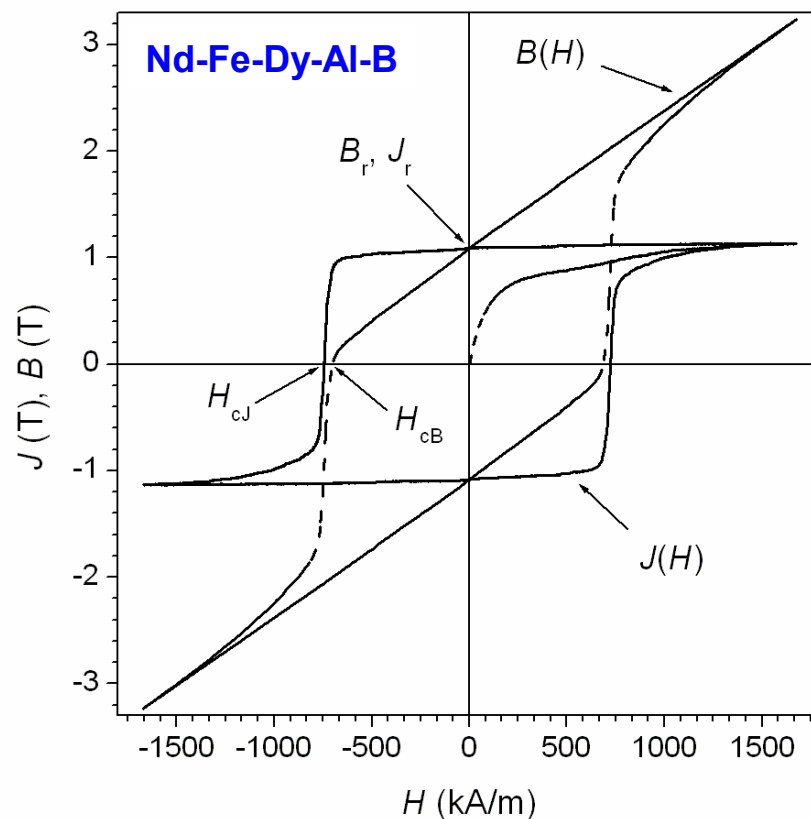
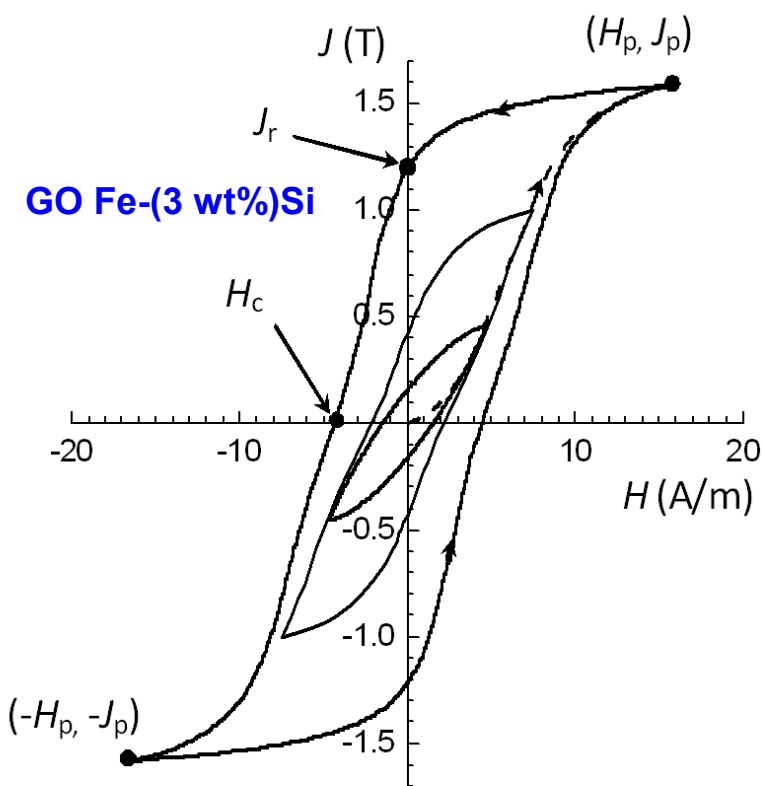
The initial magnetization curve is obtained by means of a pulsed field magnetizer



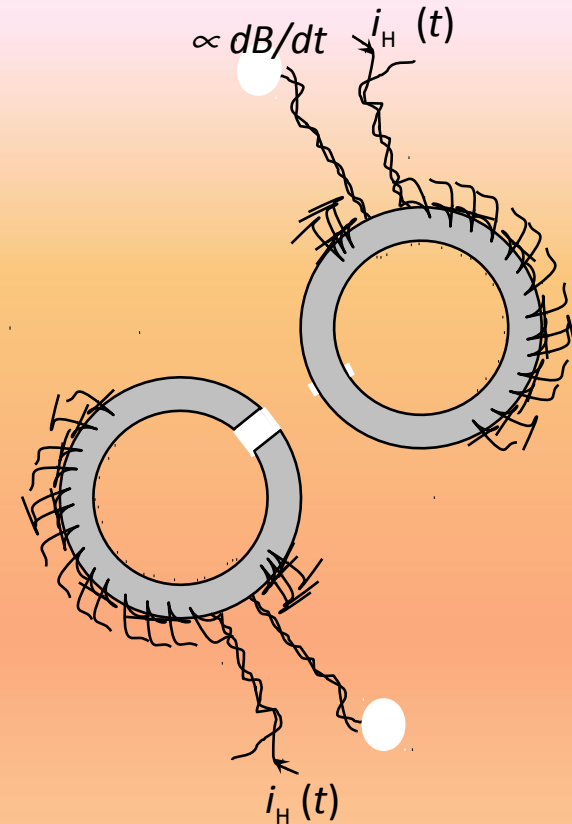
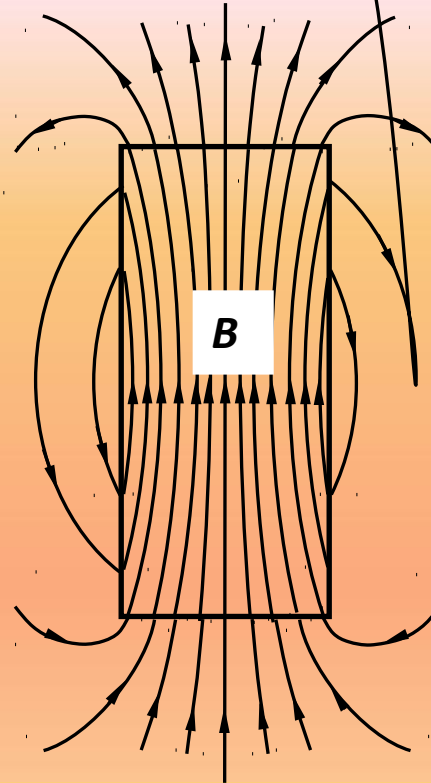
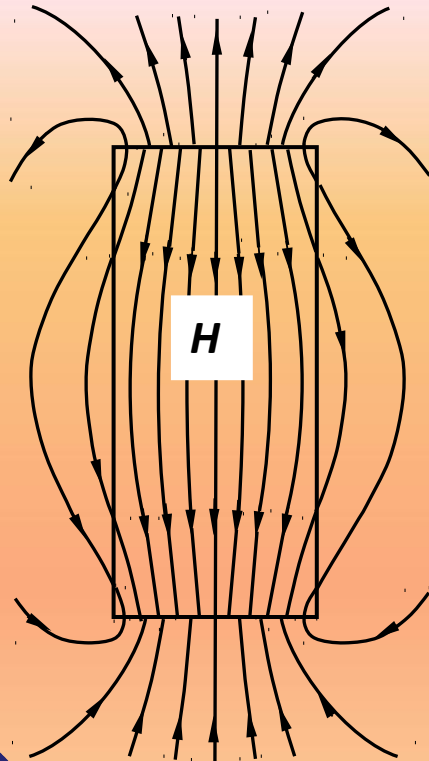
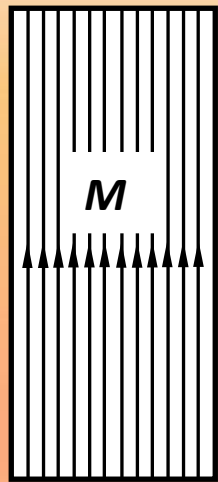
G. Asti and S. Rinaldi, *J. Appl. Phys.* 45 (1974), 3600.

MEASUREMENTS OF MAGNETIZATION CURVE, HYSTERESIS, AND THE RELATED PARAMETERS IN SOFT AND HARD MAGNETS

The applications of magnetic materials are based on their technical characterization, that is, the determination of the $J(H)$ relationship, as embodied by the magnetization curves, the hysteresis loops, and their parameters.



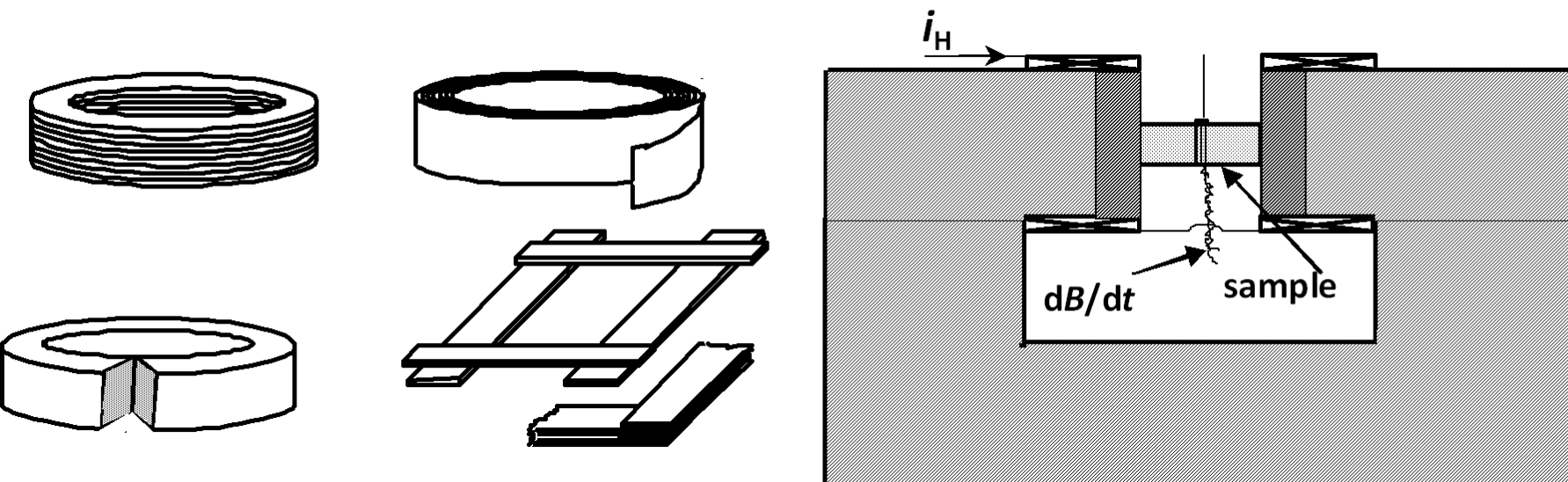
To measure the intrinsic $J(H)$ behavior in soft and hard materials is an ideal and somewhat elusive goal, because the long-range nature of the demagnetizing fields makes the measured properties of any test specimen crucially related to its geometrical features.



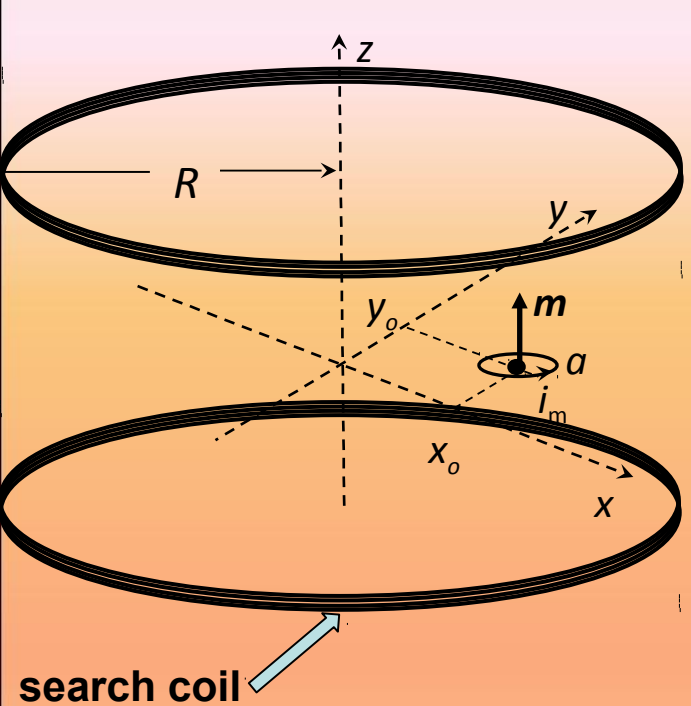
The problem chiefly lies in the role of the demagnetizing field $H_d = -N_d M$. This should be avoided when characterizing soft magnets, while it is tolerated with hard magnet testing, provided it is accurately known and is possibly uniform.

In a **fluxmetric** measurement the magnetic behavior of the material is obtained by detecting the flux variation ensuing from the application of a time-varying magnetic field.

The fluxmetric characterization most frequently calls for vanishing demagnetizing field. This condition is realized either by shaping the test specimen or by resorting to a flux-closing yoke. The latter can be supplied by a magnetizing current, so as to provide both the exciting field and the flux closure.



Measurements on open samples are generally of **magnetometric** type, where the magnetic moment of a small specimen and its dependence on the applied field strength are determined exploiting the **reciprocity principle**.



When the specimen fulfills the dipole approximation, its magnetic moment can be determined by measuring the flux linked with a surrounding coil, which is related to it by a definite relationship of proportionality.

Magnetic moment $\longrightarrow m = a \cdot i_m$

Flux linked with the search coil via the mutual inductance $M \longrightarrow \Phi_{sm} = M \cdot i_m$

M proportionally relates both the flux generated by the test dipole linking with the search coil and the flux generated by a hypothetical current i_s flowing into the search coil and linking with the equivalent test coil of area a .

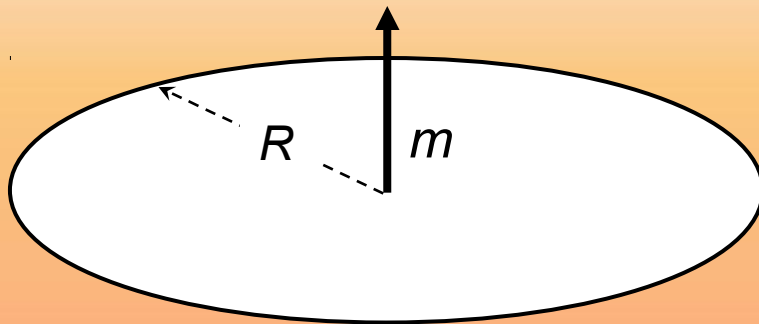
search coil $M = \Phi_{sm} / i_m = \Phi_{ms} / i_s$

$M = \frac{B_z(x_0, y_0)}{i_s} \cdot a = k(x_0, y_0) \cdot a \longrightarrow \Phi_{sm} = k(x_0, y_0) \cdot m$

If the magnetic dipole is in the generic point of coordinates (x, y, z) and has components (m_x, m_y, m_z) , the general relationship holds

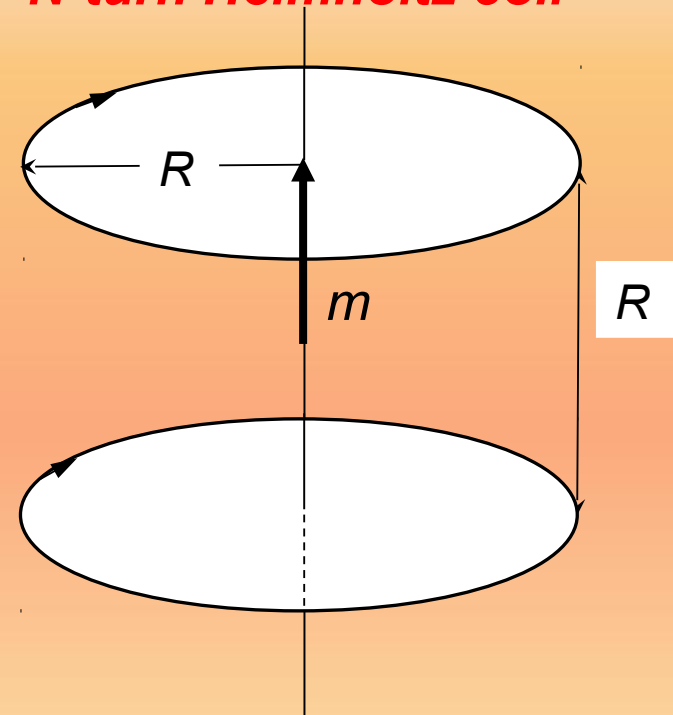
$$\Phi_{sm} = \mathbf{k}(x, y, z) \cdot \mathbf{m} = k_x(x, y, z) \cdot m_x + k_y(x, y, z) \cdot m_y + k_z(x, y, z) \cdot m_z$$

with $k_i(x, y, z) = B_i(x, y, z) / i_s$



$$\Phi_{sm} = \frac{\mu_o}{2R} m_z$$

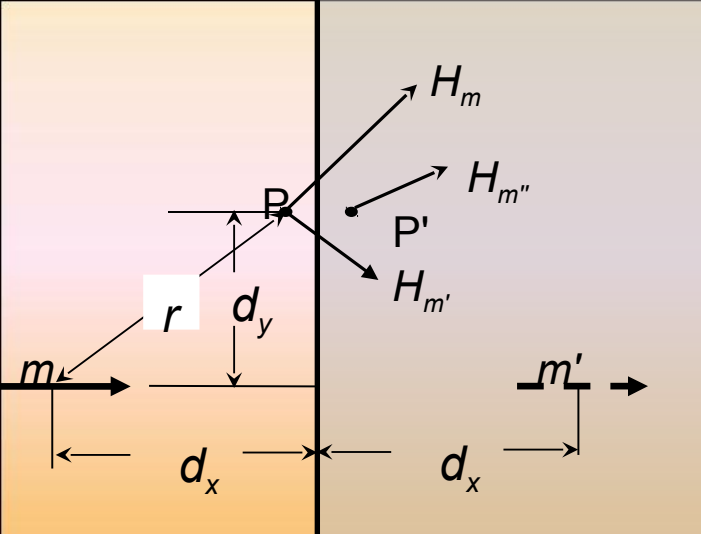
N-turn Helmholtz coil



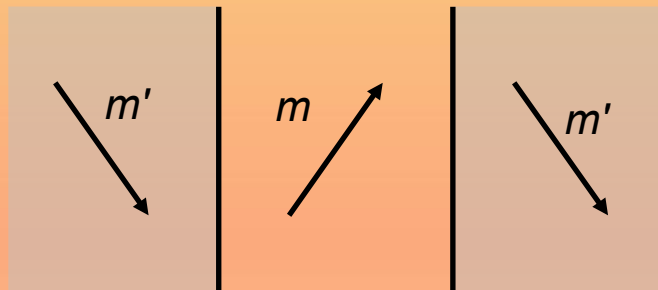
$$\Phi_{sm} = 0.1755 \cdot \frac{\mu_o N}{R} m_z$$

Image effect

The field distribution around a magnetic dipole is perturbed in proximity of a magnetic medium. For a dipole of strength m this amounts to the presence of a fictitious dipole of strength $m' = m[(\mu_r - 1) / (\mu_r + 1)]$ mirroring the real one. It can be demonstrated that with such an image dipole the continuity conditions for the tangential field and the normal induction component through the air-medium boundary are satisfied.

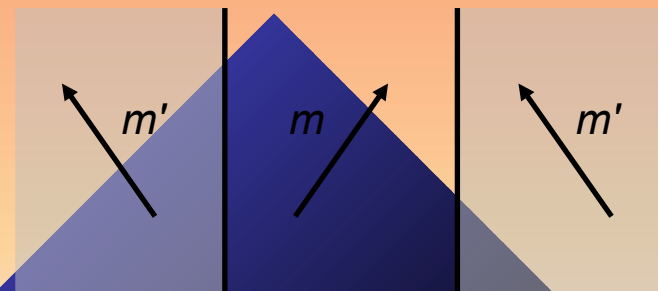


Ferromagnetic body ($\mu_r > 1$)



Open sample in the air-gap of an electromagnet

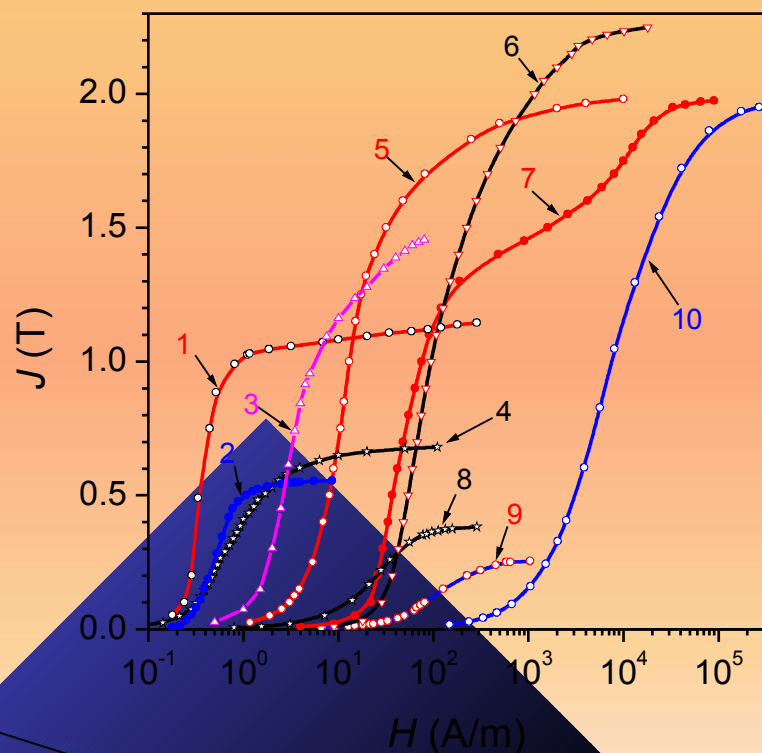
Diamagnetic body ($\mu_r < 1$)



Open sample in a superconducting solenoid

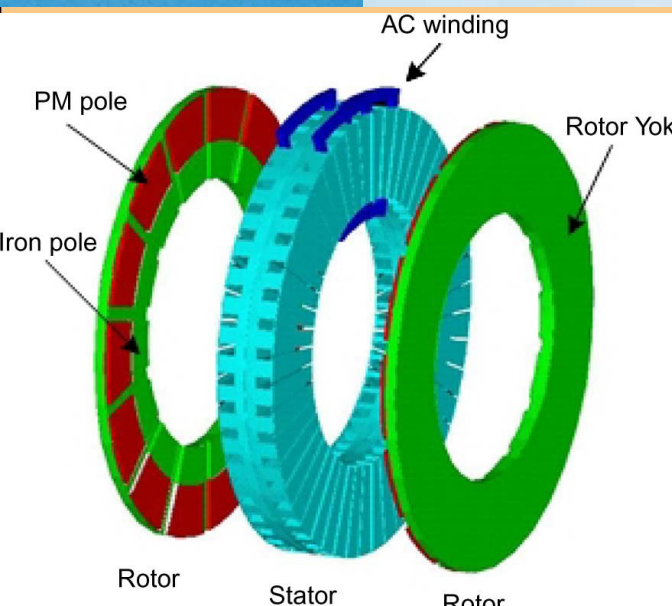
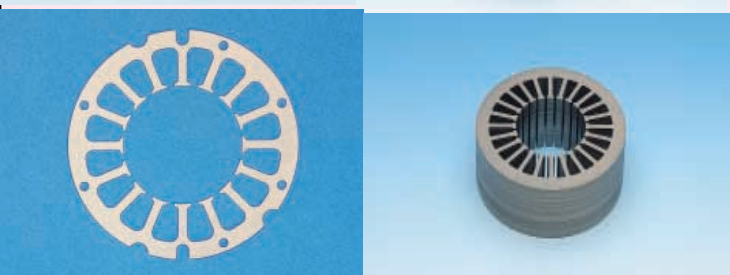
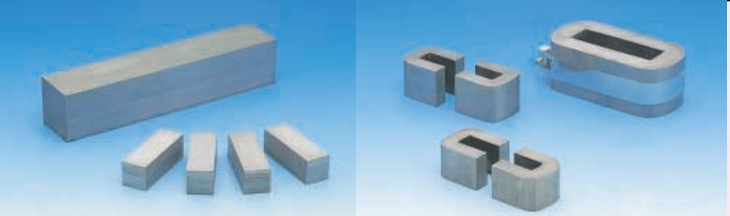
MEASUREMENTS IN SOFT MAGNETIC MATERIALS

In defining and measuring the $M(H)$ relationship in a magnetic material we must specify whether we are looking for **DC** or **AC** properties. If we are to determine the magnetization curves, we necessarily have to change the strength of the applied field with time. Strictly speaking, we talk of **DC** curves when this change is accomplished in such a way that every recorded point corresponds to a stable microscopic configuration of the system.



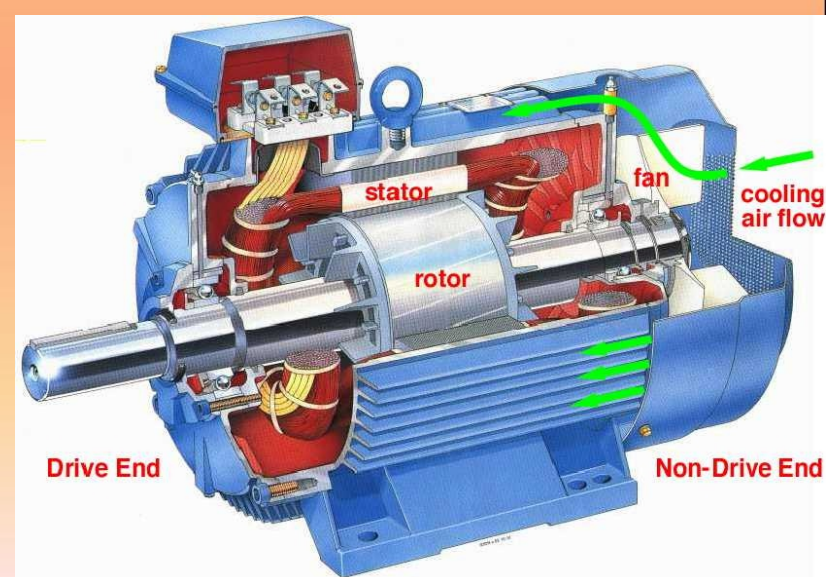
Initial magnetization curves in several types of soft magnets: 1) FINEMET nanocrystalline alloys $Fe_{73.5}Cu_1Nb_3B_9Si_{13.5}$; 2) amorphous alloys $Co_{67}Fe_4B_{14.5}Si_{14.5}$; 3) amorphous alloys $Fe_{78}B_{13}Si_9$; 4) $Fe_{15}Ni_{80}Mo_5$ (mumetal); 5) grain-oriented Fe-(3 wt %) Si laminations; 6) $Fe_{49}Co_{49}V_2$ alloys; 7) non-oriented Fe-(3.5 wt%)Si laminations; 8) Mn-Zn soft ferrites; 9) Ni-Zn soft ferrites; 10) Fe powder cores (Soft Magnetic Composites)

The applications of soft magnets (electrical machines, electronic devices, sensors and actuators, etc.) cover an outstanding range of frequencies (from DC to microwaves) and pose demanding requirements to the testing methods and apparatus.



Axial-flux rotating machine

Induction motor

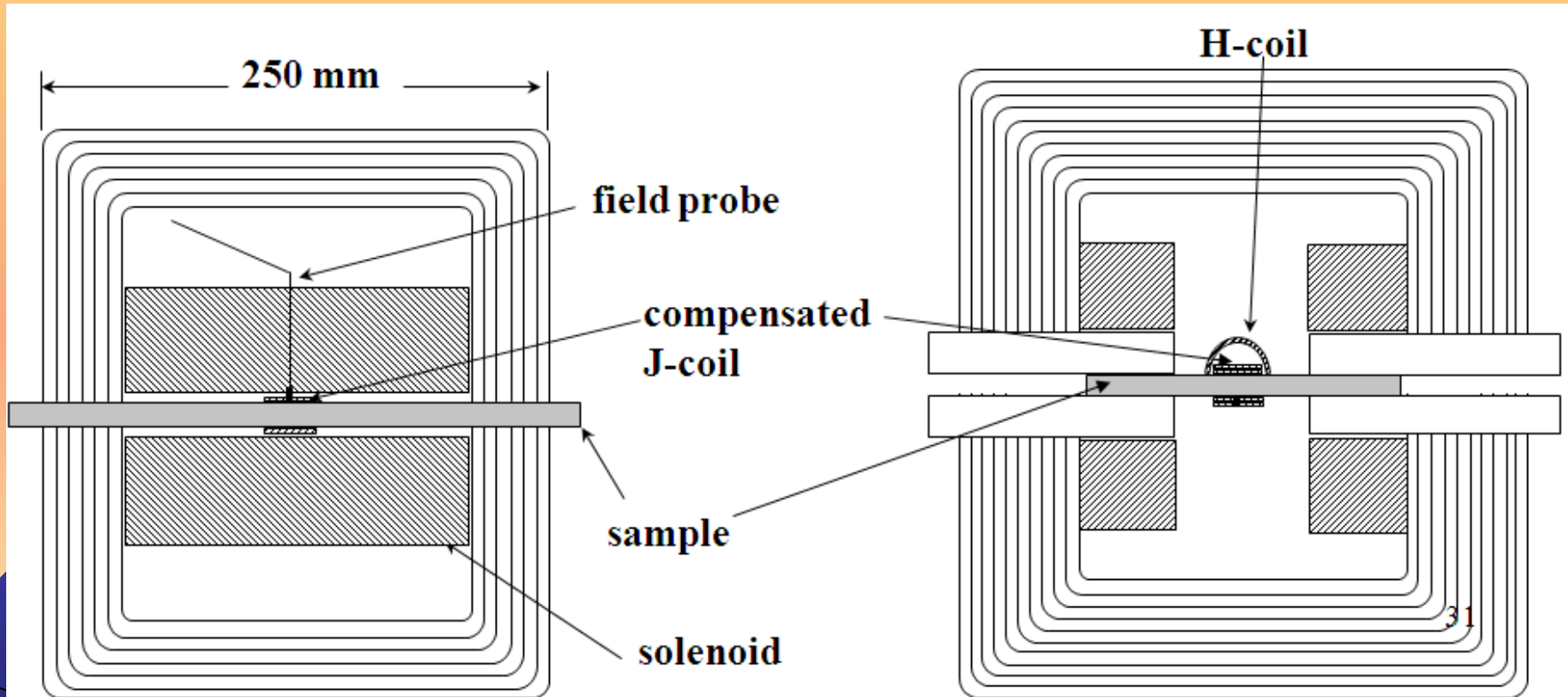


European School on Magnetism ESM2013



Metallic magnetic materials in **bulk form** are subjected to DC characterization only, because eddy currents shield the interior of the core already at very low induction rates. With ferrites and sintered or bonded metal particle aggregates, AC characterization can also be performed.

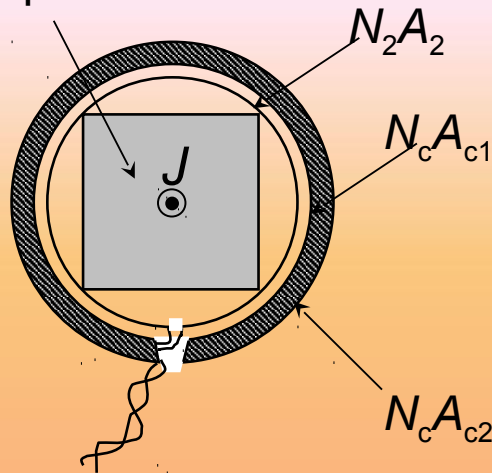
Bars, rods and thick strip specimens, as obtained, for example, by means of casting, forging, extrusion, hot rolling, powder compacting or sintering, are tested with the use of **permeameters**.



Measuring standard: IEC 60404-4

The material polarization J is obtained subtracting the signals detected by means of coils connected in series opposition.

test specimen



An inner winding of turn-area N_2A_2 is series connected with two outer compensating windings of turn-areas N_cA_{c1} and N_cA_{c2} , which are connected in series opposition. The flux linked with the outer coils, related to the shaded annulus, is

$$\Phi_c = N_c (A_{c2} - A_{c1}) \cdot \mu_o H$$

and totally compensates for the air-flux linked with the inner winding if

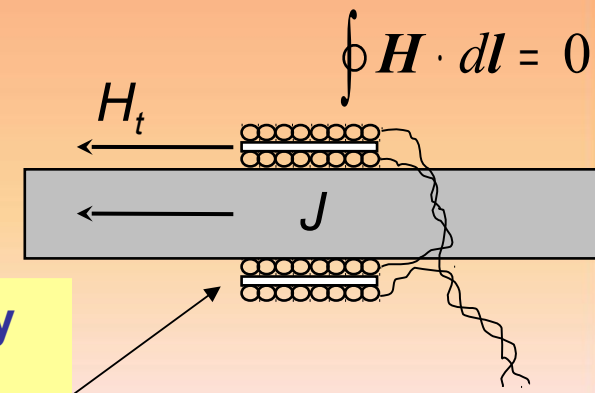
$$N_2A_2 = N_c (A_{c2} - A_{c1})$$

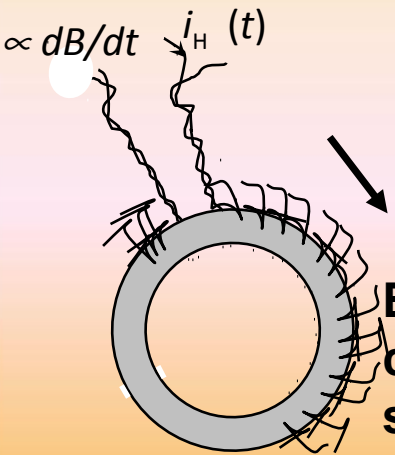
The flux globally linked with this triple-coil arrangement becomes then

$$\Phi_c = N_2AJ$$

where $A \equiv$ specimen cross-sectional area

Tangential field determined by means of a double H -coil



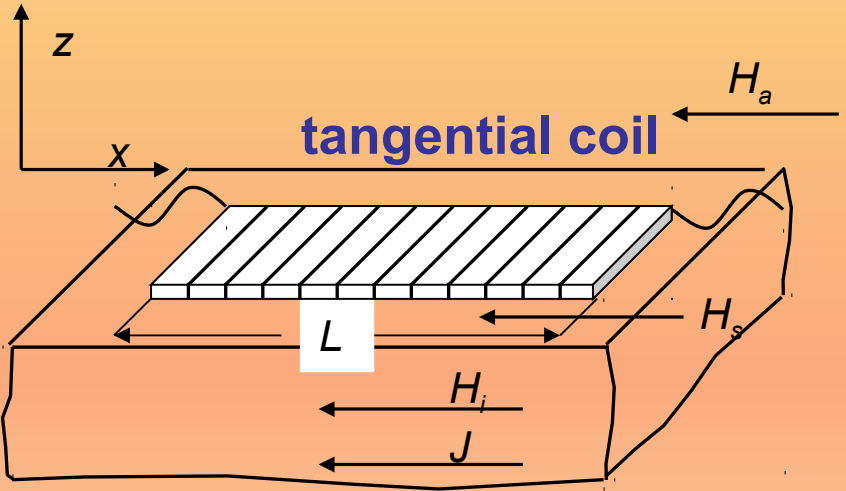
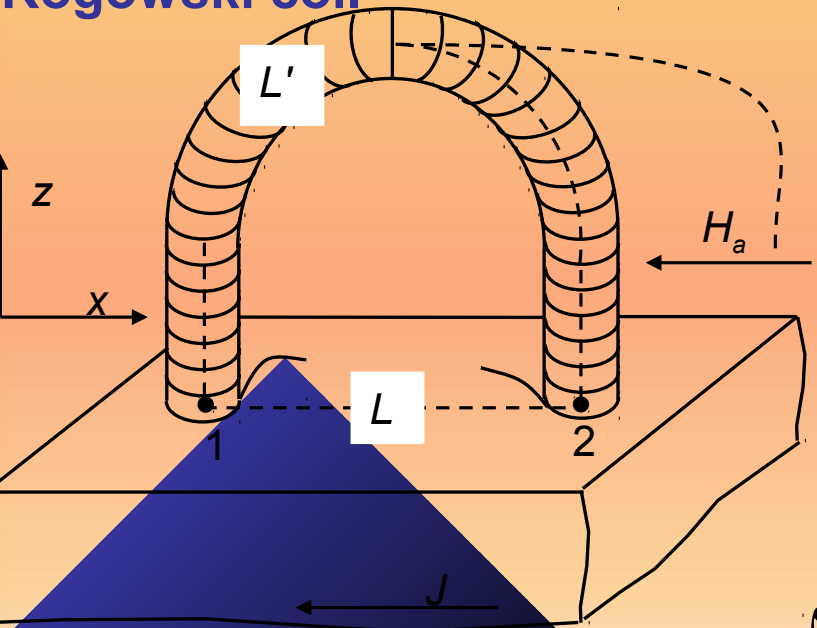


With a ring sample of mean circumference l_m , the effective field is easily obtained by knowledge of the magnetizing current i_H .

$$H = Ni_H / l_m$$

But under many measuring conditions (e.g. when using flux-closing yokes) the effective field must be directly measured at the specimen surface, either by an **H-coil** or field-sensing probe (e.g. **Hall plate**).

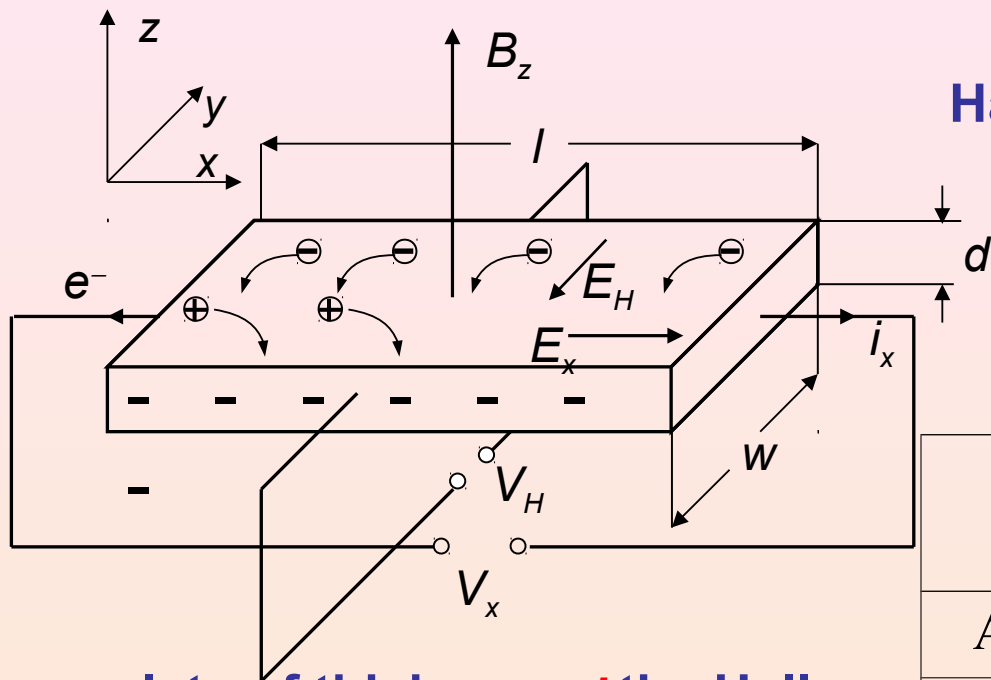
Rogowski coil



$$\int_L \mathbf{H}_i \cdot d\mathbf{x} = \int_L \mathbf{H}_s \cdot d\mathbf{x} = \int_{L'} \mathbf{H} \cdot d\mathbf{l}$$

$$H_i L = \int_{L'} \mathbf{H} \cdot d\mathbf{l} \rightarrow \mathbf{H}_i = \Phi / \mu_o nAL$$

The Hall probe: the most popular galvanomagnetic field sensor.



Hall field
$$E_H = - \frac{e\tau}{m_e} E_x B_z$$

Hall voltage
$$V_H = E_H w$$

For a plate of thickness d the Hall voltage is

$$V_H = \frac{R_H i_x B_z}{d}$$

with the Hall coefficient

$$R_H = - \frac{1}{n_e e} = - \frac{\mu_e}{\sigma}$$

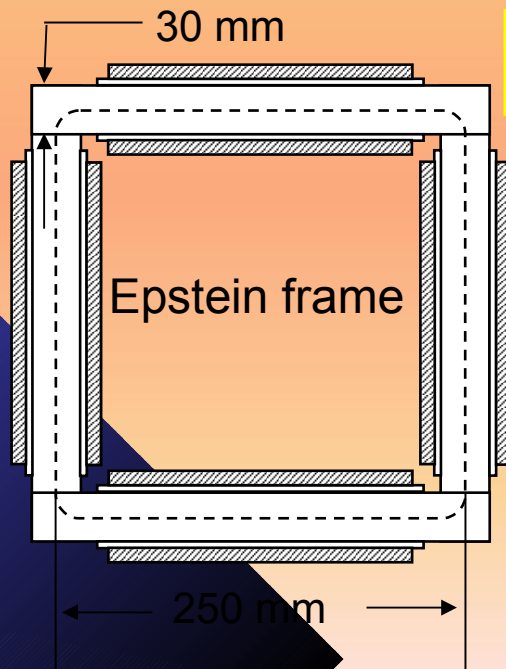
	R_H ($\text{m}^3 \cdot \text{C}^{-1}$)	$(1/R_H) \cdot dR_H/dT$ (K^{-1})
Ag	$-9 \cdot 10^{-11}$	---
Be	$2.4 \cdot 10^{-10}$	---
Sb	$-2 \cdot 10^{-9}$	---
Bi	$-6 \cdot 10^{-7}$	$5 \cdot 10^{-3}$
Si	$-1 \cdot 10^{-5}$	$-1 \cdot 10^{-3}$
InAs	$-1 \cdot 10^{-4}$	$1 \cdot 10^{-4}$
GaAs	$-2 \cdot 10^{-4}$	$3 \cdot 10^{-4}$
InSb	$-7.5 \cdot 10^{-4}$	$8 \cdot 10^{-4}^{49}$

Sheet and strip specimens

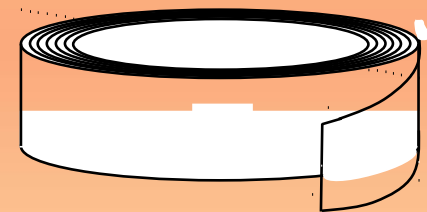
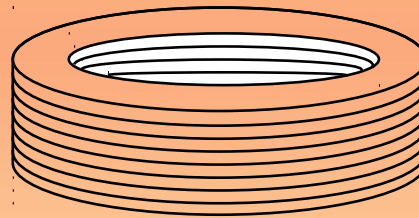
Soft magnets are applied for the most part in AC devices and for that reason they are generally produced as sheets and ribbons. To characterize them under a closed magnetic circuit configuration, we can either build ring or Epstein frame samples, or resort to flux-closure by a means of high-permeability large cross-sectional area yokes.

Conventional magnetic laminations are usually delivered as wide sheets (typically in the range 0.5 m - 1.5 m), from which testing samples must be cut. Rapidly solidified alloys are instead produced and tested as ribbons of variable width, from 1-2 mm to around 100 mm, and sometimes as wires.

Measuring
standard:
IEC 60404-2



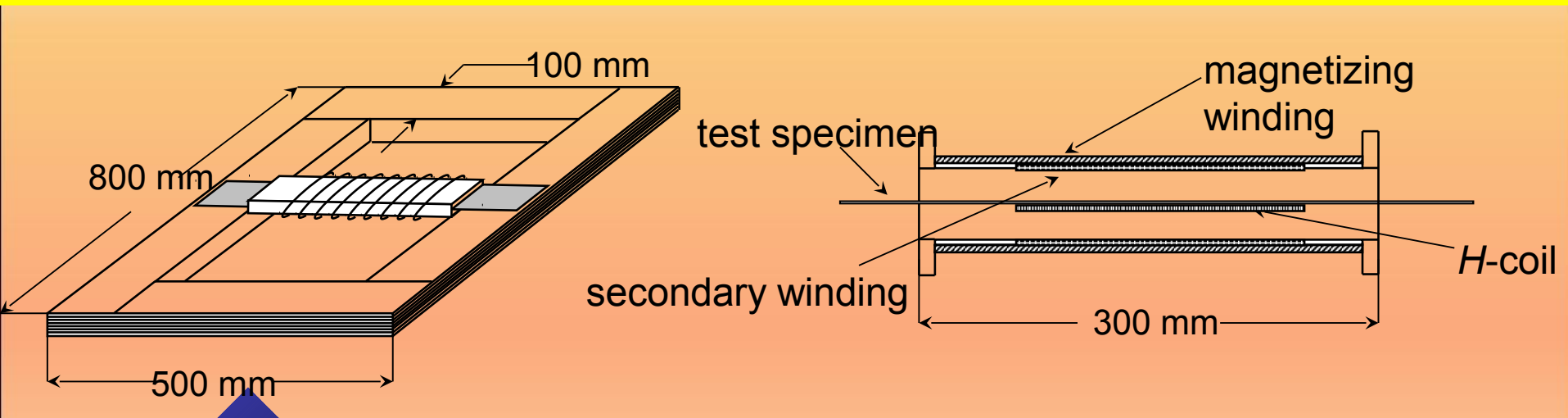
$$H = Ni_H / l_m$$



Maximum stress in a lamination of thickness d bent over a radius R ($E_y \equiv$ Young modulus)

$$\sigma_{\max} = E_Y d / 2R$$

The Epstein test method is a widely accepted industry standard, characterized by a high degree of reproducibility, as shown by intercomparisons carried out by National Metrological Institutes. Indeed, the reproducibility of measurements is central to the acceptance and assessment of a method as a standard, because it attaches to the economic value of the material being characterized. For all its merits, including many years of solid experience by laboratories worldwide, the Epstein method has certain drawbacks, making its application difficult or not totally appropriate.

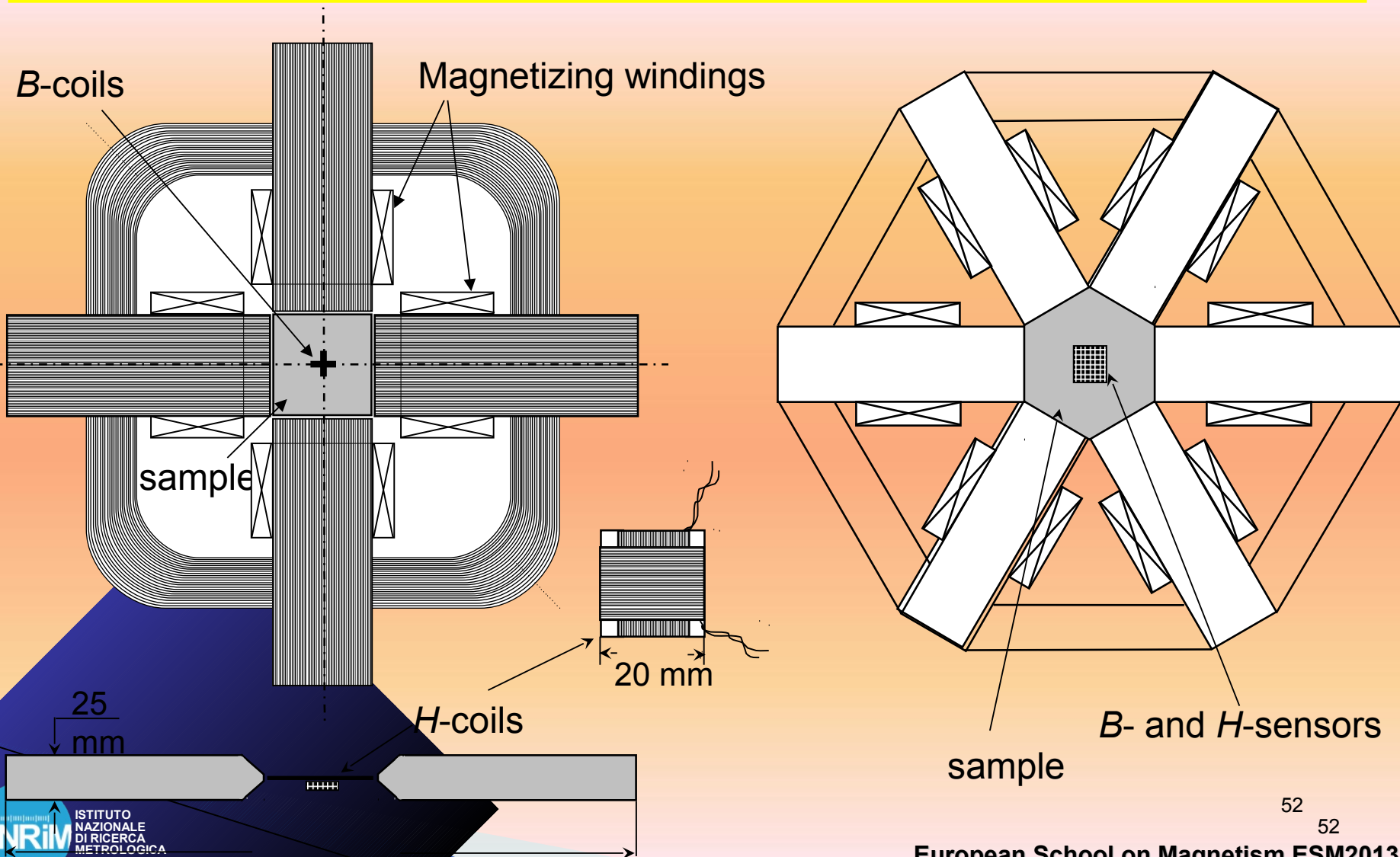


Different kinds of **single strip/single sheet testers (SST)**, like the ones employing horizontal single, double, and symmetrical yokes, or the vertical single and double C-yokes, have been investigated in the literature and have been variously adopted in national and international measuring standards.



Measuring standard: IEC 60404-3

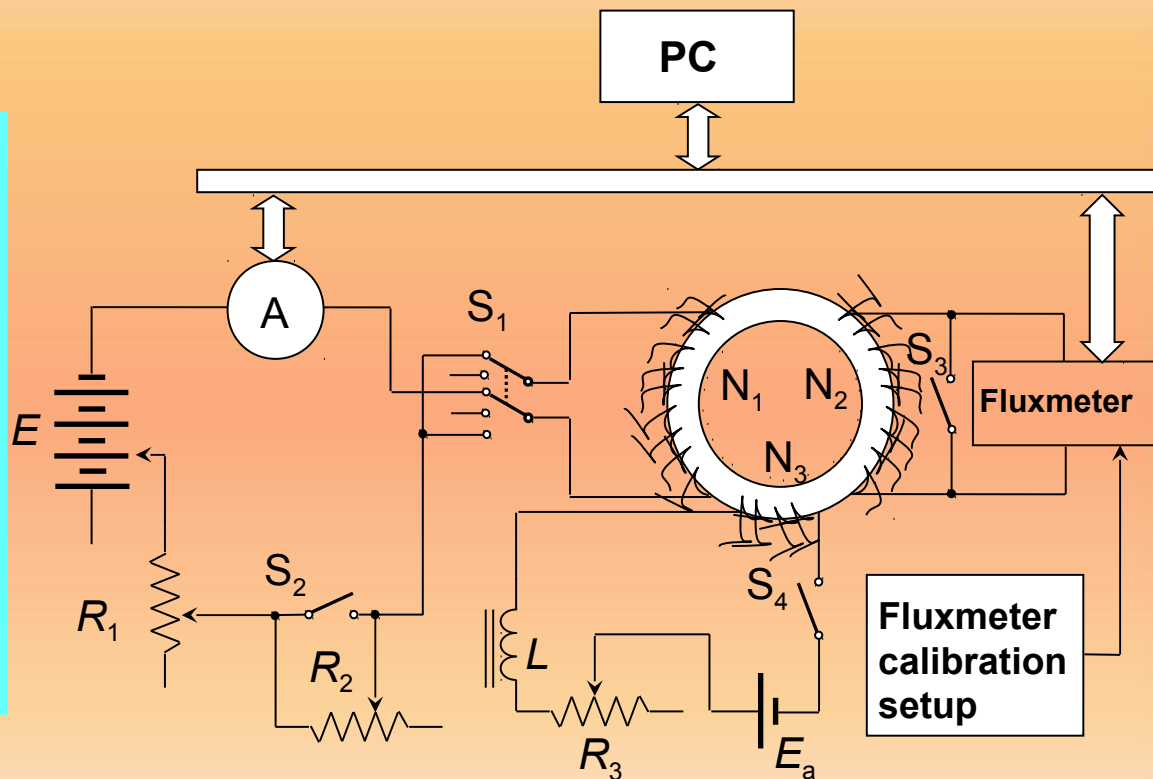
Recent trends in the development of magnetizers for soft magnetic laminations have favored a comprehensive approach to material testing, where the same setup is employed for measurements under one (1D)- and two-dimensional (2D) fields.



Fluxmetric characterization of soft magnets: DC measurements

There are two ways to determine the magnetization curves under quasi-static conditions: 1) The magnetizing field strength is changed in a step-like fashion and the curves are obtained by a point-by-point procedure; 2) The magnetizing field is changed in a continuous fashion, as slowly as reasonable to avoid eddy current effects (hysteresisgraph method). Ideally, the two methods should lead to same results, but differences are often found.

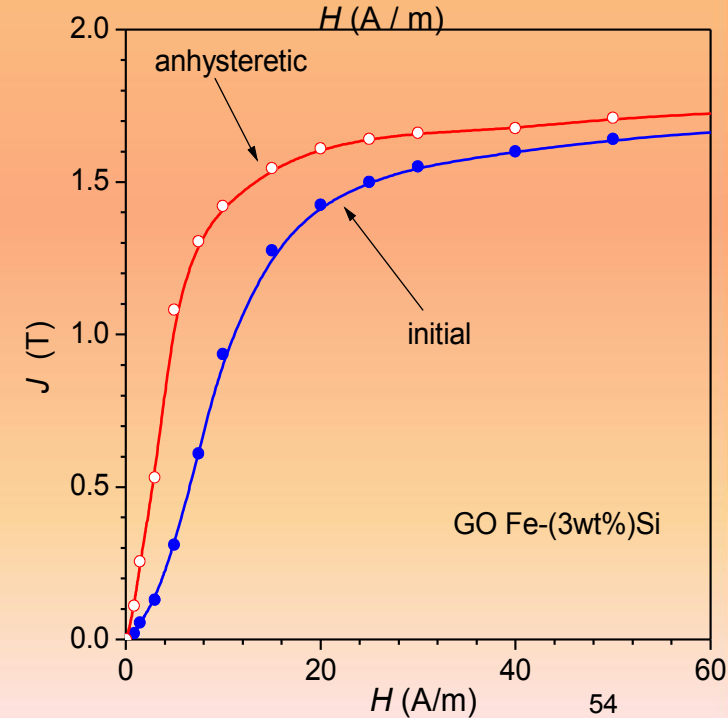
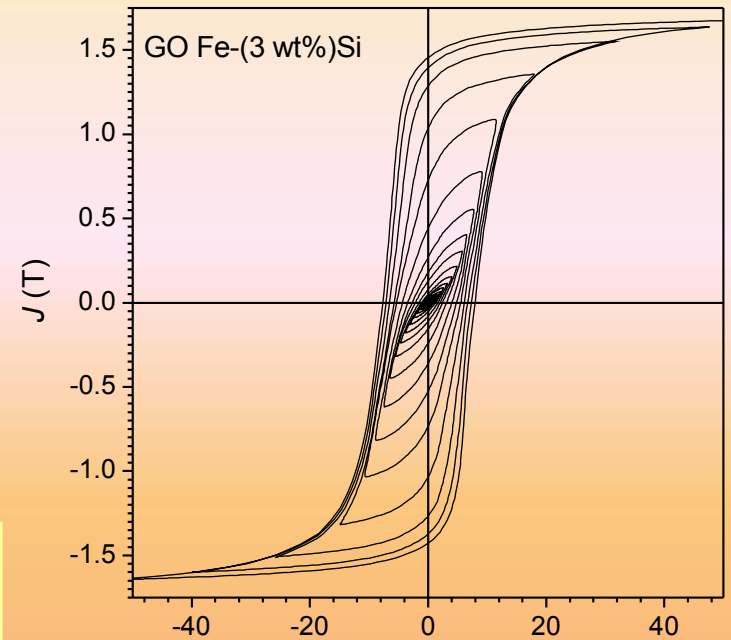
With the point-by-point procedure we detect the transient voltage induced on a secondary winding by a step-like applied field variation ΔH_a , which is integrated over a time interval sufficient to allow for complete decay of the eddy currents, in order to determine the associated flux variation $\Delta\Phi$



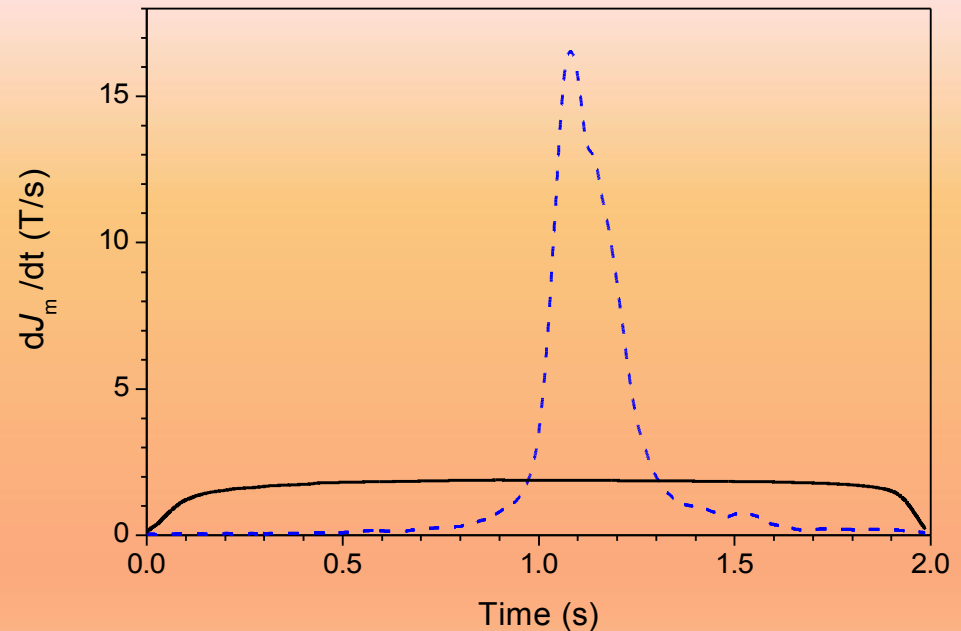
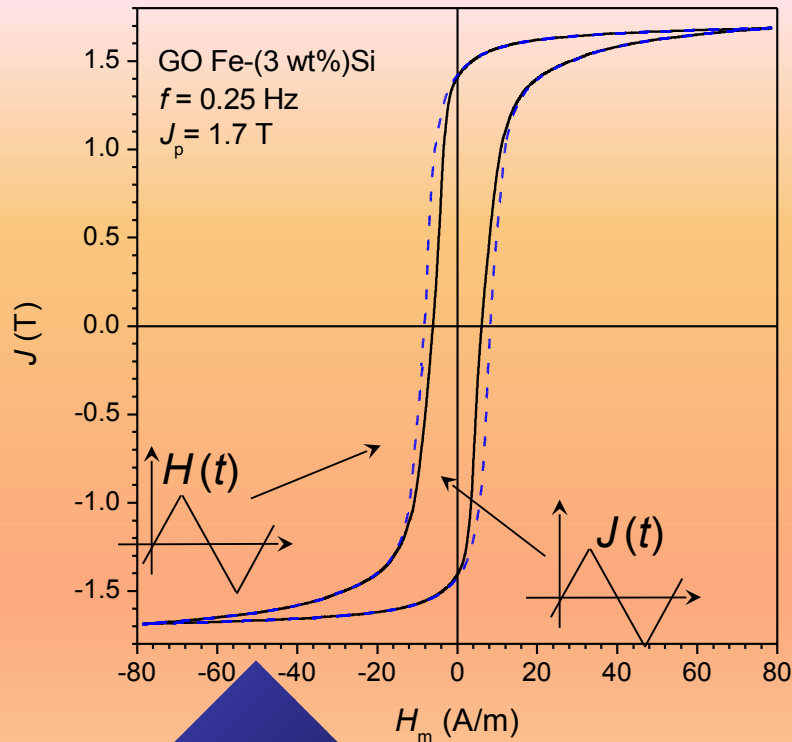
In a lamination of relative permeability μ_r , conductivity σ , and thickness d , we obtain a time constant

$$\tau \approx \mu \sigma d^2 / 8$$

τ is found to be sufficiently small for making drift problems negligible with conventional fluxmeters. In the quite limiting case of a 10 mm thick pure Fe slab of relative permeability $\mu_r = 10^3$, $\tau \sim 0.2$ s. Substantial immunity to drift (under the proper sequence of field steps) is the basic reason for the persisting interest in the point-by-point method, in spite of the apparent complication and tediousness of the measuring procedure.

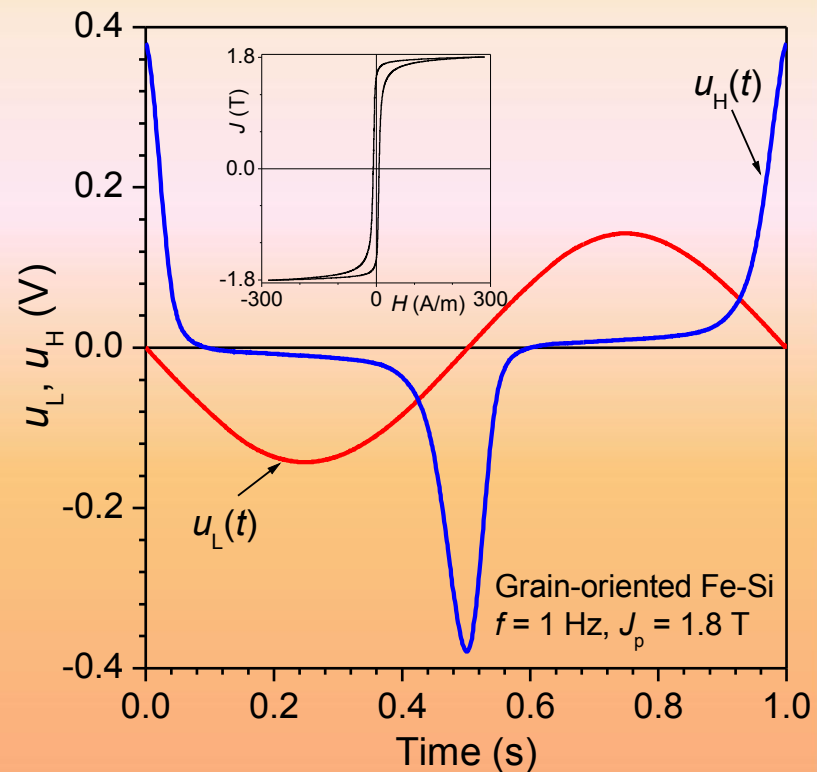
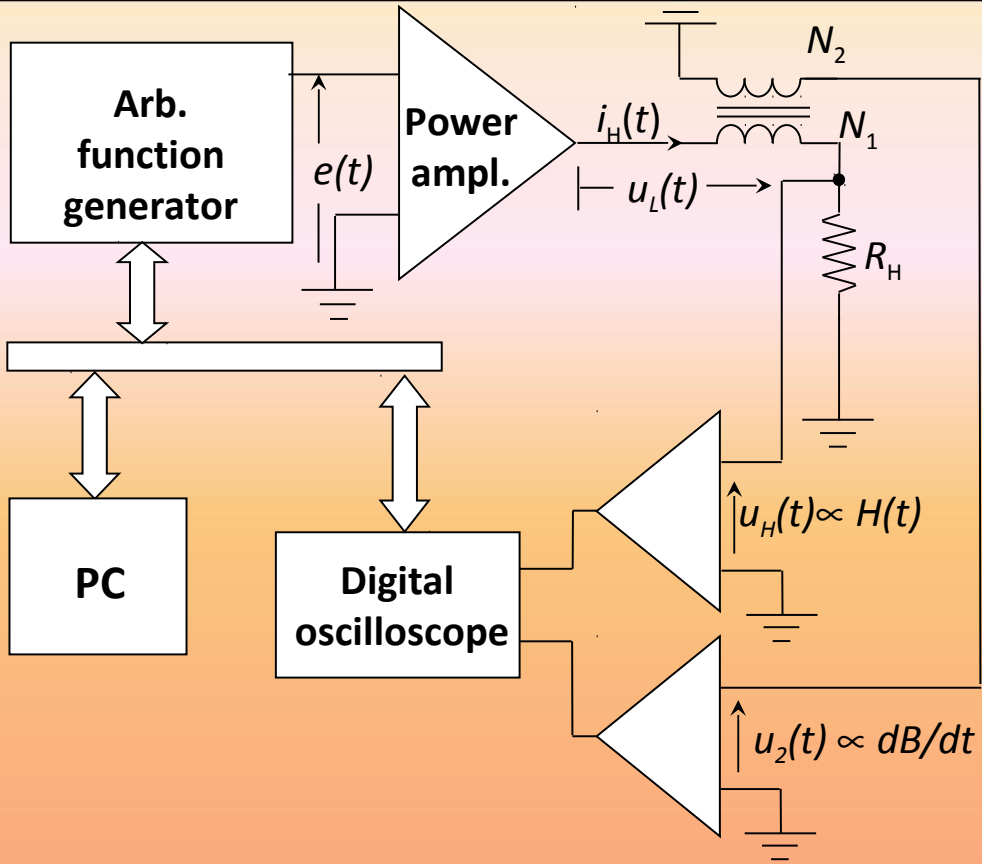


In the continuous recording method it is often required that $\frac{dB}{dt}$ is held constant. Besides being an obvious reference condition for the investigation of the magnetization process, the constant magnetization rate permits one to unambiguously define and minimize the role of eddy currents.



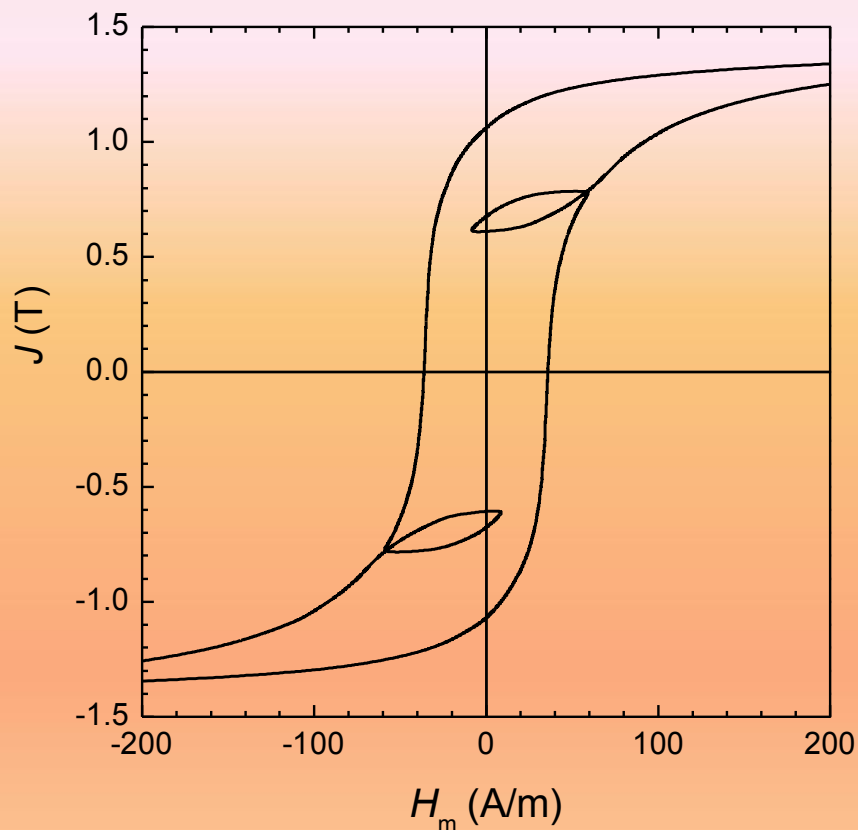
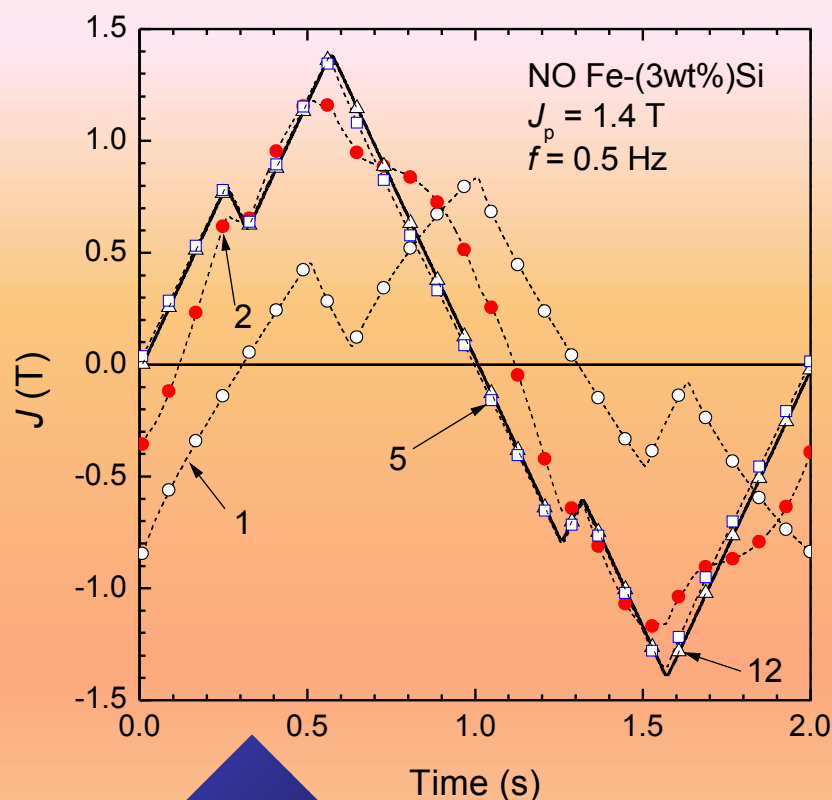
Quasi-static hysteresis loop in a grain-oriented Fe-Si lamination measured at the frequency $f = 0.25$ Hz under two different conditions:

- 1) Constant polarization rate of change ($\frac{dJ}{dt} = 1.7$ T·s⁻¹, solid line).
- 2) Constant field rate of change ($\frac{dH}{dt} = 80$ A·m⁻¹·s⁻¹, dashed line).



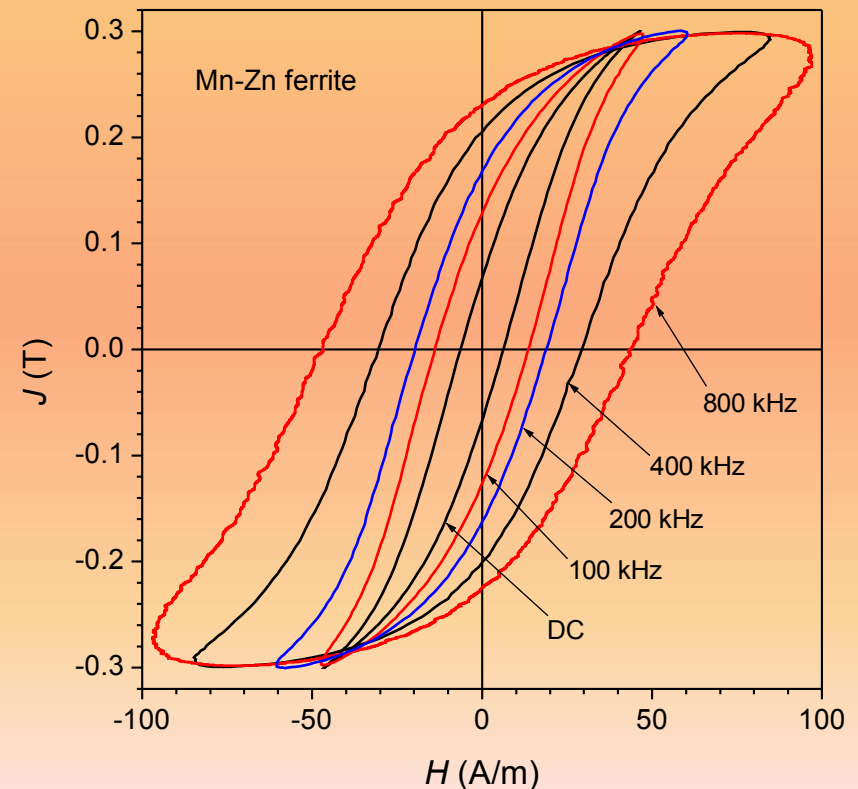
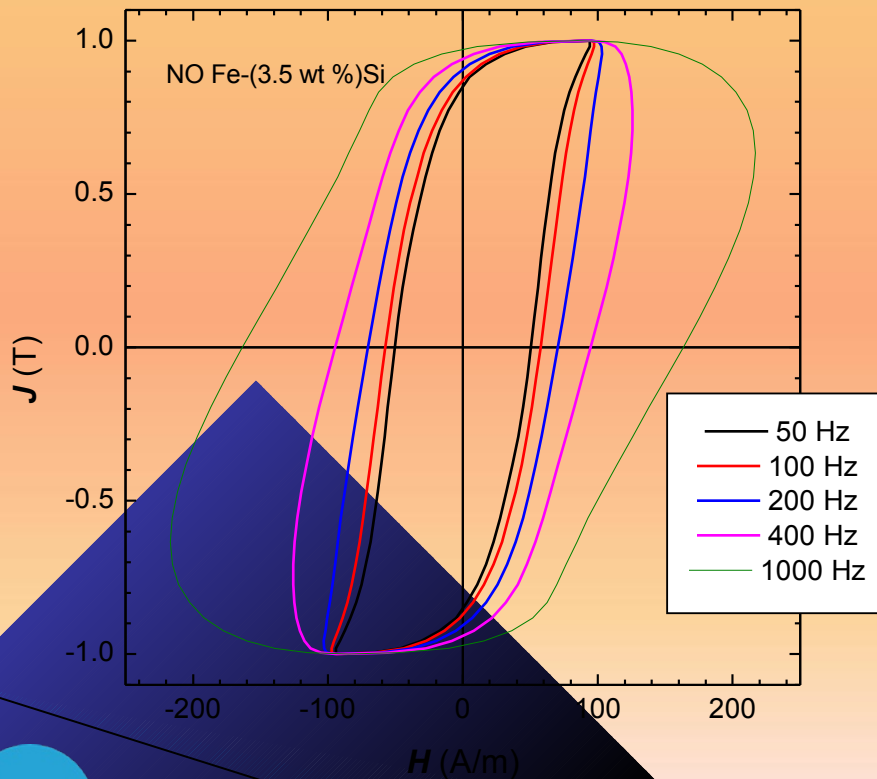
Wattmeter-hysteresisgraph implementing digital control by recursive process of the dB/dt waveform and example of final voltage signals in the primary circuit over a period. The hysteresis loop, shown in the inset, is measured at 1 Hz and $J_p = 1.8$ T on a grain-oriented Fe-Si lamination using the Epstein test frame. The voltage $u_H(t)$ is proportional to the applied magnetic field. The sinusoidal voltage $u_L(t)$ is proportional to dB/dt .

Digital recursive techniques can be exploited to obtain tight control of complex $J(t)$ waveforms.



The prescribed time dependence with local minima of the polarization in a non-oriented Fe-(3 wt%)Si lamination (solid line) is attained upon a convenient number of iterations.

Whatever the specimen configuration, any digital hysteresis graph-wattmeter built according to the previous DC testing scheme can deliver a most complete information on the magnetic properties of the material over the appropriate range of magnetizing frequencies and defined induction waveforms: major and minor hysteresis loops, normal magnetization curve, permeability, apparent power, power losses. All desired quantities are obtained in it by numerical elaboration after *A/D* conversion. Using high-resolution high sampling rate acquisition devices with synchronous sampling over the different channels, we can achieve excellent reproducibility of results.



$\bar{u}_2 = 4 f N_2 A J_p$ Mean secondary voltage \longrightarrow peak value of magnetic polarization

$H_p = \frac{N_1}{l_m} \cdot \frac{\hat{u}_H}{R_H}$ Peak value of the magnetic field

$$P = \frac{f}{\delta} \int_0^T H(t) \cdot \frac{dJ(t)}{dt} dt = - \frac{1}{m_a} \cdot \frac{N_1}{N_2} \cdot \frac{1}{T} \int_0^T u_2(t) i_H(t) dt$$

Power loss per unit mass (with δ the density and $m_a = \delta l_m A$)

$S = \tilde{i}_H \tilde{u}_2 \cdot \frac{N_1}{N_2} \cdot \frac{1}{m_a}$ Apparent power

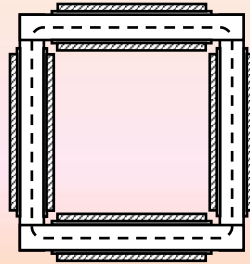
It is noted that we can also write the power loss as $P_w = \frac{f}{\delta} \int_0^T H(t) \cdot \frac{dB(t)}{dt} dt$

Since $B(t) = \mu_o H(t) + J(t)$

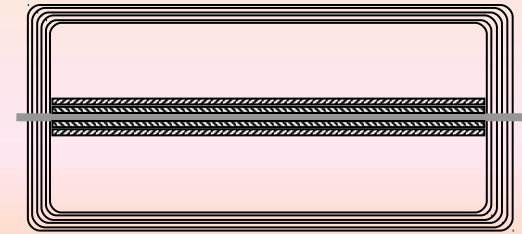
$$P_w = \frac{f}{\delta} \int_0^T \left[\mu_o H(t) \cdot \frac{dH(t)}{dt} + H(t) \cdot \frac{dJ(t)}{dt} \right] dt = \frac{f}{\delta} \int_0^T H(t) \cdot \frac{dJ(t)}{dt} dt = P$$

**IEC
60404-2
&
IEC
60404-3**

IEC 60404-2 (Epstein frame)



IEC 60404-3 (Single Sheet Tester)



Frequency

DC - 400 Hz

Power frequencies.

Temperature

23 ± 5 °C

23 ± 5 °C

Windings

Primary (outer) and secondary (inner) windings distributed on the four arms. $N_1=N_2= 700$.

Length of the magnetizing winding: 445 mm. $N_1=400$, N_2 depending on the acquisition setup.

Specimen size

Strip length: $280 \text{ mm} \leq l \leq 320$ mm, width of strips: $30 \text{ mm} \pm 0.2$ mm.

Sheet: length > 500 mm, width > 300 mm. Specimen placed inside a double-C laminated yoke $500 \text{ mm} \times 500$ mm.

Magnetic path length

$l_m = 0.94$ m

$l_m = 0.45$ m

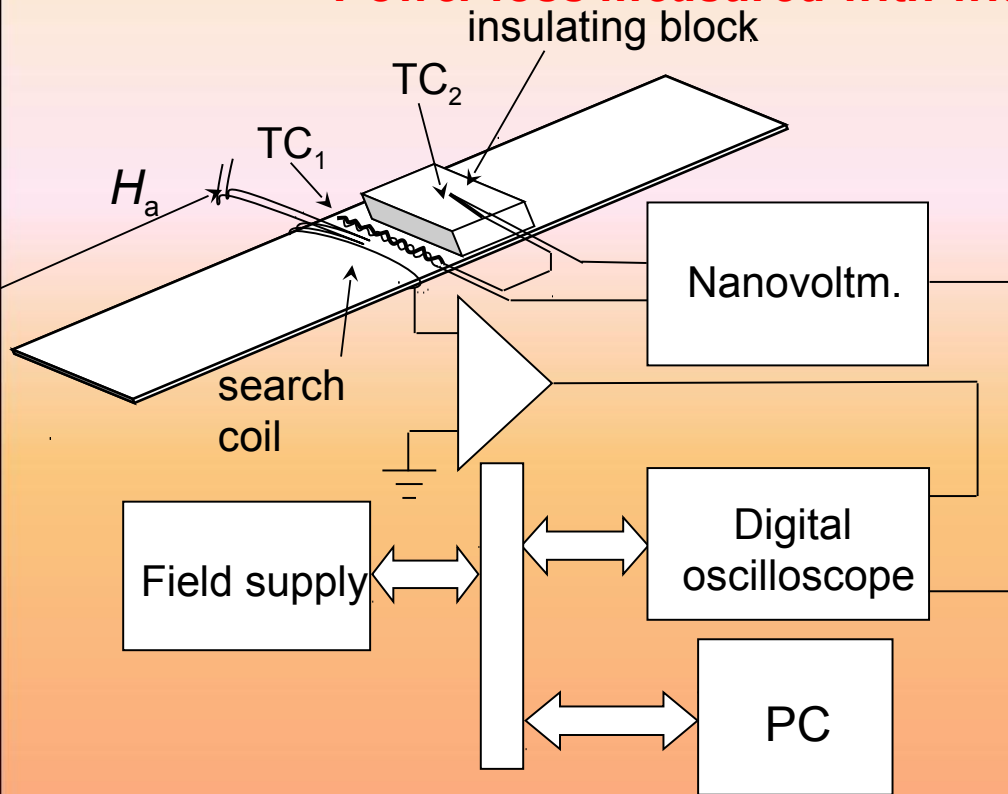
Polarization waveform

Sinusoidal: form factor of the secondary voltage $FF = 1.1107 \pm 1\%$

Sinusoidal: form factor of the secondary voltage $FF = 1.1107 \pm 1\%$

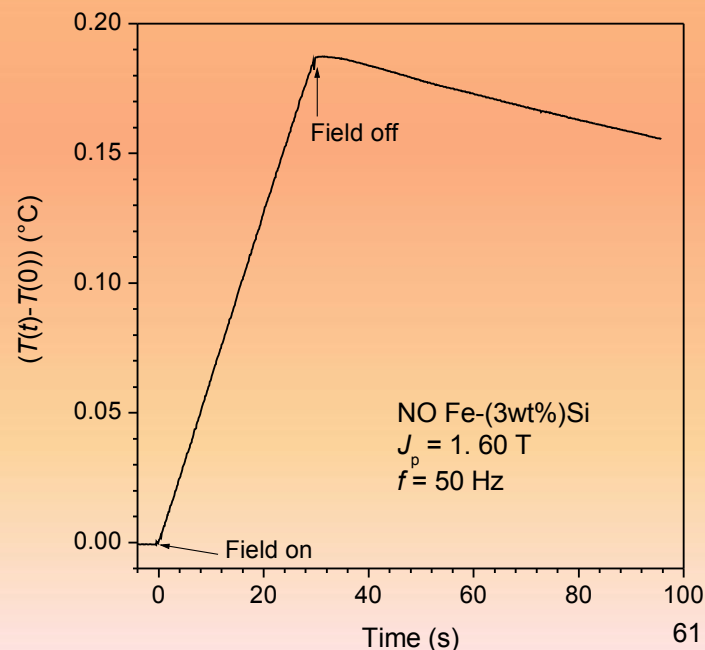
60

Power loss measured with with the calorimetric method



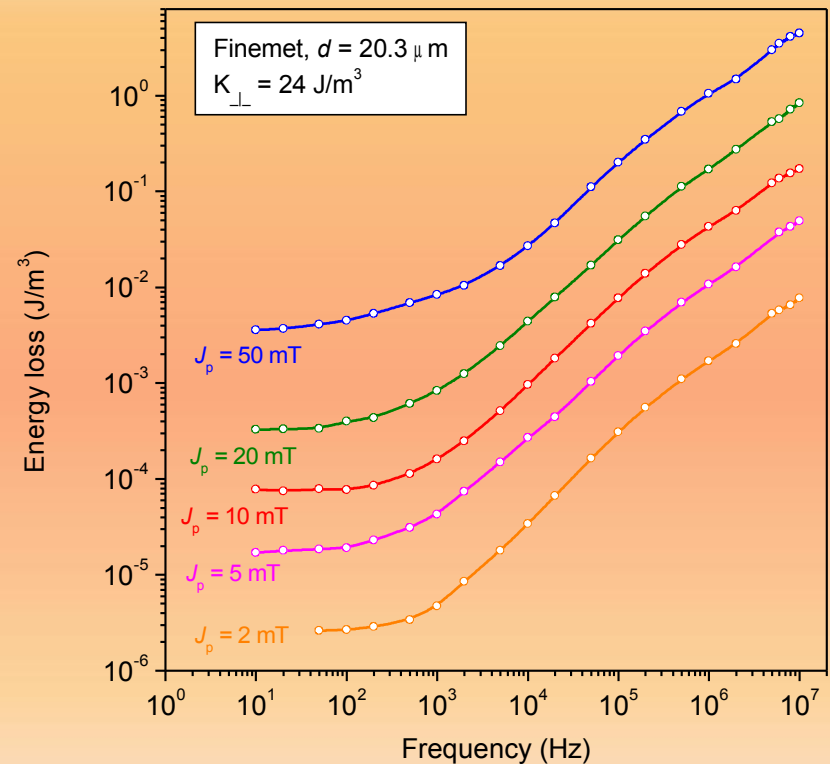
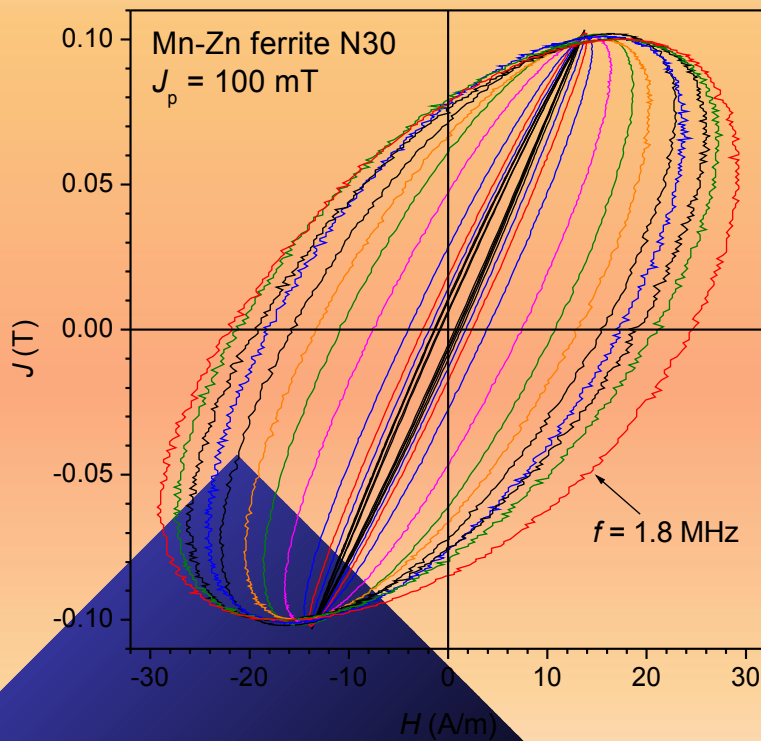
The rate of change of the sample temperature is determined by placing either thermocouples or thermistors on the sample surface. For an adiabatic process this quantity is in fact proportional to the dissipated power

$$P = c_p \frac{dT}{dt} = c_p \cdot \frac{dV}{dt} \cdot \frac{1}{(dV/dT)}$$



Medium-to-high frequency measurements

There is an increasing trend towards the use of electrical machines and various types of devices over a wide range of frequencies and with a variety of supply methods, which call for the precise characterization of soft magnetic materials beyond the assessed DC and power frequency domain. However, to adapt the conventional measuring setups to the characterization of soft magnets up to the MHz range might become a relatively complex task.



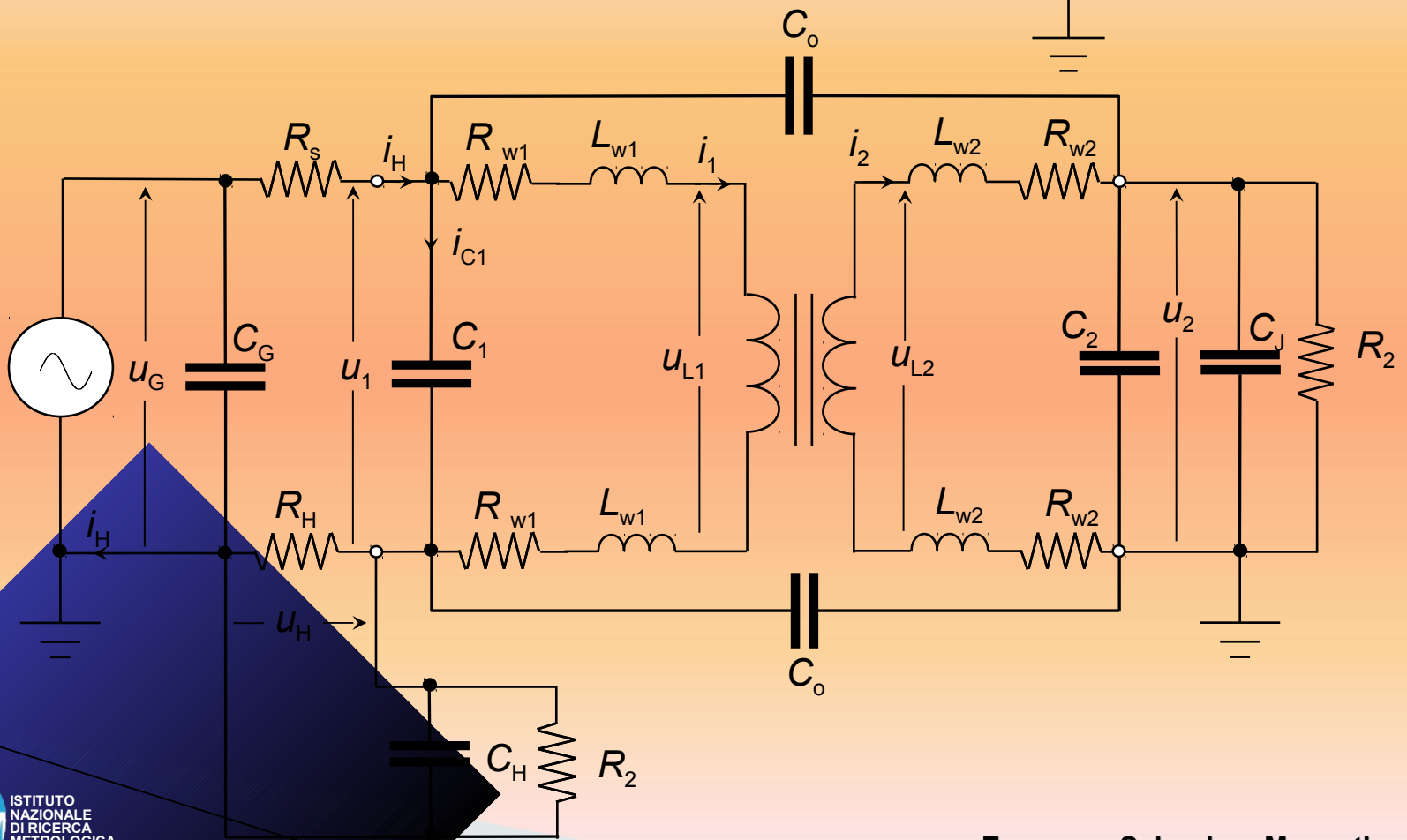
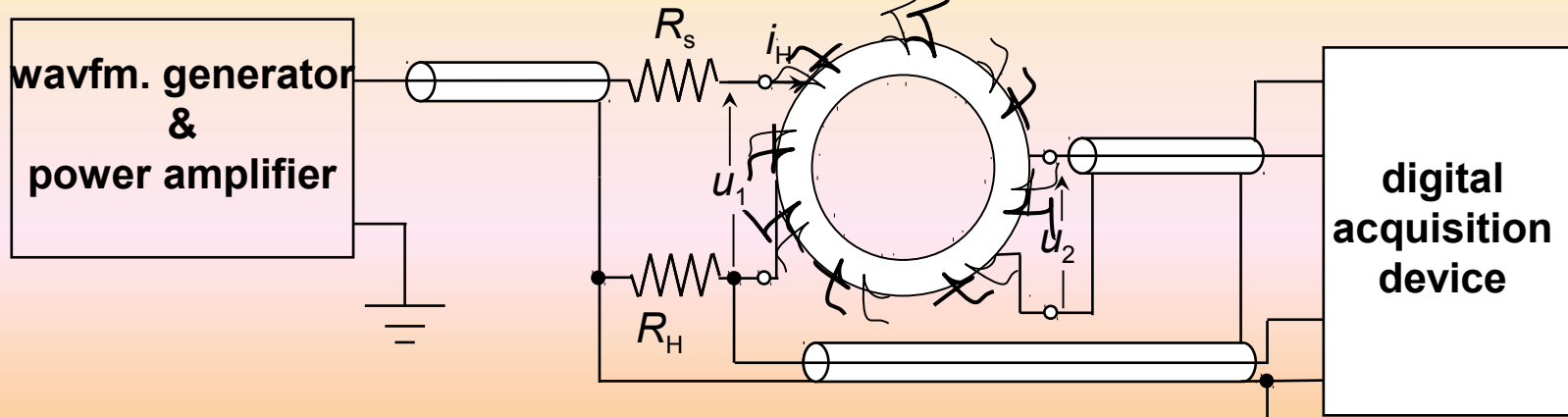
1) The flux penetration in the test sample can be incomplete (skin effect).

2) The temperature of the sample can appreciably rise during the measurement. A 0.050 mm thick grain-oriented sheet, suitably developed for high-frequency applications, can display, for example, a power loss of about 500 W/kg at 1.0 T and 10 kHz. The sample temperature is correspondingly expected to rise at a rate around 1 °C/s.

3) The increase of the required exciting power with the frequency poses serious limitations on the achievable peak polarization value.

4) Fast A/D converters are required to satisfy our requirement of single-shot signal acquisition and real time analysis.

5) With the increase of the magnetizing frequency above the kHz range, it becomes important to consider the role of stray inductances and capacitances. This is a most basic issue, the one making the real difference between low-frequency and high-frequency measurements, at least up to the radiofrequency domain, where the wavelength of the electromagnetic field becomes comparable with the dimensions of the test specimen.



An acceptable simplification in the analytical treatment of power loss and apparent power at high frequencies is obtained by treating the material as a linear medium. It is possible in this case to generalize the basic concept of permeability, defined as the ratio between induction and field strength when the material is taken along the normal curve or the anhysteretic curve, in order to account for the AC hysteresis.

$$H(t) = H_p \cos \omega t$$

$$B(t) = B_p \cos(\omega t - \delta) \quad B(t) = B_p \cos \delta \cos \omega t + B_p \sin \delta \sin \omega t$$

We can then describe $B(t)$ as the sum of two 90° phase-shifted sinusoids. The 90° -delayed component of the induction is connected with the dissipation of energy.

$$P = f \int_0^T H_m(t) \cdot \frac{dB(t)}{dt} dt = f\pi H_p B_p \sin \delta$$

Equivalently, we can write, using the complex notation,

$$H_m(t) = H_p e^{j\omega t} \quad B(t) = B_p e^{j(\omega t - \delta)}$$

and we can apply the definition of permeability to both in-phase and 90° out-of-phase components

$$\mu' = \frac{B_p}{H_p} \cos \delta \quad \mu'' = \frac{B_p}{H_p} \sin \delta \quad \mu = \frac{B_p e^{j(\omega t - \delta)}}{H_p e^{j\omega t}} = \mu' - j\mu''$$

It is immediate to see that power loss per unit volume and imaginary permeability are related by the equation

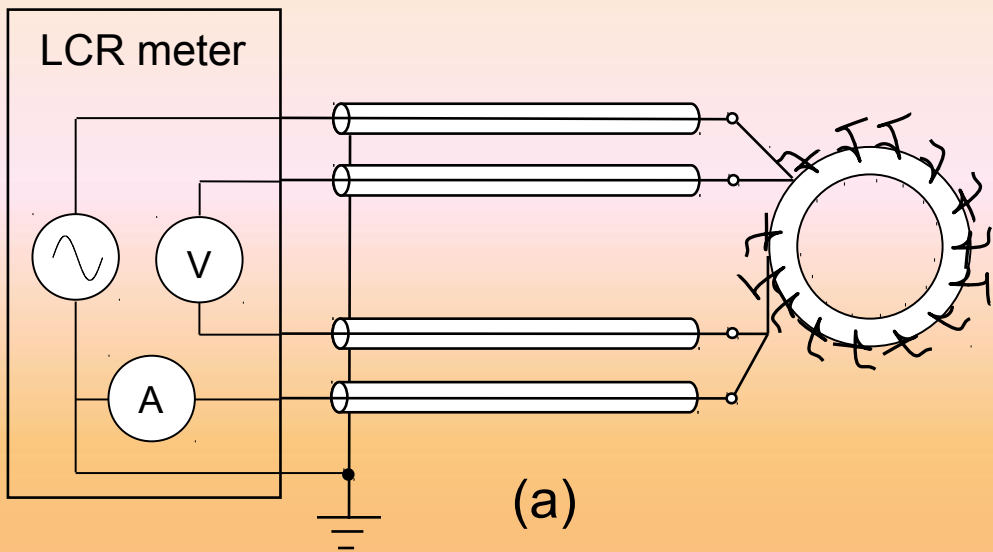
$$P = f\pi H_p^2 \mu''$$

A loss factor $\frac{\mu''}{\mu'} = \tan \delta$

can be introduced, which coincides with the inverse of the quality factor **Q** of the inductor.

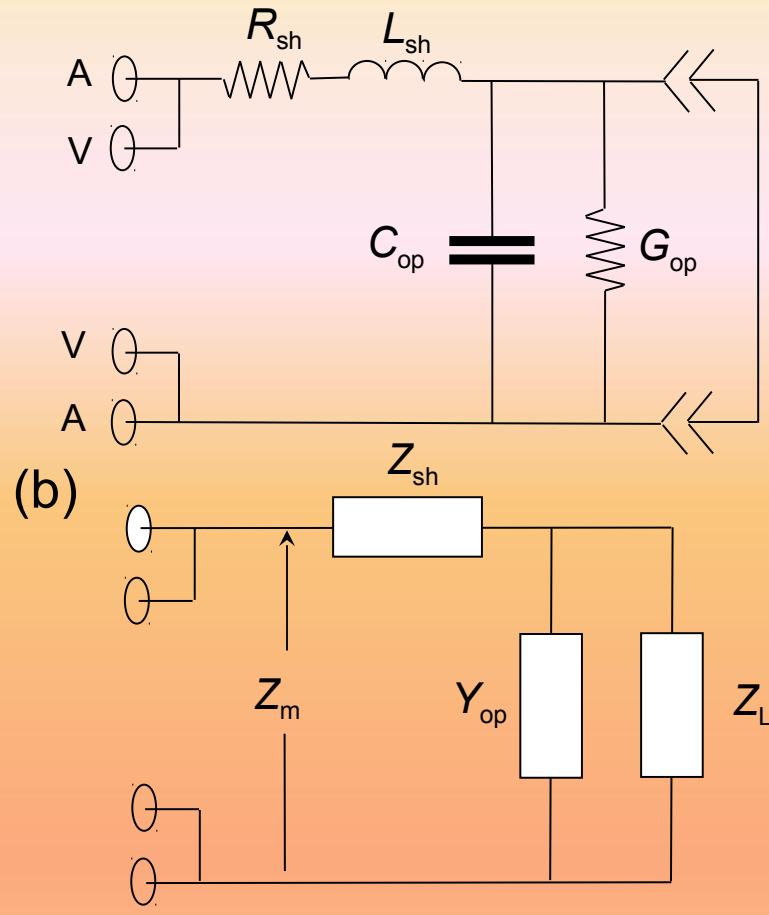
$$Q = 2\pi \frac{E_L}{E_R}$$

with $E_L = \frac{1}{2} B_p H_p \cos \delta \quad E_R = \pi B_p H_p \sin \delta$



(a)

$$Z_L = \frac{Z_m - Z_{sh}}{1 - Y_{op}(Z_m - Z_{sh})}$$

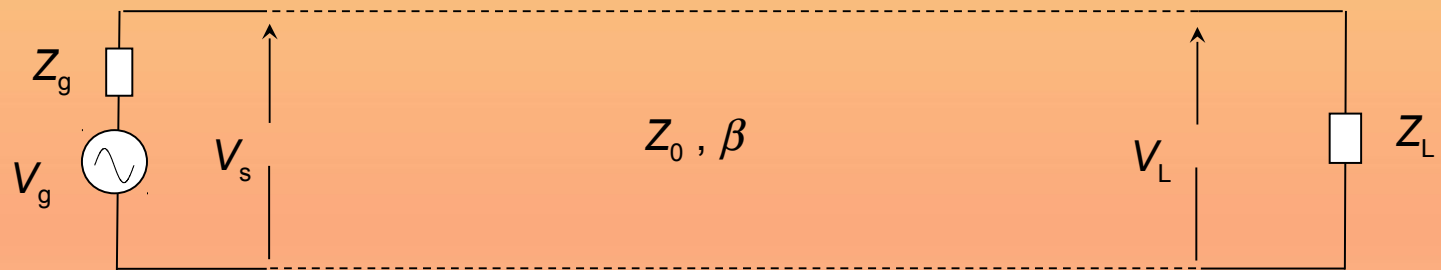


(b)

Measurement of the inductor impedance with **LCR** meter and four-terminal shielded configuration. The residual impedance of the test fixture is compensated using the equivalent circuit shown in (b), where Z_{sh} is the impedance measured with short-circuited terminals and Y_{op} is the admittance measured with open terminals (open/short compensation method). Z_m is the measured impedance and Z_L is the impedance of the inductor under test.

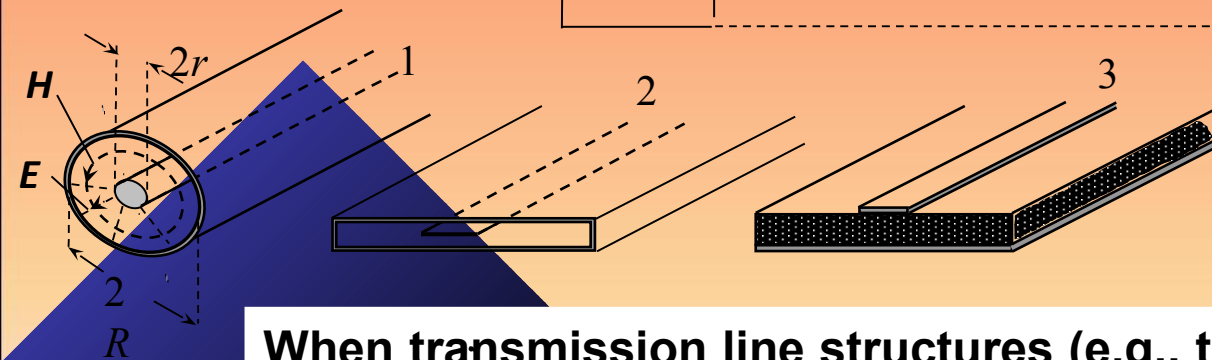
Measurements at radiofrequencies

The notion of simultaneity between cause and effect, as implied by ordinary electric circuit theory (closing a switch at some point does make ensuing currents and voltages to appear at once at all points in the circuit), must give way at high frequencies to the concept of waves traveling through connecting cables and circuits upon times non-negligible with respect to the oscillation period. A signal of frequency $f = 50$ MHz propagating at the velocity of light $c = 3 \cdot 10^8$ m/s has wavelength $\lambda = c/f = 6$ m. If we take as significant a time delay of 1/30 of a period, we conclude that traveling wave techniques should be used at such a frequency to deal with phenomena taking place over distances larger than about 20 cm.

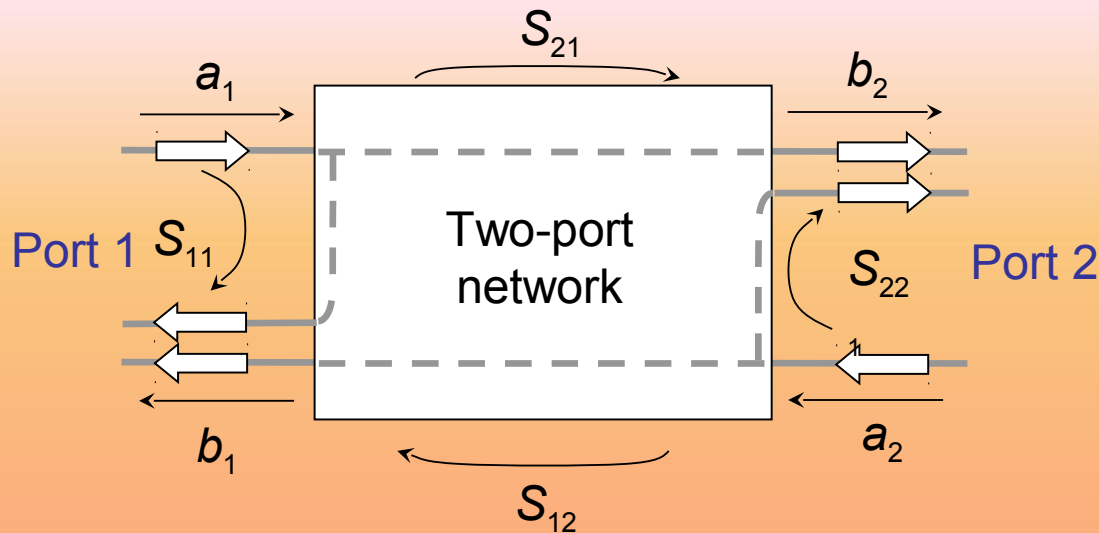


$$Z_0 = (L/C)^{1/2} \equiv \text{characteristic impedance of the line.}$$
$$\beta = \omega(LC)^{1/2} \equiv \text{propagation constant}$$

When transmission line structures (e.g., the diameter of the connecting cables) are significantly smaller than the signal wavelength, the analysis can be performed in terms of line voltages and currents.

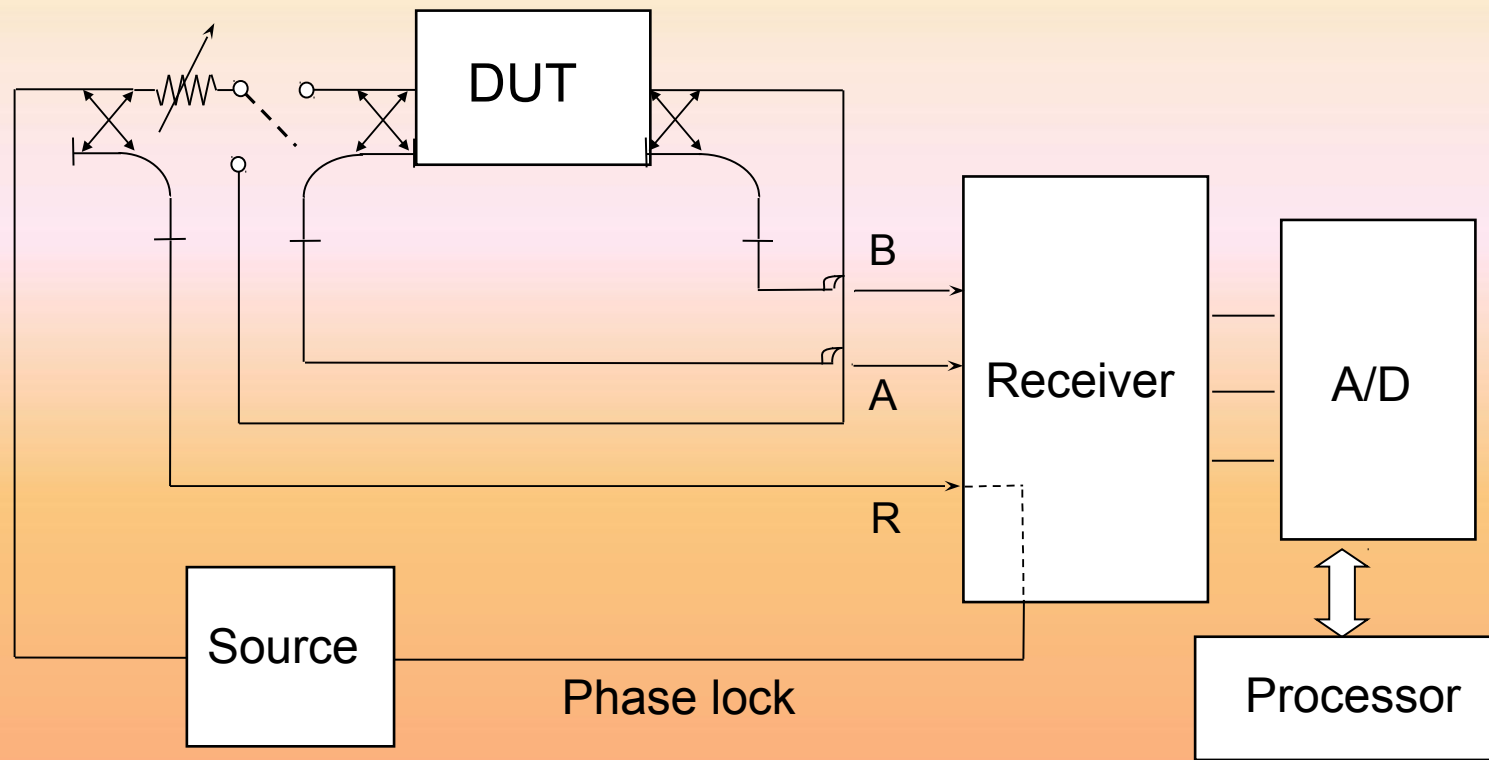


Most experiments involving transmission lines are nowadays performed using vector network analyzers. These devices have built-in signal sources and can measure the complex reflection and transmission coefficients of two-port and one-port networks over a broad range of frequencies.



The performance of such a network, that is, the quantities relating incoming and outgoing signals at the two ports, can be defined by means of the scattering matrix **[S]**. It relates the signals entering and leaving the device under test through the reflection coefficients S_{11} , S_{22} and the transmission coefficients S_{21} , S_{12} .

$$\begin{bmatrix} b_1 \\ b_2 \end{bmatrix} = \begin{bmatrix} S_{11} & S_{12} \\ S_{21} & S_{22} \end{bmatrix} \cdot \begin{bmatrix} a_1 \\ a_2 \end{bmatrix}$$



Basic scheme of a network analyzer. The swept radiofrequency signal (typically from some 100 kHz to a few GHz) generated by a high-resolution synthesized source can be delivered to either port 1 or port 2 of the device under test (DUT). Directional couplers separate incident and reflected signals. The signals leaving ports 1 and 2 are routed to the inputs A and B of the receiver, respectively, while the incident signal is sent to the reference input R. Transmission and reflection measurements can be done in both forward and reverse direction. The receiver has adapted ports A, B, and R.

$$S_{11} = \left. \frac{b_1}{a_1} \right|_{a_2=0}$$

reflection
coefficient at port 1

$$S_{22} = \left. \frac{b_2}{a_2} \right|_{a_1=0}$$

reflection
coefficient at port 2

$$S_{21} = \left. \frac{b_2}{a_1} \right|_{a_2=0}$$

transmission coefficient from port 1
to port 2 (forward gain)

$$S_{12} = \left. \frac{b_1}{a_2} \right|_{a_1=0}$$

transmission coefficient from port 2
to port 1 (reverse gain)

The input impedance of a transmission line can be expressed in terms of the reflection coefficient at the source plane $\Gamma(l)$

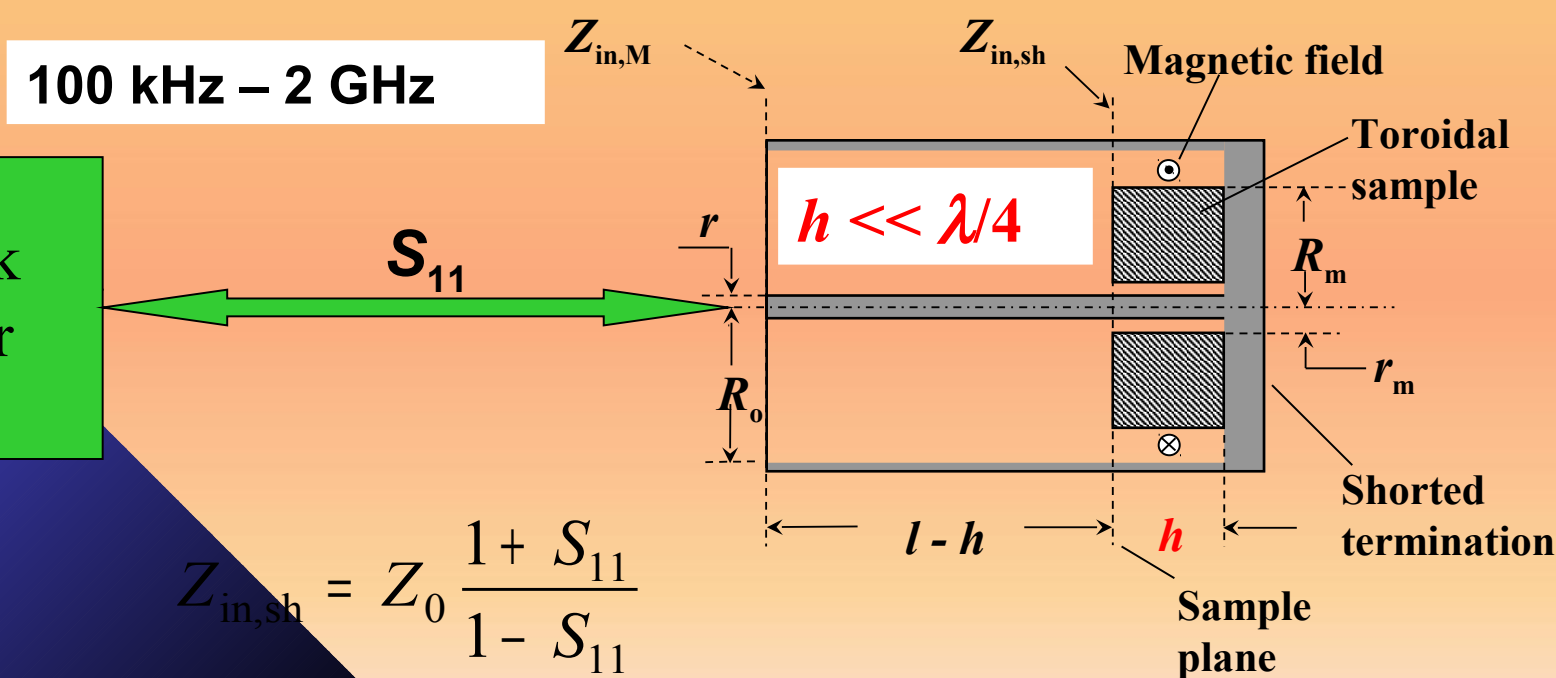
$$Z_{in} = Z_0 \frac{1 + \Gamma(l)}{1 - \Gamma(l)}$$



$$Z_{in} = Z_0 \frac{1 + S_{11}}{1 - S_{11}}$$

Measurements on ring samples using a transmission line.

Coaxial lines are the seat of a well-defined field configuration and provide a convenient fixture for sample testing. In particular, by placing the ring sample at the bottom of a shorted coaxial line, where the electric field (voltage) has a node and the magnetic field (current), azimuthally directed, is maximum, we can ignore dielectric effects, provided the sample thickness h is small with respect to the quarter wavelength $\lambda/4$ of the electromagnetic field.



$$Z_{in,sh} = Z_0 \frac{1 + S_{11}}{1 - S_{11}}$$

With network analyzers, we can move the calibration plane to the desired location using internal software, which simulates a variable length transmission line and the related phase shift. We can thus compensate for the electrical length of the piece of coaxial line separating the sample plane from the analyzer port plane.

The input impedance at the sample plane $Z_{in,sh} = jZ_0 \tan(\beta h) \cong jZ_0 \beta h$

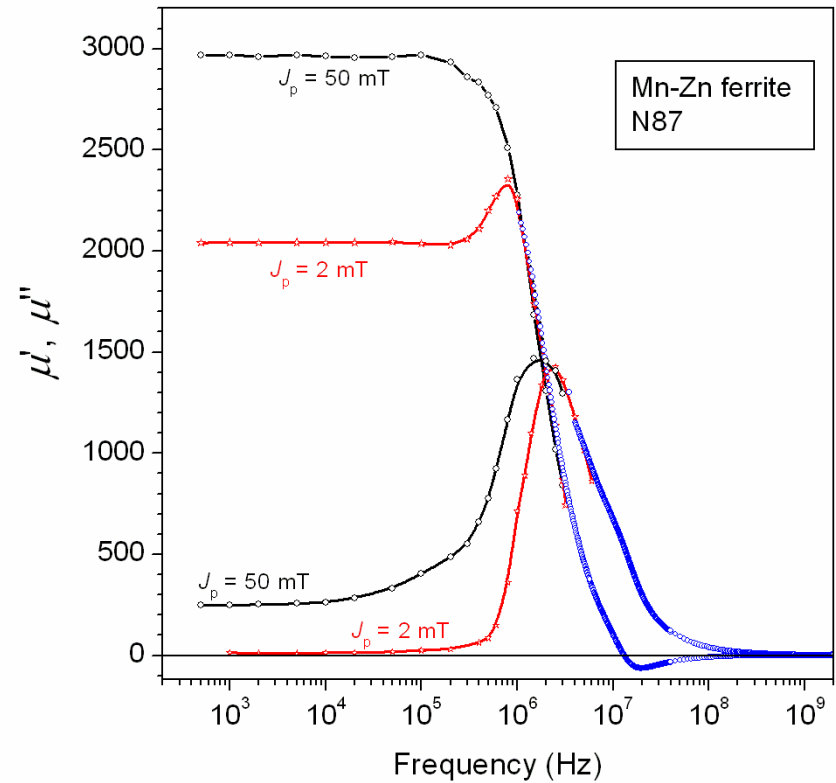
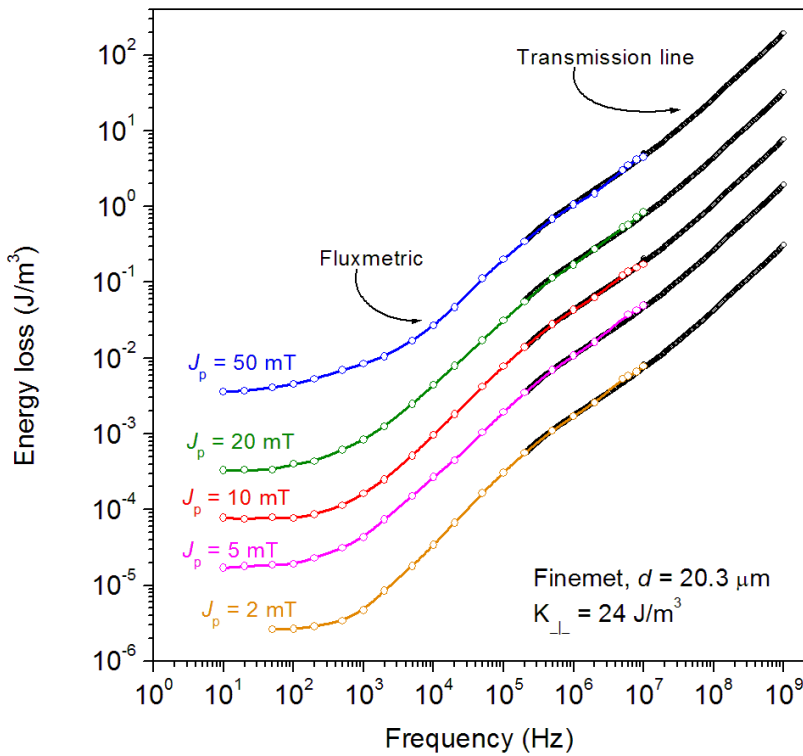
$Z_{in,sh}$ is determined via the measurement of the scattering coefficient with and without the sample inserted in the line. The real $\Re(\Delta Z)$ and imaginary $\Im(\Delta Z)$ parts of the impedance difference are separated and the real and imaginary permeabilities are thus obtained as

$$\mu'_r(\omega) = \frac{\Im[\Delta Z]}{\omega (\mu_0 / 2\pi) h \ln(R_m / r_m)} + 1 \quad \mu''_r(\omega) = \frac{\Re[\Delta Z]}{\omega (\mu_0 / 2\pi) h \ln(R_m / r_m)}$$

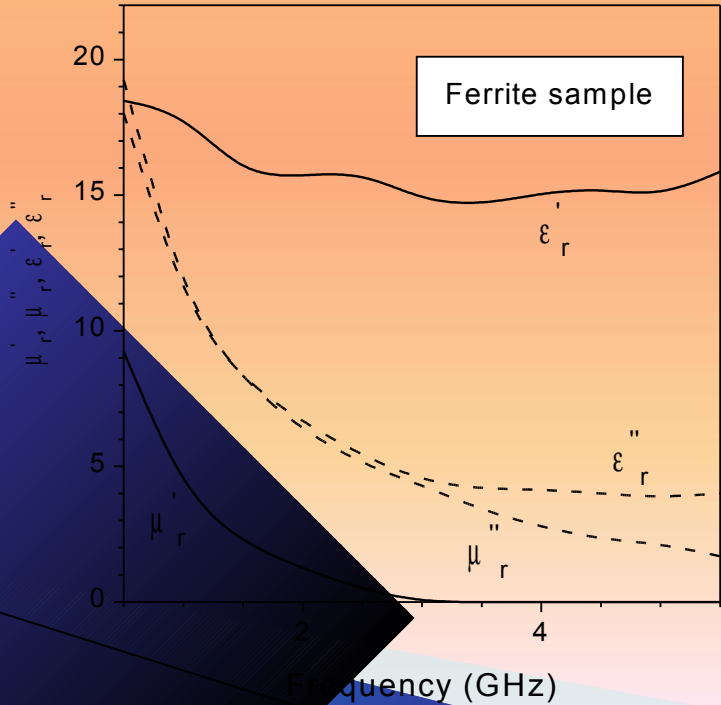
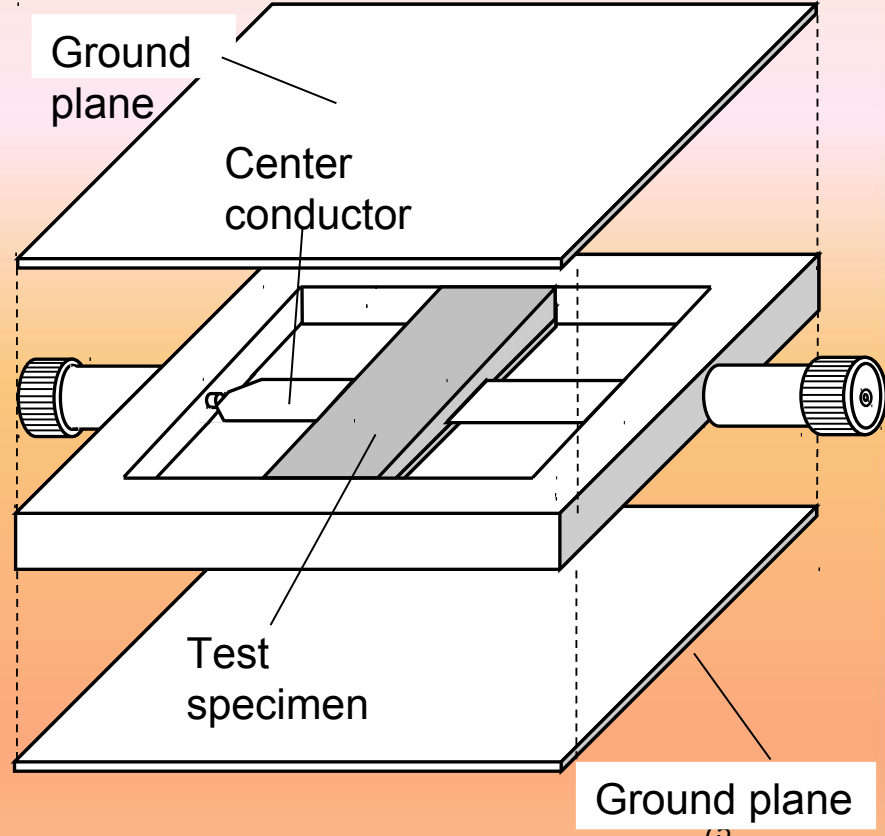
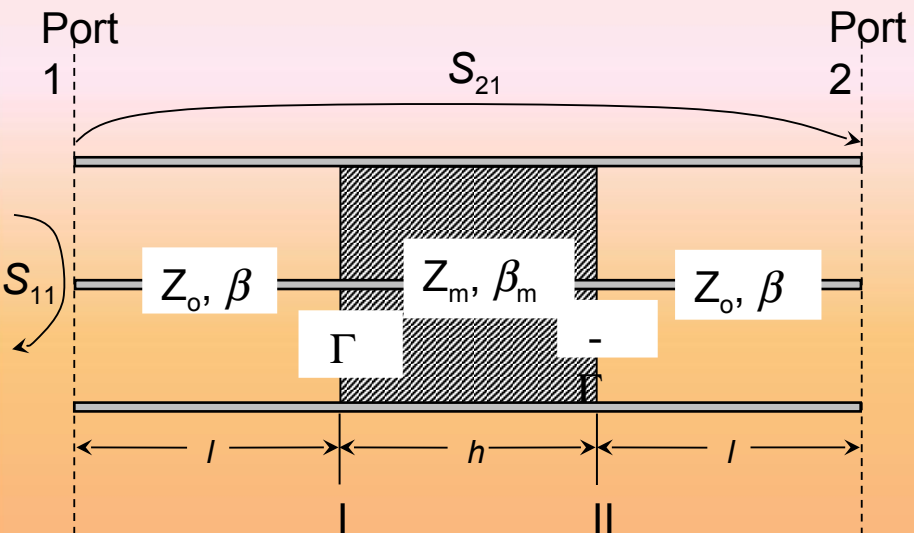
The loss tangent $\tan \delta = \mu'' / \mu'$

The Q factor $Q = 1 / \tan \delta$

Examples of broadband energy loss and permeability behaviors in nanocrystalline and soft ferrite ring samples measured with combination of fluxmetric and transmission line experiments.

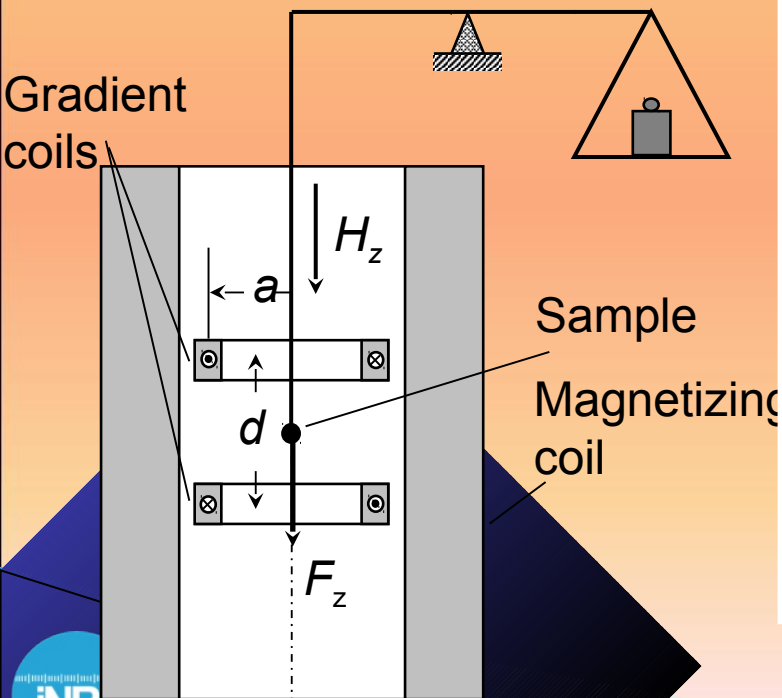


Measurement of complex permeability and permittivity with the Barry cell and two-port network (S_{11} and S_{21}).



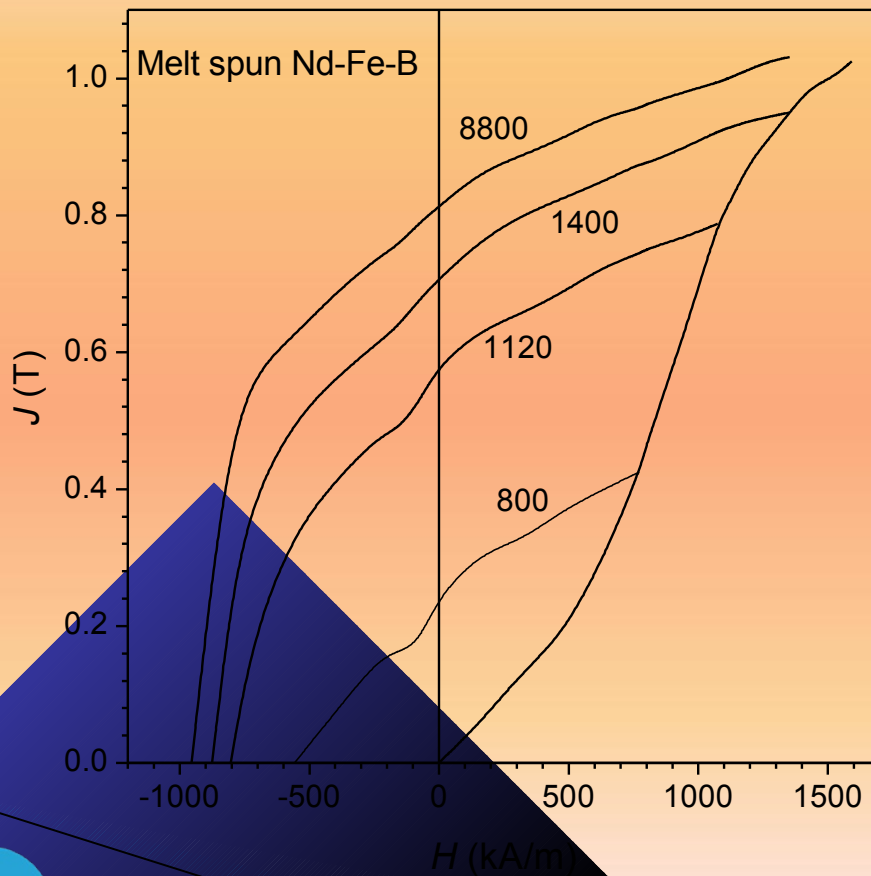
MEASUREMENTS IN PERMANENT MAGNETS

The natural approach to measurements in permanent magnets consists in the determination of the magnetic moment of a test specimen exploiting the forces arising by its interaction with a precisely known external field H . If a suspended or pivoted needle-shaped permanent magnet of total magnetic moment m is immersed in a uniform field H , it takes an orientation resulting from the equilibrium of the torque $\tau = m \times \mu_0 H$ applied by the field and a counteracting torque applied by a spring or a torsion wire.

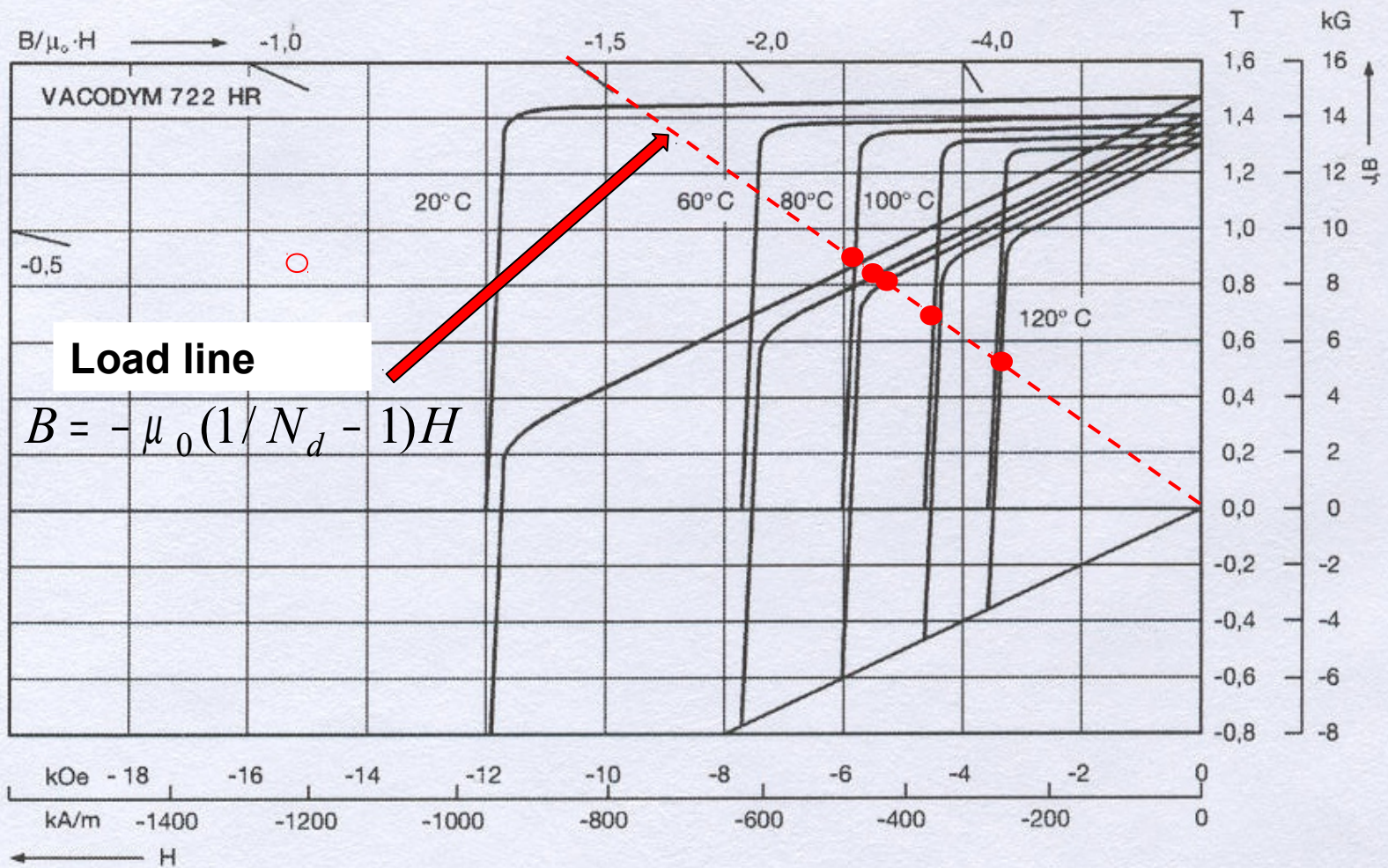


By letting such a specimen oscillate about its equilibrium position, one obtains a torsion pendulum, whose natural resonance frequency is directly related to the value m and the moment of inertia of the pendulum. If the test sample, assimilated to a dipole, is placed instead in a non-uniform field, it will be subjected to a translatory force $F = \nabla(m \cdot \mu_0 H)$, whose measurement in a known field gradient will equally provide the value of the magnetic moment.

For all their sensitivity and accuracy, the force methods require rather cumbersome apparatus and are not frequently used to measure the hysteresis behavior of permanent magnets, though they have been revived in the special case of **Alternating Gradient Force Magnetometers**. Magnetometric and inductive methods are largely employed instead in the determination of the hysteresis behavior of permanent magnets.



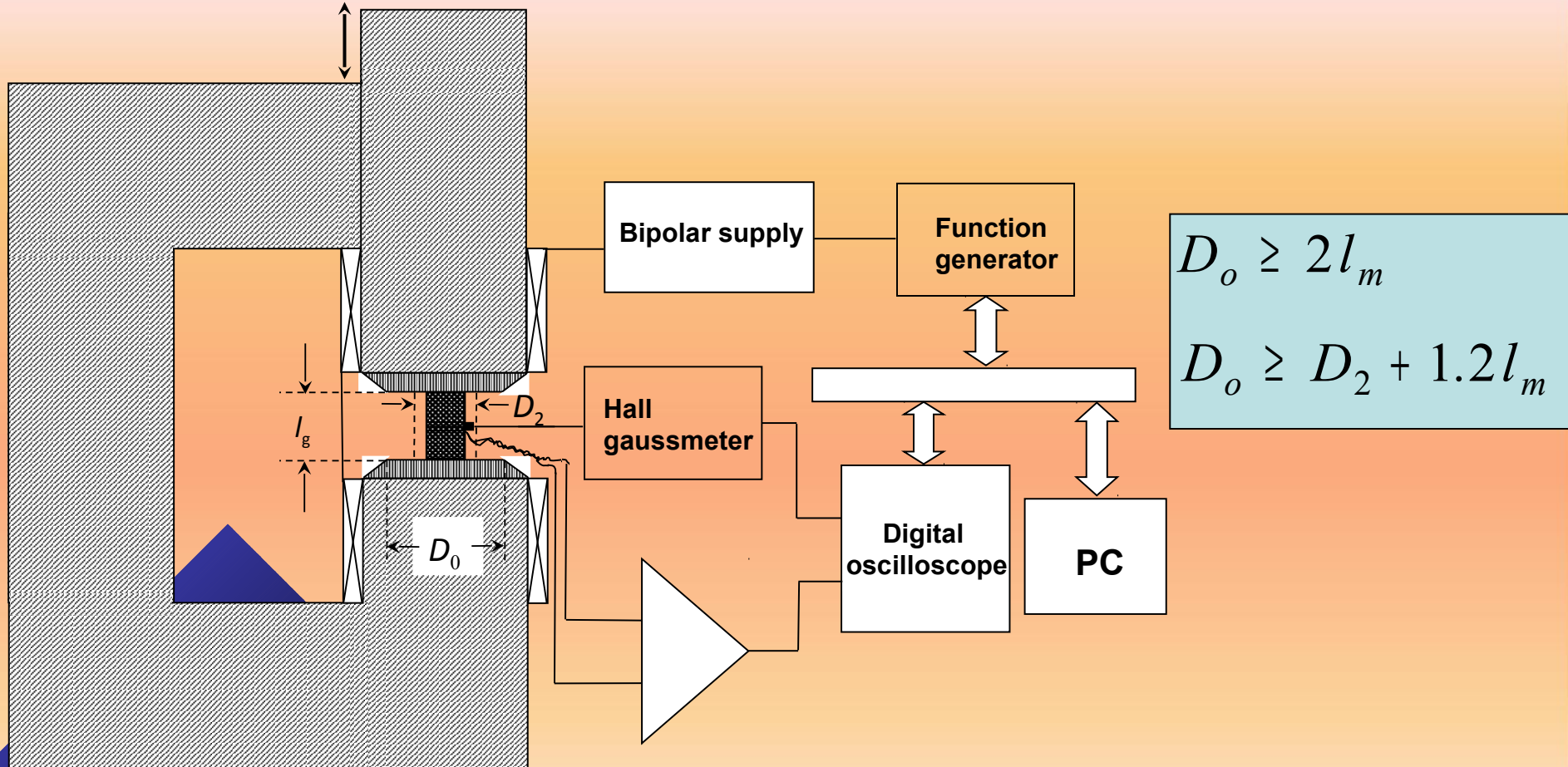
A fundamental problem arises with rare-earth based permanent magnets, because of the very high field values required for achieving technical saturation and ensuing demagnetization.



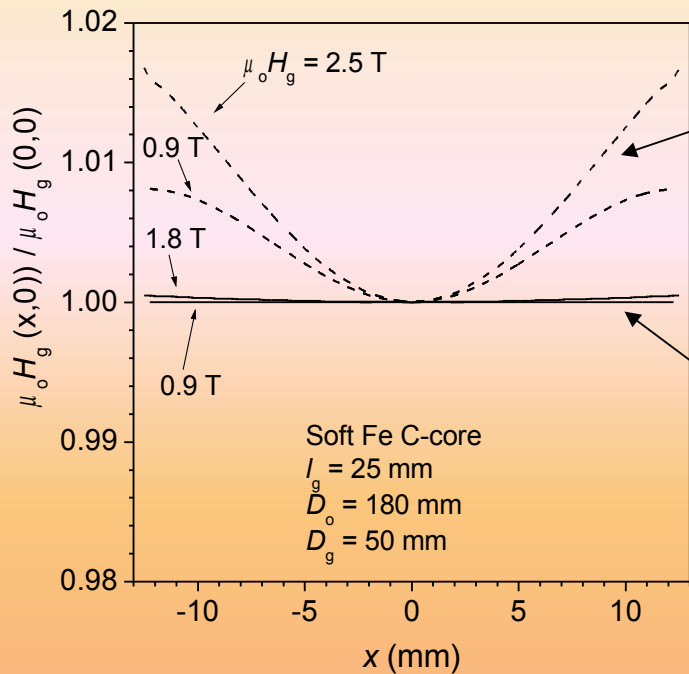
$J(H)$ and $B(H)$ demagnetization curves in a representative commercial Nd-Fe-B sintered permanent magnet between room temperature and 120 °C. Scale markers correspond to load lines with permeance coefficients $B/(\mu_0 H)$ ranging between -0.5 and -4.

Closed magnetic circuit measurements

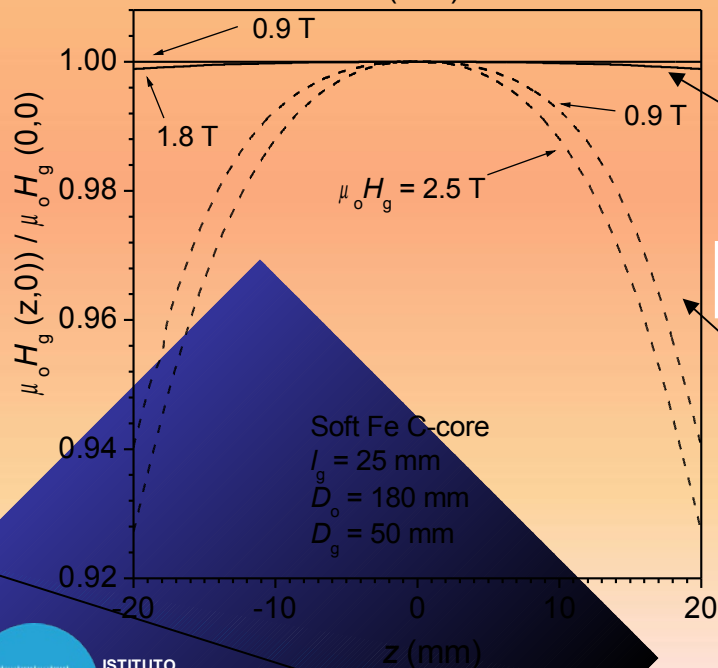
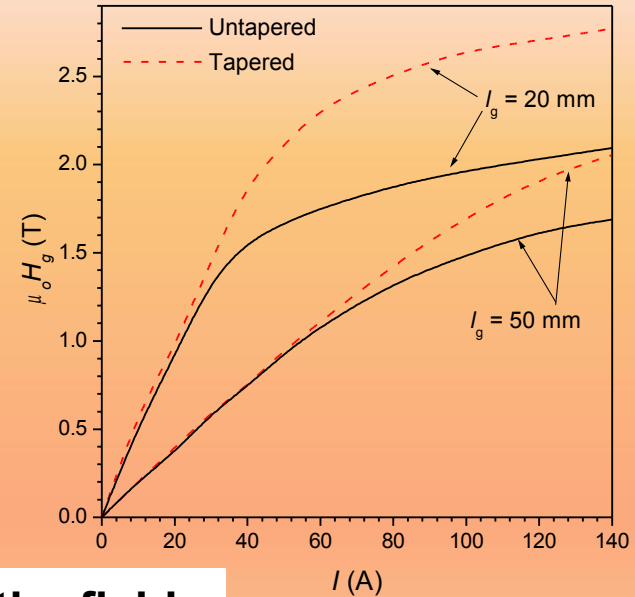
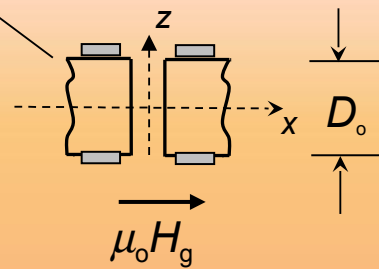
Permanent magnets are typically characterized under a closed-circuit configuration, where an electromagnet plays the role of both field source and soft return path for the magnetic flux (IEC 60404-5).



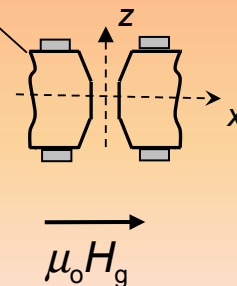
Effect of electromagnet pole tapering on the uniformity of the field in the gap

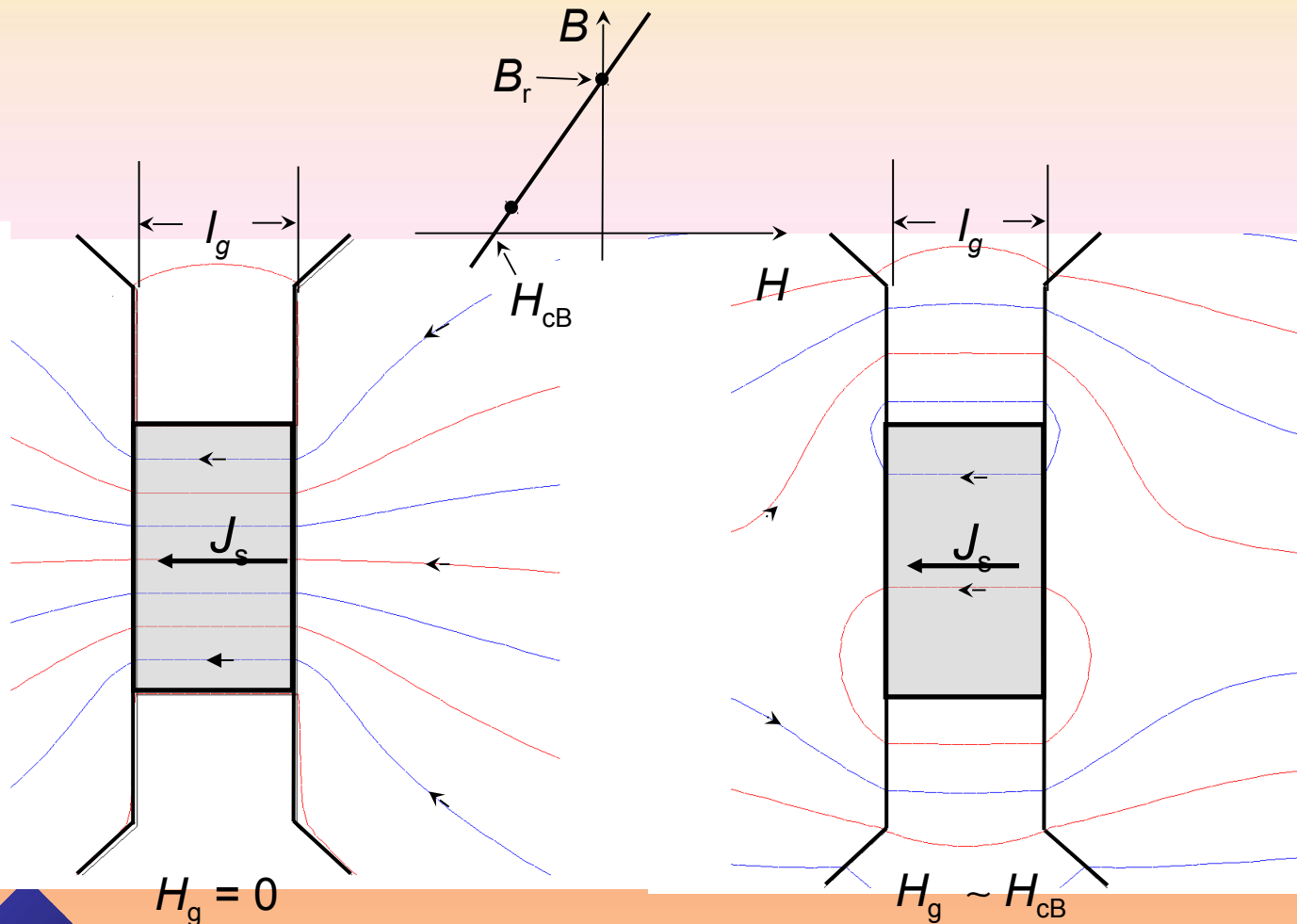


Axial uniformity of the field

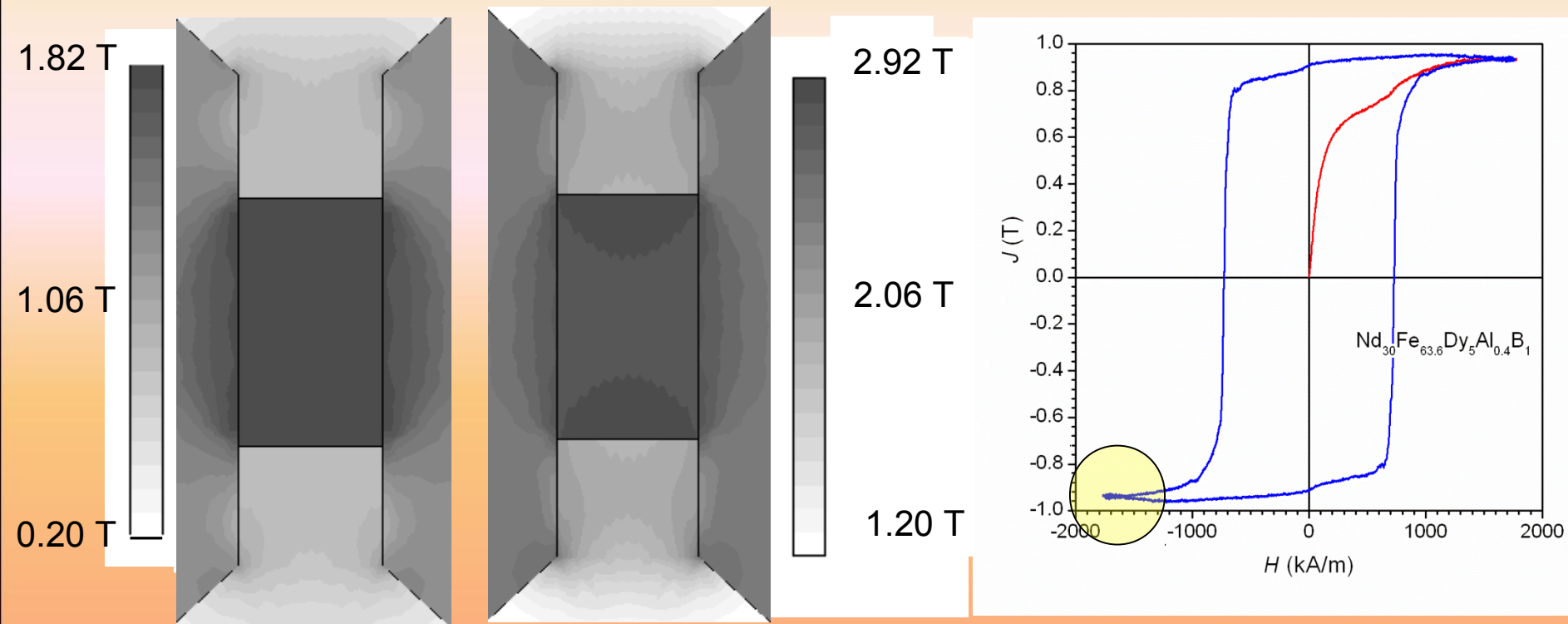


Radial uniformity of the field





FEM modeling of flux distribution in an ideal permanent magnet (saturation polarization = 1 T) and soft iron pole pieces (Armco type iron). a) The field in the gap is zero and the magnet is at remanence ($B_r = J_r = J_s$). b) The electromagnet is supplied and the magnetomotive force appears almost totally across the magnet ($Ni \sim H_g l_g$).



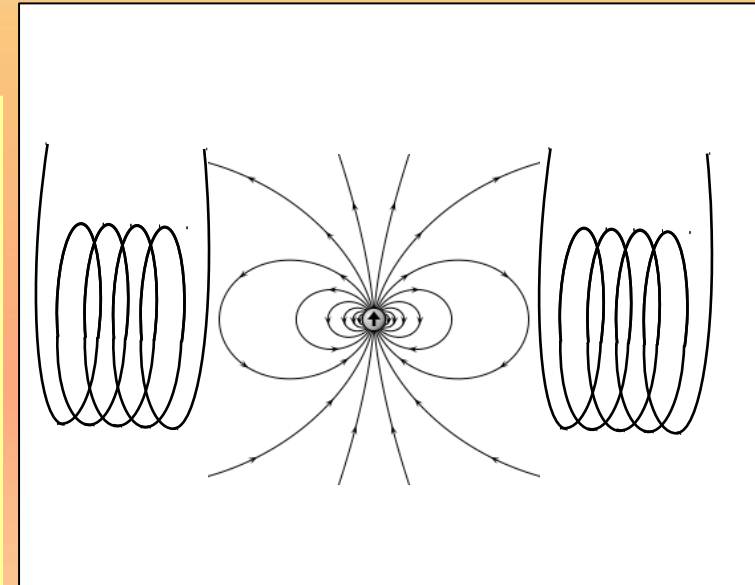
FEM calculation of magnetic flux distribution in ideal permanent magnet test sample (saturation polarization $J_s = 1$ T) and surrounding area for two largely different levels of the applied magnetomotive force. a) The induction in the sample is $B = 1.82$ T and the induction in the back-core is lower than 1 T. Consequently, the effective field in the sample is homogeneous. b) With induction in the sample overcoming 2.9 T, the induction in the back core is larger than 1.9 T, flux-closure by the iron core is poor, and both effective field and induction in the sample are inhomogeneous.

Open sample measurements

Hard magnets have properties influenced by the demagnetizing fields, but they are **little sensitive to the environmental fields**, which can disrupt or falsify measurements made on open soft magnetic sheets and strips. Consequently, testing hard magnets as open samples is not only methodologically correct, but it opens a wide scenario in terms of novel measuring techniques and flexibility as to the type of testing materials and size and shape of the specimens.

Vibrating sample magnetometer

The flux linked with a sensing coil placed at a certain distance from an open sample subjected to an intense magnetizing field can be seen as the sum of a main contribution due to such a field plus a perturbation originating from the sample. **We are interested in measuring such a perturbation**. This can be done by impressing a vibrating motion to the sample, so as to produce an AC signal in a linked coil. Any background constant flux is automatically filtered out. The popular **Vibrating Sample Magnetometer (VSM)**, is based on this principle



An opposing coil pair generates an axial field always passing through the zero value at the origin, where the gradient is maximum and attains a value depending on the ratio between the radius of the coils a and their distance d . When $d = a$, they form an **inverse Helmholtz pair** and the induction derivative at the origin is

$$\frac{dB_x(0)}{dx} = 0.8587 \mu_o \frac{Ni_s}{a^2}$$

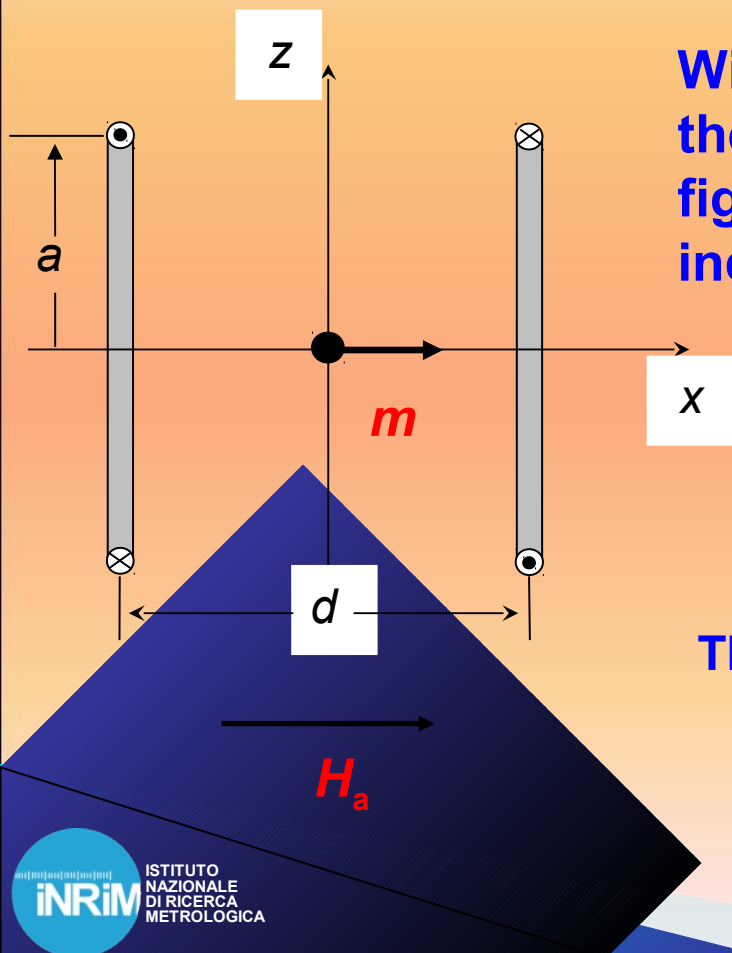
With the magnetic moment m directed along the axis of the coil pair, as shown in the figure, and moving with velocity dx/dt , the induced voltage takes the form

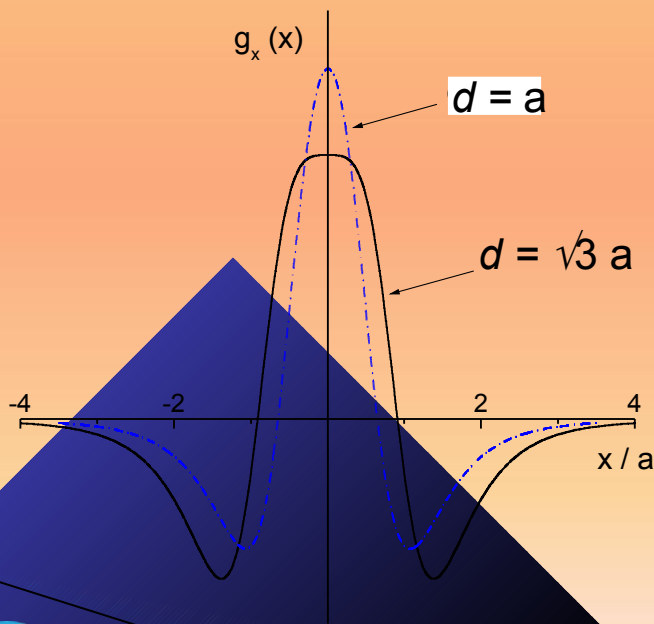
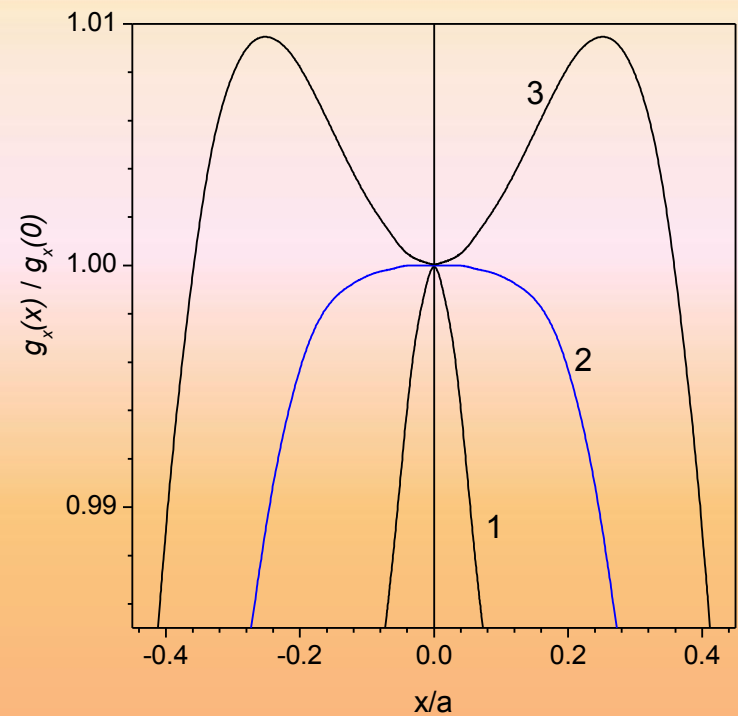
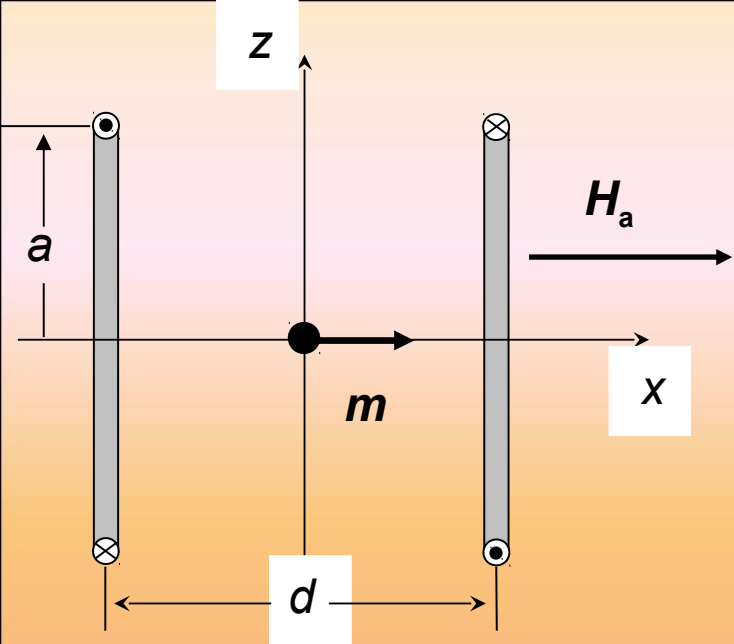
$$u(x, t) = \frac{d}{dx} (m k_x(x)) \cdot \dot{x} = m \cdot g_x(x) \cdot \dot{x}$$

The function

$$g_x(x) = \frac{dk_x(x)}{dx}$$

is called sensitivity function.





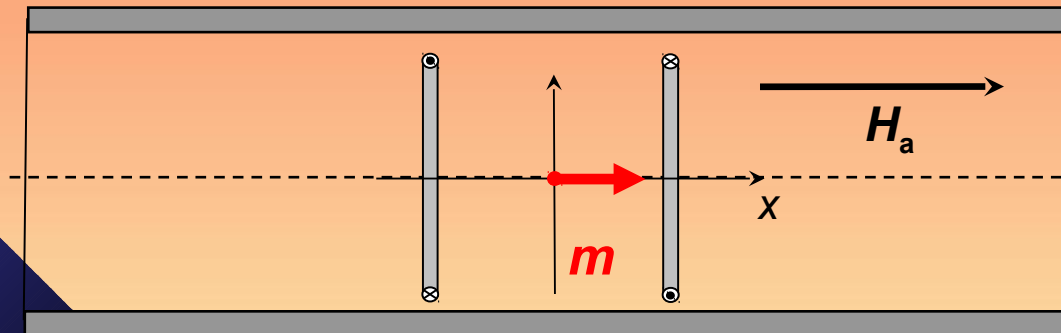
Relative sensitivity function versus displacement of a small sample of magnetic moment m along the x axis of a thin-coil pair for different values of the ratio between intercoil distance d and coil radius a . The coils are connected in series opposition. Curve 1: (inverse Helmholtz pair). Curve 2: $d = \sqrt{3}a$ (maximum homogeneity of the sensitivity function). Curve 3: $d = 1.848a$. c) The sensitivity function averages out to zero over a region of the order of $4a$.

One looks in general for sensing coil arrangements making the point at the origin a saddle point for the sensitivity function, because in the neighborhood of such a point the signal is insensitive to the first order to the sample position. For a small-amplitude vibration of the magnetic moment around the origin, we can safely assume $g_x(x) \cong g_x(0)$

For $x(t) = X_o \sin \omega t$ the voltage induced in the coils is proportional to the sample magnetic moment m , according to

$$u(t) = m g_x(0) \cdot \dot{x} = m g_x(0) \cdot X_o \omega \cos \omega t$$

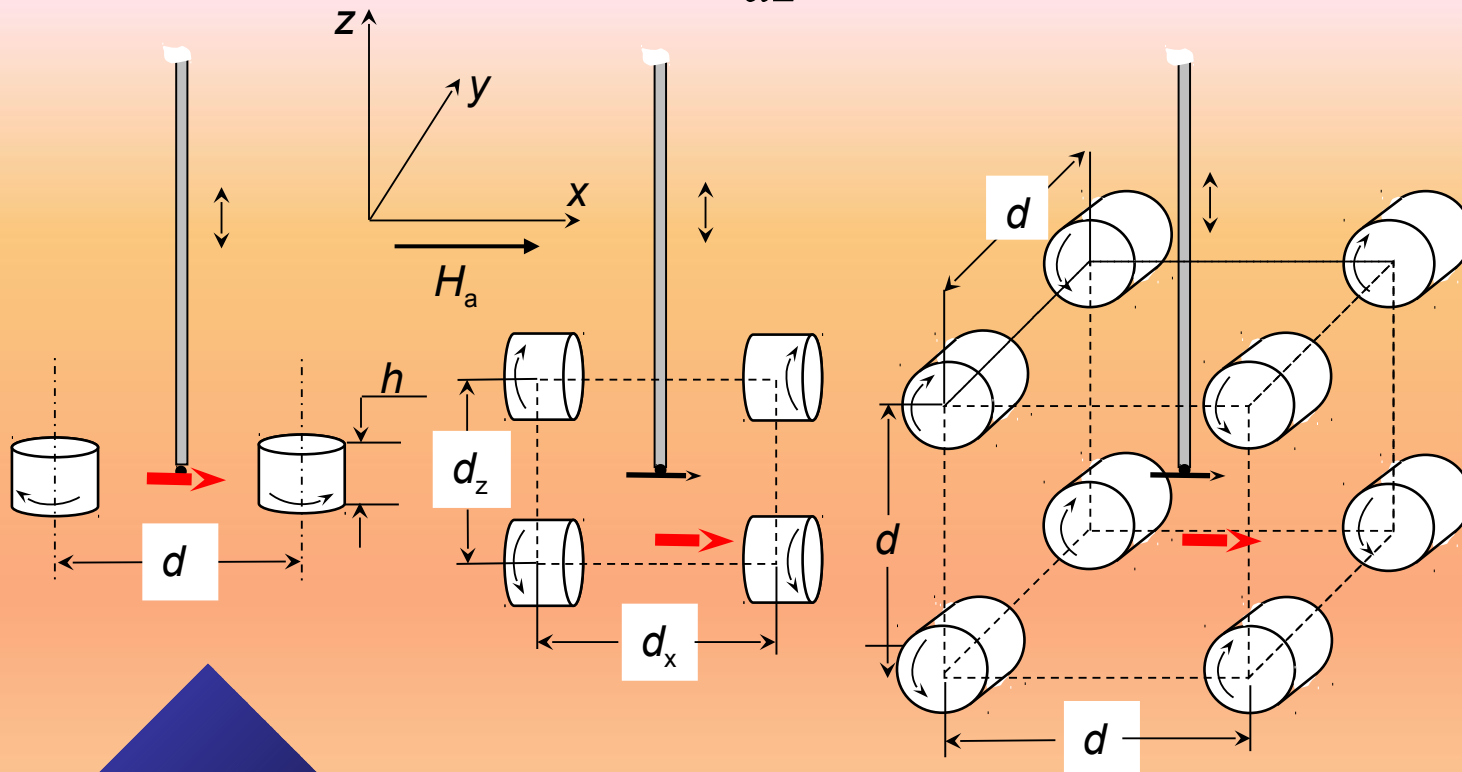
If the field is applied by means a superconducting solenoid, the vibration is necessarily impressed along the axial direction (**x-axis**) and the series opposition coil pair is employed.



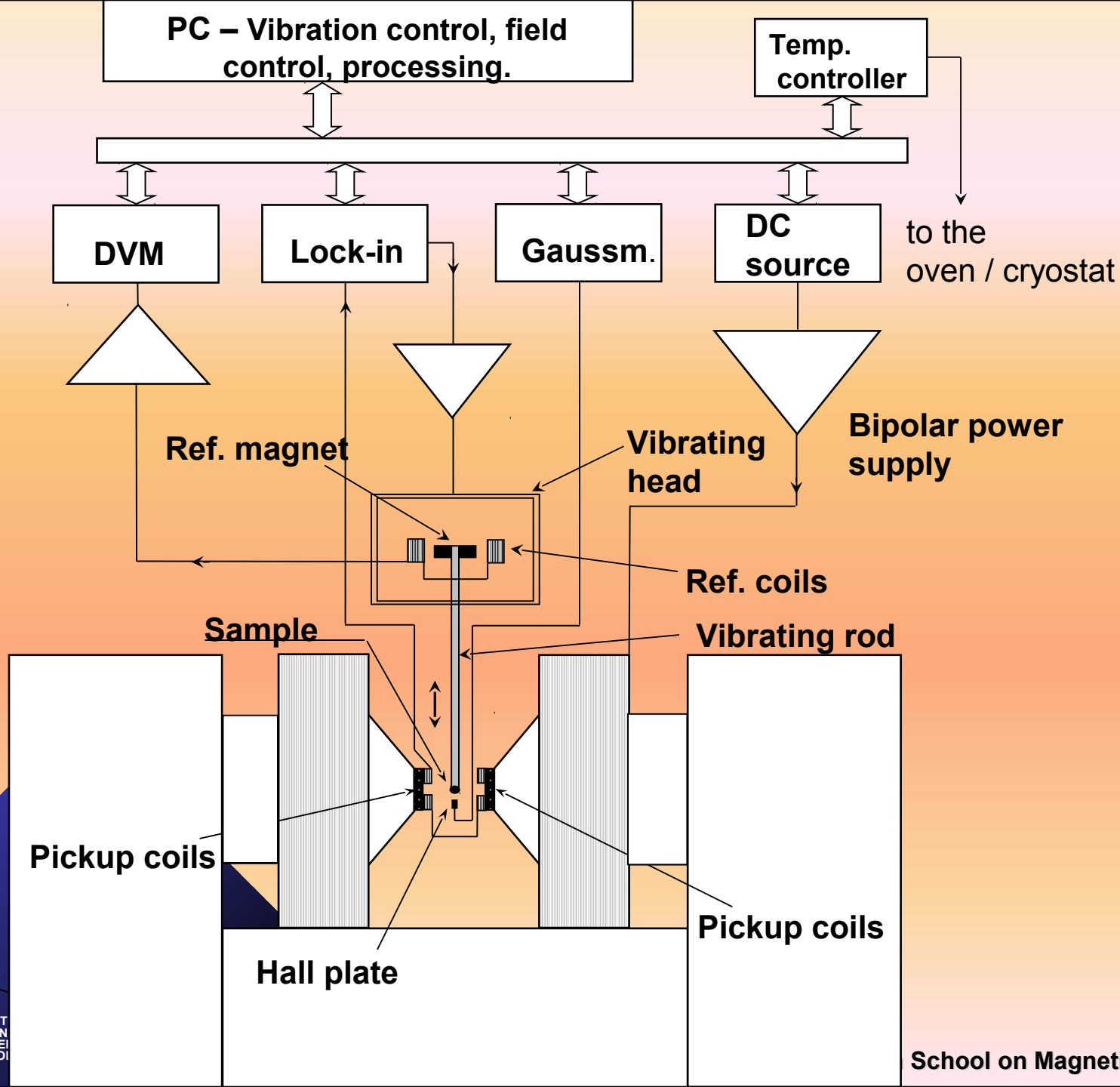
Polarization $J = \mu_0 m / V$, where V is the sample volume.

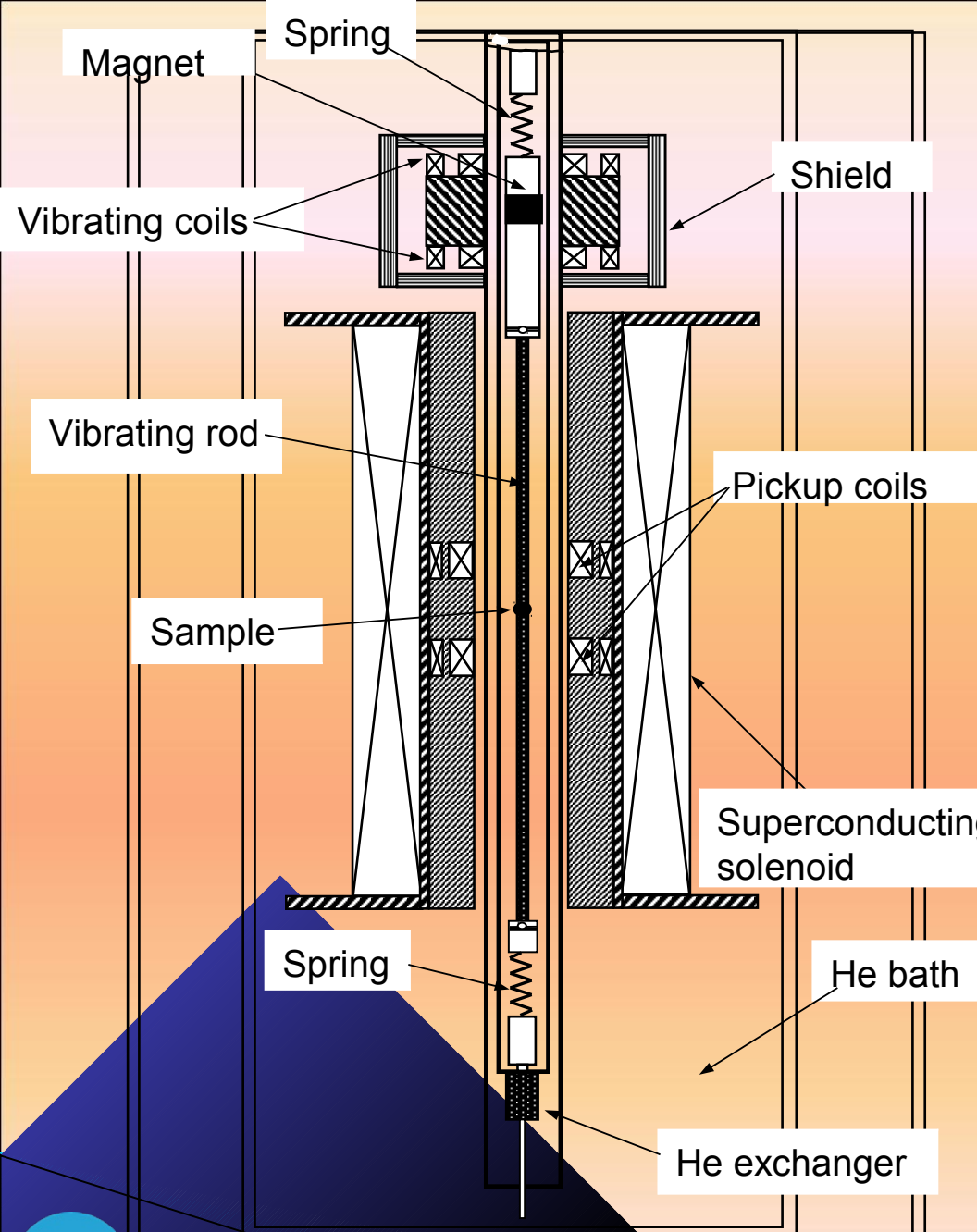
When the field is applied by conventional electromagnets or by permanent magnet sources, transverse sample vibration (z-axis) is generally adopted. In such a case we have

$$u(z,t) = \frac{d}{dz}(m k_x(z)) \cdot \dot{z} = m \cdot g_x(z) \cdot \dot{z}$$



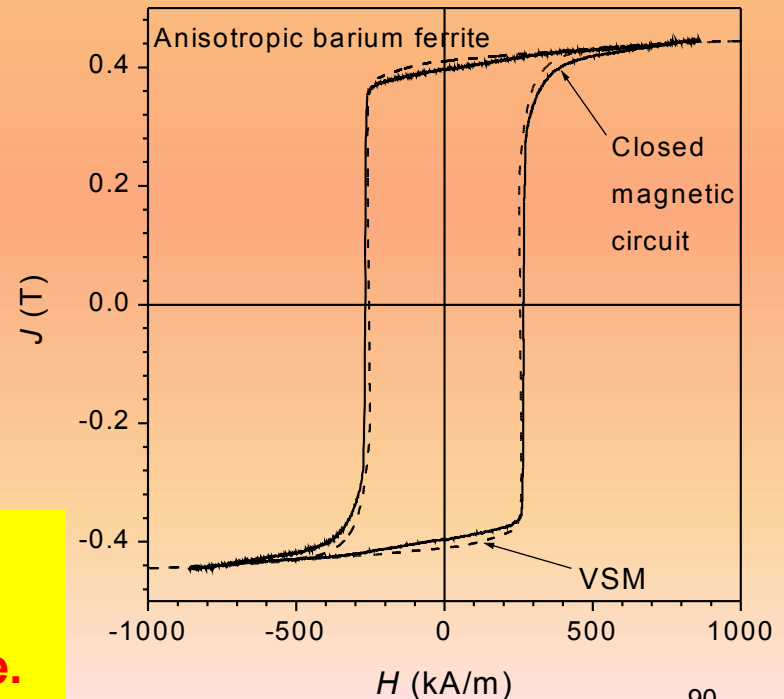
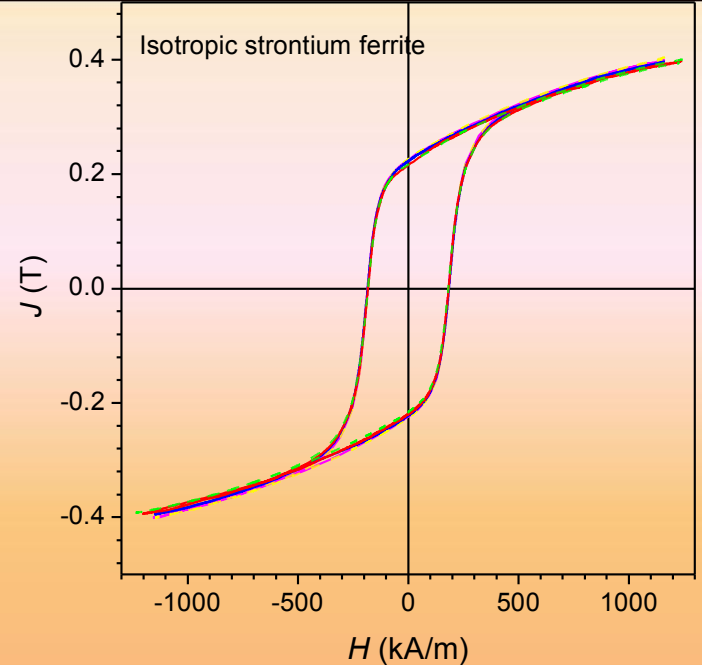
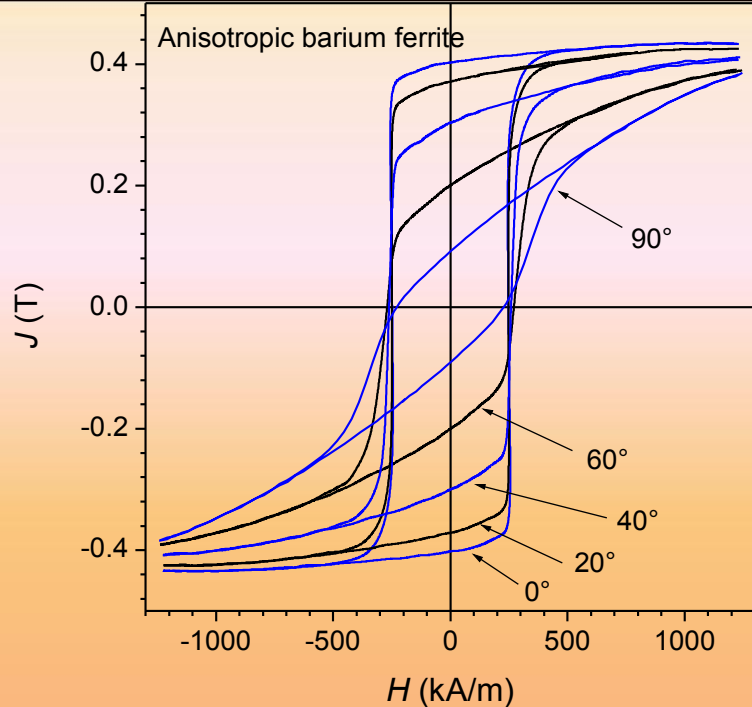
Examples of saddle point coil arrangements in a **VSM** for vibration perpendicular (**z-axis**) to the direction of the magnetic moment (**x-axis**). The sample is attached to a non-magnetic vibrating rod. The arrows marked on the coils identify the way in which the signals from the coils have to be added.





Example of **VSM** setup using a superconducting solenoid field source. The axial pickup coils are compensated by concentric coils connected in series opposition. They have same area-turn product and far lower sensitivity function. The vibration is generated by a couple of AC-supplied superconducting coils connected in series opposition, which create an AC force on a magnet affixed to the vibrating rod. The vibration frequency is **14 Hz** and the peak-to-peak oscillation amplitude is **4 mm**

D. Dufeu and P. Lethuillier, *Sci. Instr.* **70** (1999), 3035-3039). *Rev.*

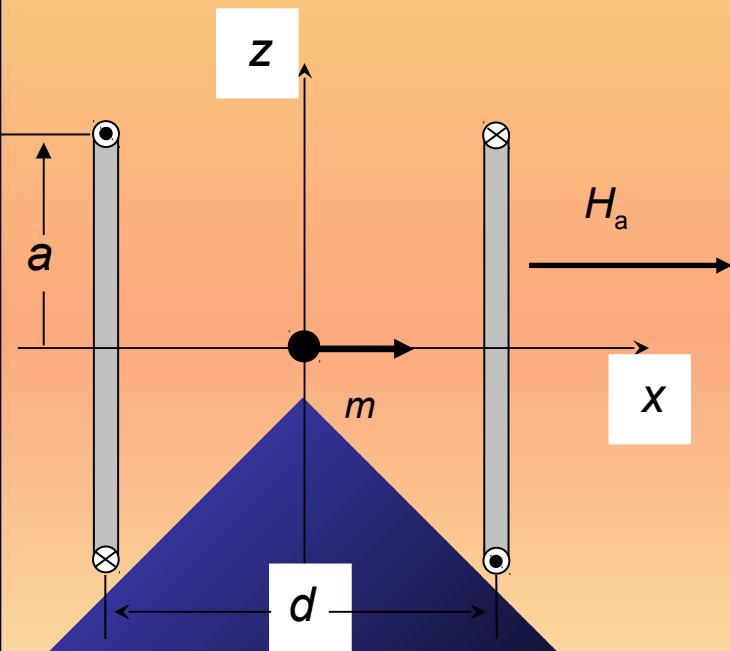


Hysteresis loops measured with a VSM on sintered $\text{BaFe}_{12}\text{O}_{19}$ sample, tested as a 3mm diameter sphere. The effective field is obtained as $H = H_a - (1/3\mu_0)J$. a) Anisotropic material. b) Isotropic $\text{SrFe}_{12}\text{O}_{19}$ spherical sample. c) Comparison with the result obtained with the hysteresisgraph method and closed magnetic circuit

VSM does not provide absolute measurements and must be calibrated with a reference sample.

Alternating Gradient Force Magnetometer

The **VSM** is the preferred solution for the determination of low magnetic moments, down to the some $10^{-8} - 10^{-9} \text{ A}\cdot\text{m}^2$. But we may need to measure magnetic moments lower than typical **VSM** noise floor. A $\text{BaFe}_{12}\text{O}_{19}$ single particle of size about $5 \mu\text{m}$ has a moment of the order of $5 \cdot 10^{-11} \text{ A}\cdot\text{m}^2$, far below the **VSM** sensitivity. For this we can resort to the Alternating Gradient Force Magnetometer (**AGFM**). It is a sort of inverted **VSM**, also called **Vibrating Reed Magnetometer**.



With a sinusoidal current $i(t) = i_o \sin \omega t$

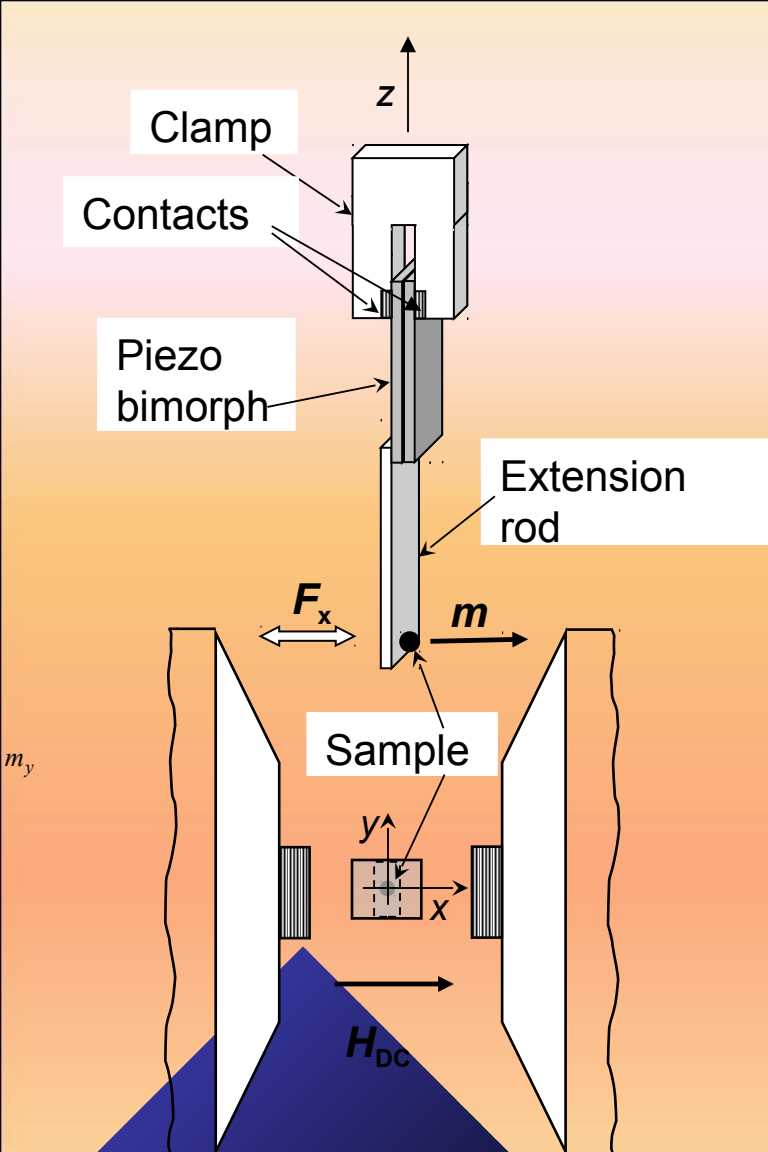
supplying the coils, a sinusoidally varying force

$$F_x(t) = F_o \sin \omega t$$

is applied to the sample. For small oscillations around the center, we obtain

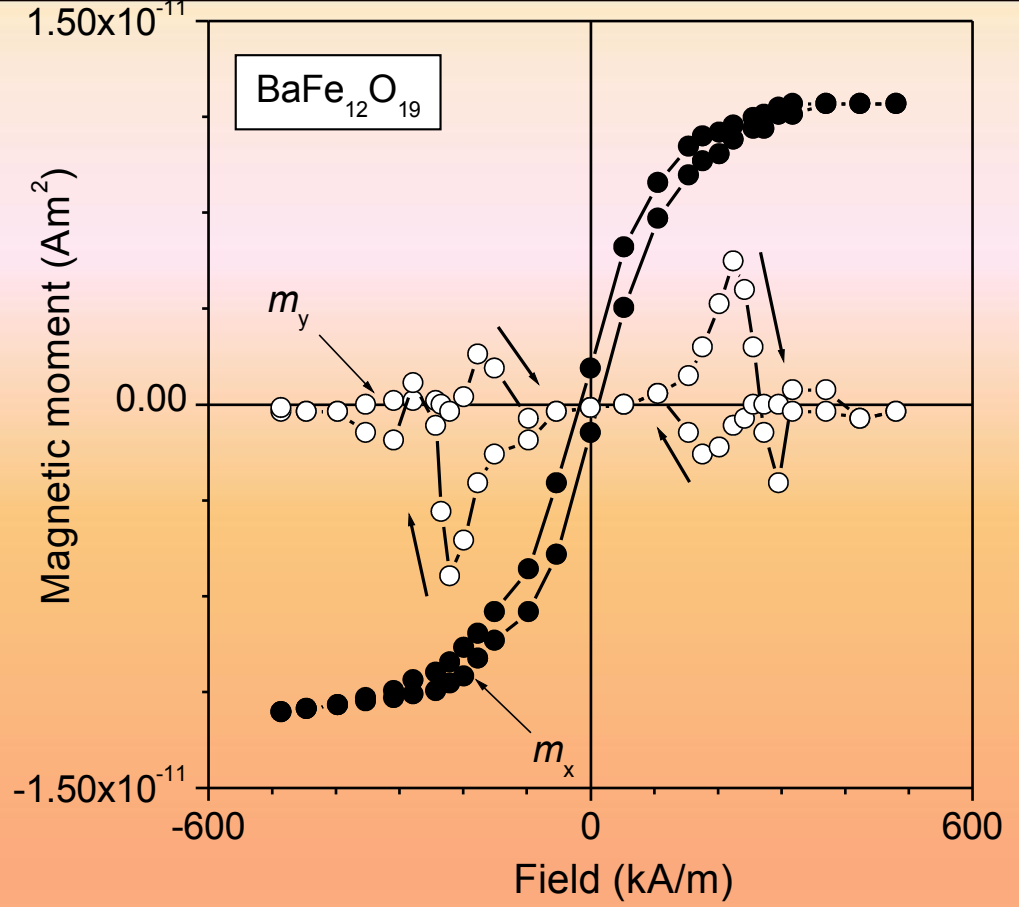
$$F_o = m g_x(0) i_o$$

with $g_x(0)$ the value of the sensitivity function at the origin.



Horizontal gradient AGFM

P.J. Flanders, J. Appl. Phys. 63 (1988) 3940.



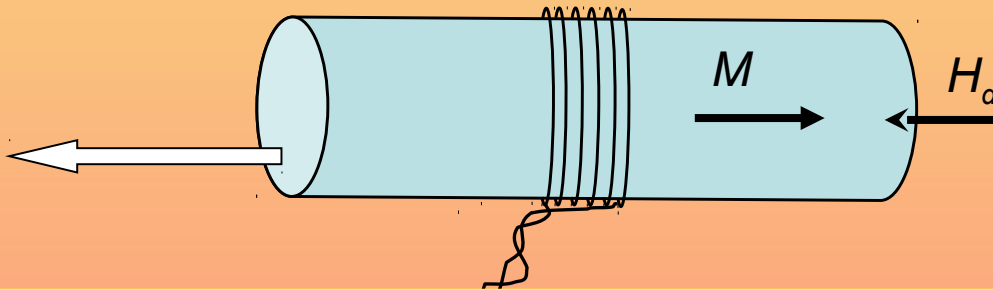
Vector **AGFM** measurement on a **BaFe₁₂O₁₉** single particle, with diameter around **2 μm** and easy axis (**y** direction) oriented at **90°** with respect to the applied DC field (**x** direction). The observed variation of **m_y** versus applied field provides information on the irreversible magnetization processes.

G. Zimmermann, et al., IEEE Trans. Magn. 32 (1996) 416.

Extraction method

The extraction method does provide a practical approach to the measurement of the magnetic moment of the permanent magnets. In its classical realization, a magnetized bar specimen is removed from a rest position, where it is **fully inserted** within a short search coil, to a distant place, where flux linkage with the coil is zero. The ensuing flux variation, measured by a fluxmeter connected with the coil, is

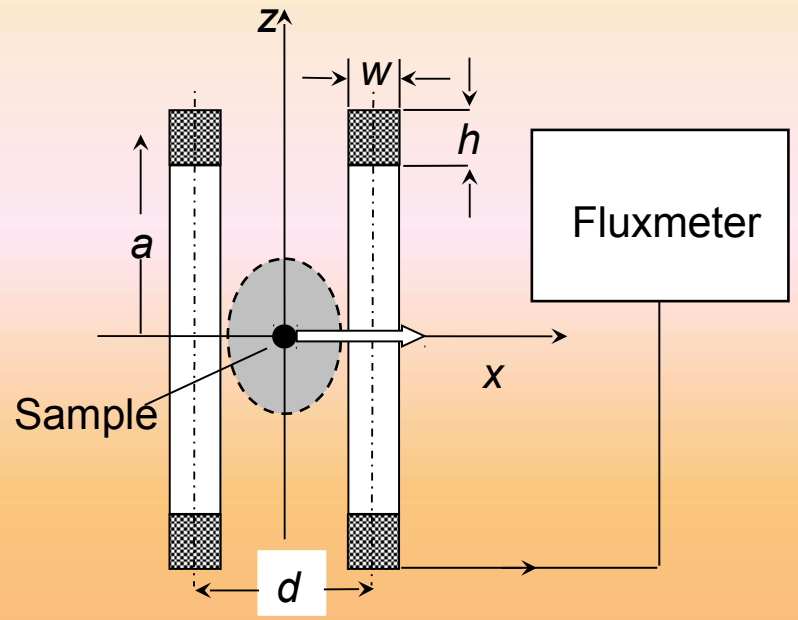
$$\Delta \Phi = BA = \mu_o (M - H_d) A = \mu_o MA(1 - N_d)$$



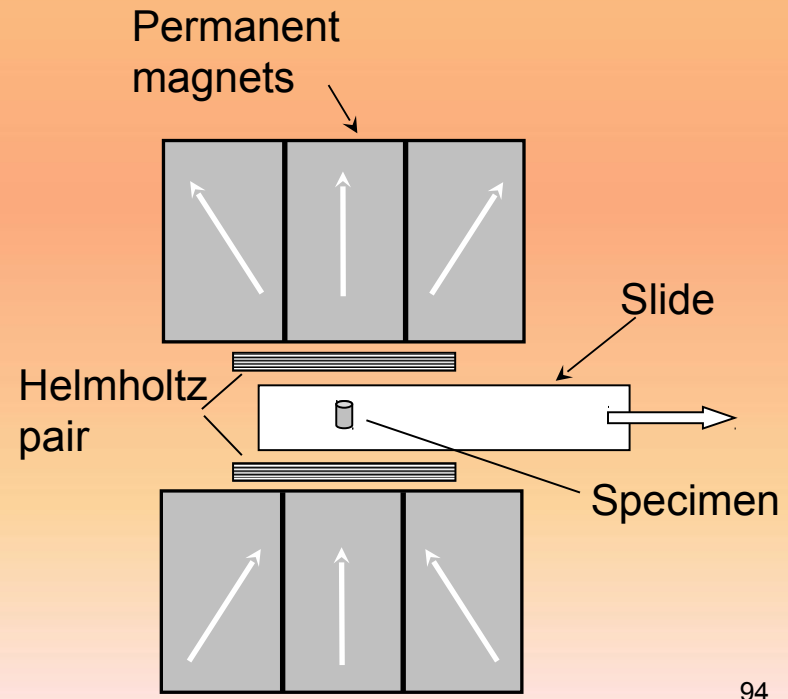
Permanent magnets typically come as short samples, because the induction behaves nearly linearly in the second quadrant and the maximum energy product is obtained with a high value of the demagnetising coefficient ($N_d \sim 1/2$). An elegant solution to the measurement of the magnetic moment of a short sample by the extraction method is offered, as in the VSM and AGFM methods, by the reciprocity principle. Any coil brought in proximity of a small sample having magnetic moment m is linked with a certain amount of flux $\Phi = k(x, y, z) \cdot m$, where $k(x, y, z)$ is the coil constant at the sample position.

Measurement of the magnetic moment of permanent magnets by sample extraction.

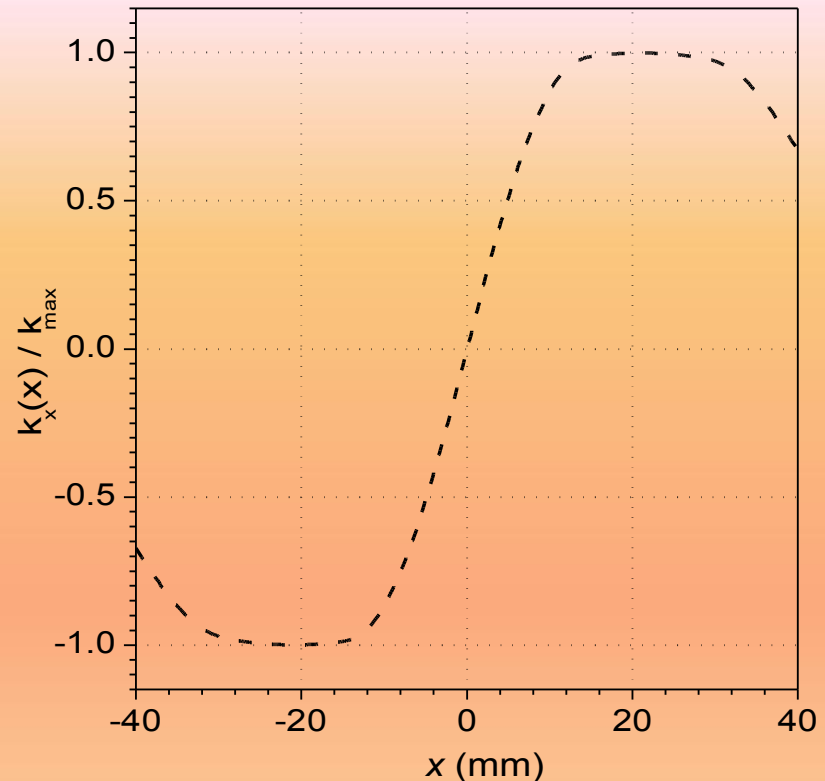
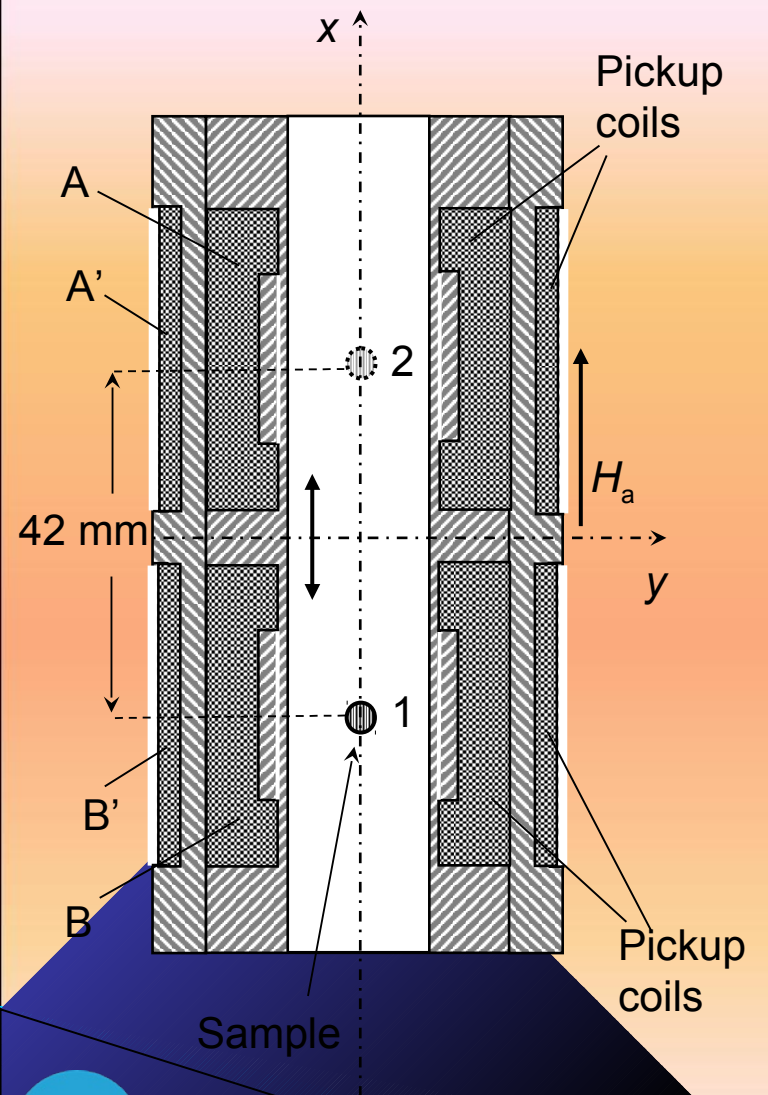
The flux variation detected upon withdrawal of the sample from the center of a Helmholtz pair up to a distant position is proportionally related to the component of the magnetic moment along the coil axis. The saturation magnetization of hard materials can also be determined using an assembly of high-coercivity permanent magnets to generate a conveniently high field at the center of the Helmholtz pair.



IEC standard 60404-14



An interesting variant of the extraction method involves the movement of the sample between the centers of two identical search coils connected in series opposition and placed at a convenient distance along their common axis x .



$$\Delta \Phi = 2k_x m_x$$

D. Dufeu, T. Eryraud, P. Lethuillier, Rev. Sci. Instr. 71 (2000) 458.

References

- [1] T.C. Bacon, *Neutron Diffraction* (Oxford: Clarendon Press) 1975.
- [2] G.I. Squires, *Thermal Neutron Scattering* (New York: Cambridge Univ. Press) 1978.
- [3] H. Zjilstra, *Experimental Methods in magnetism* (Amsterdam: North-Holland) 1967.
- [4] M. McCaig and A.G. Clegg, *Permanent Magnets in Theory and Practice* (London: Pentech Press) 1987.
- [5] E. Steingroever, *Magnetic Measuring Techniques* (Köln: Magnet Physik) 1989.
- [6] P. Lethuillier, *Magnétisme Pratique et Instrumentation*, in *Magnétisme*, vol. II (E. du Trémolet de Lacheisserie, ed., Presses Universitaires de Grenoble, 1999), p. 435.
- [7] F. Fiorillo, *Measurement and Characterization of Magnetic Materials* (Elsevier-Academic Press, Amsterdam) 2004).
- [8] B.D. Cullity and C.D. Graham, *Introduction to Magnetic Materials* (Piscataway, NJ: IEEE Press and Wiley) 2009.
- [9] J.M.D. Coey, *Magnetism and Magnetic Materials* (Cambridge Univ. Press) 2010.

- [10] F. F. Fiorillo, *Measurements of magnetic materials*, Metrologia, vol. 47, pp. S114-S142, 2010.[11]
- [12] S. Tumanski, *Handbook of Magnetic Measurements* (CRC Press) 2011.
- [13] BIPM, IEC, IFCC, ISO, IUPAC, IUPAP, OIML, “*Guide to the expression of uncertainty in measurement*,” (International Organization for Standardization, Geneva, Switzerland) 1993.
- [14] BIPM, “*Mutual recognition of national measurement standards and of calibration and measurement certificates issued by the national metrology institutes*,” (Bureau International des Poids et Mesures, Sèvres, 1999); <http://www.bipm.fr/BIPM-KCDB>
- [15] IEC Standard Publications, 60404 Series.